CHAPTER ONE
Physical and biological processes

(a)

(b)

(a) Experimentally produced turbidity current. Courtesy Jeff Peakall. (b) Upper part of sediment slide deposits (Facies F2.1) draped by siltstone turbidites (Facies D2.2 and D2.3) in deep-marine volcaniclastics, Miocene Misaki Formation, Miura Peninsula, southeast Japan.

1.1   Introduction

This chapter has two main functions. First, there is an introduction to the main processes responsible for the physical transport and deposition of sediments derived from land areas and carried into the deep sea. Second, the origin of pelagic sediments (oozes, chalks, cherts) and organic-rich muds (e.g., black shales and sapropels with >2% organic matter) is explained. For these sediments, transport of material from an adjacent land mass is either not required, for example in the case of accumulation of biogenic skeletons, or is far less important than the chemistry of the seawater at the site of deposition. The biogenic process of bioturbation is considered in Chapter 3.

The three main processes responsible for transporting and depositing particulate sediments seaward of the edges of the world's continental shelves are (i) bottom-hugging sediment gravity flows (e.g., turbidity currents and debris flows), (ii) thermohaline bottom-currents that form the deep circulation in the oceans and (iii) surface wind-driven currents or river plumes that carry suspended sediment off continental shelves. Tidal currents, sea-surface waves and internal waves at density interfaces in the oceans appear to be only locally important as transport agents on the upper parts of slopes and in the heads of some submarine canyons.

In order to appreciate how sands and gravels encountered in deep-marine petroleum reservoirs are deposited, it is essential to understand the dynamics of sediment gravity flows. A *sediment gravity flow* (SGF; Middleton & Hampton 1973) is a bottom-hugging density underflow carrying suspended mineral and rock particles, mixed together with ambient fluid (most commonly seawater). A SGF is a special type of *particulate gravity current* (McCaffrey *et al.* 2001) – in other flows belonging to this broad category the particles can be snow and ice (e.g., in a powder snow avalanche), or the fluid phase can be hot volcanic gases (e.g., in a pyroclastic surge). In engineering practice, such mobile solid and fluid mixtures are called *granular flows*, *slurry flows* or *powder flows*, depending on the size of the particles, whether the fluid phase is a liquid or a gas and whether cohesive forces are significant. In this book, we will use the more geologically relevant term 'sediment gravity flow', but anyone undertaking a literature search needs to be aware of the alternative terminology used in other disciplines.

The particles in SGFs spend most of their time in suspension rather than in contact with the seafloor. In the more dilute SGFs, particles in suspension eventually settle to the seafloor where they accumulate, either with or without a phase of traction transport. This is called *selective deposition* (Ricci Lucchi 1995; *incremental deposition* of Talling *et al.* 2012), because particles are deposited one by one according to size, shape, density or some other intrinsic property. In concentrated dispersions or cohesive debris flows, the particles are not fully free to move independently of one another and therefore accumulate by massive deposition (Ricci Lucchi 1995; *en masse* deposition of Talling *et al.* 2012). The distinction between *selective deposition* and *massive deposition* (or en masse deposition) is a useful one, because the former deposits are commonly laminated and the latter commonly structureless, poorly organised, plastically deformed, or contain evidence of intense particle interaction and/or pore-fluid escape. The ultimate end-member example of en masse deposition is *coherent sliding* in which masses of semi-consolidated material move downslope while retaining some of the organisation and stratigraphy of the original failed successions. Sediment slides come to rest as deformed, folded and/or sheared units.

Let us start by considering a typical event responsible for basinward sediment transport along a continental margin. The transport can be divided into four phases: (i) a phase of flow initiation; (ii) a period during the early history of the flow when characteristics of the transporting current change rather quickly to a quasi-stable equilibrium state; (iii) a phase of long-distance transport to the base of the continental slope or beyond and (iv) a final depositional phase. In many cases, the concentration of solid particles changes systematically along the flow path. Particle concentration is an important variable because mixtures of sediment and water can only become fully turbulent if the concentration is low. Without turbulence, it is difficult to suspend and transport mineral-density particles for long distances, and tractional sedimentary structures like current-ripple cross-lamination cannot form. Figure 1.1 shows how a range of deep-marine transport processes can be assigned to one or more of these four stages of flow evolution, and shows how the flow concentration might change through time. For example, sediment suspended by a storm on a continental shelf or by tidal currents in the head of a submarine canyon forms low-concentration suspensions that might continue to move downslope as turbidity currents, transferring particulate sediment tens to hundreds of kilometres farther seaward. Other initiation processes, like the disintegration of sediment slides on steep slopes, can generate more concentrated SGFs such as submarine debris flows. These debris flows may never become more dilute or develop turbulence, and therefore are less likely to transport their sediment load far into the deep-marine basin.

There is a fundamental difference in the way that non-turbulent, highly concentrated SGFs (e.g., debris flows) deposit their sediment load and evolve as compared to turbulent and water-rich flows like turbidity currents. As a highly concentrated SGF decelerates, the internal resistance to flow (e.g., friction between adjacent particles, or electrostatic cohesive forces between clay minerals) eventually exceeds the gradually decreasing gravitational driving force. When this happens, the flowing mass ceases to travel basinward and is deposited. Because the shear stress responsible for internal deformation and therefore 'flow' increases downward toward the base of the moving mass (due to the cumulative weight of the overlying material), it is the basal part of the mass which last stops deforming. This final immobilisation of the basal part of the flow only occurs after higher levels have ceased to deform (Fig. 1.2). In the case of a slowly decelerating, texturally homogeneous debris flow, the top of the flow will stop deforming first, and then internal deformation will cease in a sequential manner from the top of the flow (where the shear stress is lowest) downward. If we equate the cessation of internal deformation to the phenomenon called 'deposition', then such flows might be said to deposit (and acquire their textures and fabrics) 'from the top downward'. In the case of decelerating debris flows, this gradually thickening zone with little or no internal deformation at the top of the flow has been called a 'rigid plug' (Johnson 1970). In contrast, most decelerating turbulent SGFs deposit their load selectively, grain by grain, during a period when solid particles rain downward to the base of the flow. This can be thought of as deposition 'from the base upward', with the result that many deposits of this type show graded bedding because of a progressive decline in flow energy during the depositional phase. Unlike the non-turbulent flows, these low-concentration SGFs become increasingly dilute as they lose their sediment load (Fig. 1.1), eventually losing their identity when the flow density decreases to a value close to that of clear seawater.

Although the way in which deposition proceeds can help explain the development of texture and the internal organisation of many deep-sea facies, the distinction between deposits formed 'from the top downward' and those formed 'from the base upward' is sometimes blurred. This happens in some SGFs of intermediate concentration or
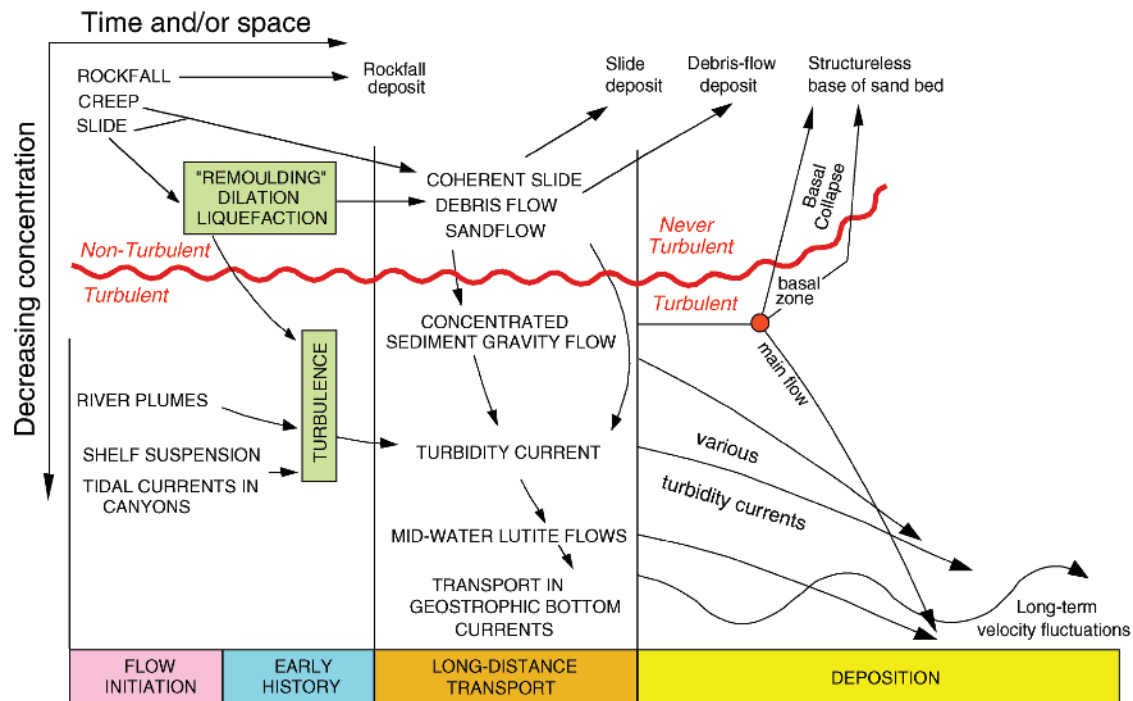
Fig. 1.1 Simplified conceptual overview of the evolution of sediment gravity flows and other deep-marine transport processes as a function of concentration. The horizontal axis is time and/or space, but no units are implied because the evolution of some flows is much longer than for others. For example, turbidity currents might flow for only hours to days, whereas contour-following geostrophic bottom-currents (i.e., thermohaline currents) have velocity fluctuations lasting thousands of years. Notice that non-turbulent flows tend to deposit en masse, so that the deposit is simply the original flow, arrested in place when driving forces are no longer adequate to keep the material moving. In contrast, turbulent flows lose their sediment load by settling, and therefore become increasingly less concentrated during the depositional phase. Modified from Middleton and Hampton (1973) and Walker (1978).

clay content (e.g., Baas *et al.* 2011), because the downward rain of solid particles during times of rapid deceleration suppresses turbulence in the near-bed region of the flow. Such flows are strongly stratified in terms of their density and concentration, so that the basal and upper parts of the flow behave differently. If the average concentration is low (<5% by volume), particles are lost by settling from the upper fully turbulent part of the flow and the flow becomes progressively more dilute. Near the base of the flow, however, frictional resistance can eventually in some cases immobilise a basal sheared layer, and the properties of the resulting deposit will be more akin to those of the more highly concentrated SGFs. If the average concentration is high (>5% by volume) and a significant amount of clay is present, rapid deceleration leads to the accumulation of a bipartite bed with an upper division of *fluid mud* containing variable quantities of silt and sand, as well as clay (Baas *et al.* 2011). Above this bipartite deposit, the upper part of the still-moving viscous flow may be immobilised, because of insufficient shear stress, to form a variably thick semi-rigid plug that thickens downward with decreasing flow velocity, leading to a very complicated final deposit.

With this brief introduction behind us, let us now probe more deeply into the processes responsible for deep-marine sedimentation. What is the best point of departure for a systematic assessment of sedimentary processes in the deep sea? We take our guidance from Figure 1.1, and begin with shelf-edge processes that can either initiate SGFs or independently move sediment into deeper water. In deep parts of the ocean basins, thermohaline currents locally are important agents of sediment transport, but mostly these areas receive their

sediment from infrequent SGFs, separated in time by long periods of relative quiescence. SGFs are responsible for a wide spectrum of modern and ancient facies, so their classification and description form a significant part of this chapter. Each type of SGF creates unique sedimentary textures and structures, which are described after each flow process is explained. The chapter concludes with other issues that are important in understanding the deep-marine environment, like the accumulation of pelagic sediments and deep-sea bioturbation.

1.2 Shelf-edge processes

1.2.1 High-level escape of mud from the shelf

Suspended sediment concentrations in shelf areas may be quite high due to the input of mud-laden river water, or stirring of the bottom by waves (Geyer *et al.* 2004), tidal currents or internal waves at density interfaces (Cacchione & Southard 1974). This suspended sediment may be advected off the shelf by ambient currents, possibly wind-driven, or by transport in cascading cold water that may flow off the shelf in the winter months (Postma 1969; McCave 1972; McGrail & Carnes 1983; Wilson & Roberts 1995; Ivanov *et al.* 2004). Suspensions of fine-grained sediment may also leave the shelf as dilute turbidity currents (lutite flows), moving along the bottom onto the lower slope and rise, or along density interfaces in the ocean water (Fig. 1.3) (Postma 1969; McCave 1972; Gorsline *et al.* 1984). These dilute suspensions may move down a smooth upper slope as
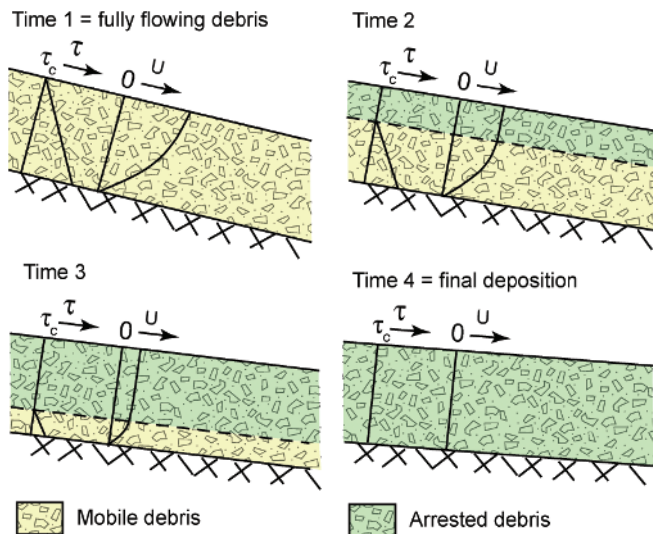
Mobile debris

Arrested debris

Fig. 1.2 Four snapshots during the deceleration and eventual deposition (Time 4) of a non-turbulent debris flow, showing how textures, fabrics and internal structures of the eventual deposit are locked into place by the progressive downward thickening of a 'rigid plug' (arrested debris). These are streamwise vertical cross-sections through the flow. In the 'rigid plug', there is little to no internal deformation because gravity-induced shear stress (τ) is less than the critical shear stress (τ_c) needed to overcome resisting forces (due to internal grain friction and electrostatic cohesive forces). Decreasing slope explains the decreasing shear stress. Profiles of shear stress (τ) and velocity (U) are shown in each case. In the 'rigid plug', the change in velocity with depth is zero, although the velocity of the plug itself is positive up until Time 4. In SGFs of this type, the material is effectively deposited 'from the top downward', and the base of the flow is the last part to be deformed by shearing (e.g., Time 3).

unconfined sheet flows, or may be confined by gullies or canyons in which suspension is augmented by weak tidally forced flows (Shepard *et al.* 1979; Gorsline *et al.* 1984). There is evidence that most mud transported off the shelf by dilute turbidity currents (lutite flows)
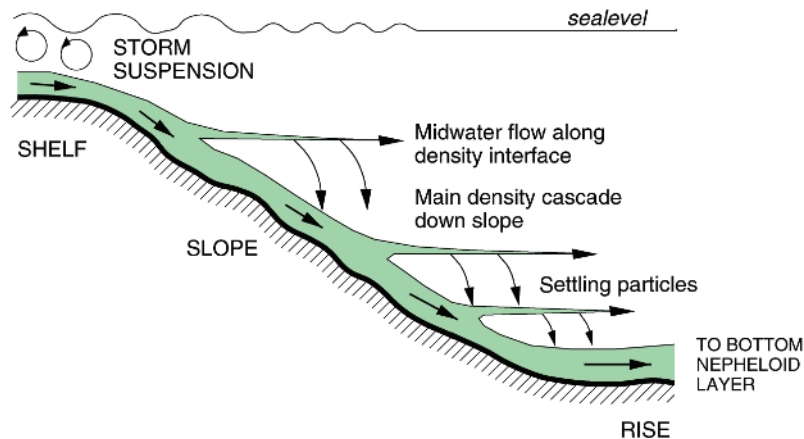
bypasses the slope, leading to maximum rates of accumulation on the continental rise (Nelson & Stanley 1984).

On narrow shelves, plumes of suspended sediment from river deltas can extend beyond the shelf-slope break (Emery & Milliman 1978; Thornton 1981, 1984), directly contributing fine-grained sediments to slope and rise areas. In polar areas, sediment-laden spring meltwater may actually flow from the land across the surface of floating sea ice and deposit its load directly onto the continental slope (Reimnitz & Bruder 1972).

Mud that leaves the shelf either by 'high-level' escape in river plumes, by dilute turbidity-current flow, or by movement along density interfaces in the water column over the slope eventually settles to the seafloor to form the bulk of what are called *hemipelagic deposits*. Deposition rates are on the order of 10–60 cm kyr^{-1} (Krissek 1984; Nelson & Stanley 1984). As is true for strictly pelagic sediments, the finest particles in the high-level suspensions are probably carried to the bottom as aggregates in the form of faecal pellets (Calvert 1966; Schrader 1971; Dunbar & Berger 1981). In regions of higher mud concentration, for example off river mouths, a significant quantity of mud forms aggregates called *floccules* (or flocs). The 'stickiness' that holds silt- and clay-sized particles together in flocs is provided by electrostatic attraction, organic matter and bacteria (Gibbs & Konwar 1986; Curran *et al.* 2002; Geyer *et al.* 2004). Flocs from a number of environments settle at speeds very close to 1 mm s^{-1} ($\sim$100 m day^{-1}), which is much faster than the settling rates of the same material once disaggregated (Gibbs 1985a, b; Hill 1998; Geyer *et al.* 2004). Even in mud-laden turbidity currents, the percentage of sediment deposited as flocs may commonly exceed 75% (Curran *et al.* 2004). The diameters of flocs, based mainly on measurements on continental shelves, are >100–200 µm, although floc densities are low and decrease with increasing floc size (Hill & McCave 2001).

Fine-grained suspensions that move seaward across the edges of continental shelves may vary seasonally in (i) grain size and (ii) content of suspended organics. In anaerobic/dysaerobic basins, this fine-scale seasonal cyclicity can be preserved in the sediment record; on oxygenated basin slopes all such lamination would be destroyed by burrowers. Dimberline and Woodcock (1987) and Tyler and Woodcock (1987) convincingly argue that submillimetre-thick interlaminations of silt and organics in the Silurian Welsh Basin are a result of alternations of (i) spring algal blooms with (ii)
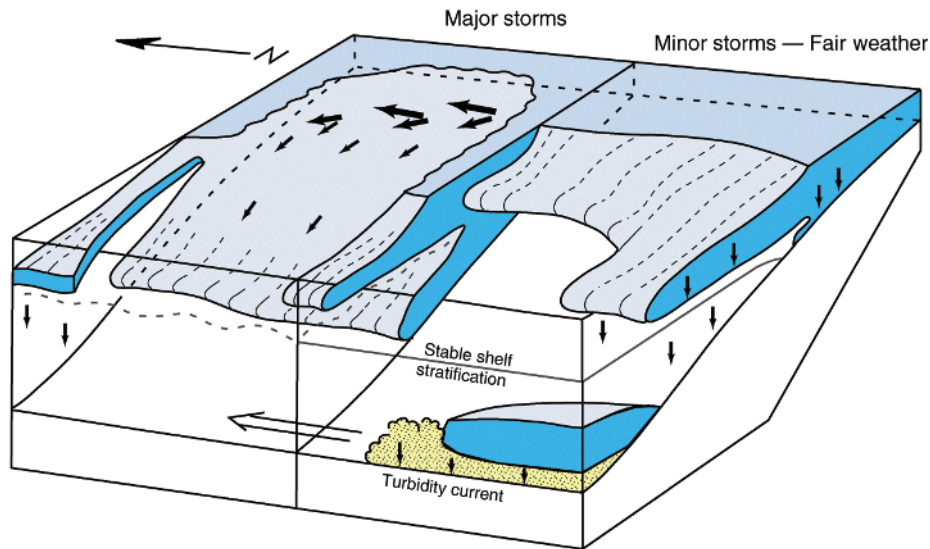

Fig. 1.3 Schematic representation of lutite flows cascading downslope. The increase in length of the arrows indicates an increase in concentration toward the base of the continental slope. The *nepheloid layer* is a part of the water column near continental margins where the suspended sediment concentration is particularly high because persistent currents prevent deposition of fine-grained suspended load. Redrawn from McCave (1972).

Fig. 1.4 Model for hemipelagites (Silurian Bailey Hill Formation) and turbidite sandstones (Brimmon Wood Member) in the Welsh Basin. Suspended silts, fine sands and organics (blue 'tongues') were advected off the shelf by waves and currents (large arrows and smaller downslope-oriented arrows), forming dilute bottom- and mid-water flows. The particulate materials then settled vertically from these flows (short vertical arrows). Annual seasonal layering in the hemipelagites was preserved under anaerobic/dysaerobic conditions. Redrawn from Dimberline and Woodcock (1987).

increased winter discharge of silt into the basin. The assumption of annual cyclicity leads to reasonable sediment accumulation rates of 60–150 cm kyr^{-1} (Dimberline & Woodcock 1987). A general depositional model (Fig. 1.4) involves bottom-hugging and midwater dilute flows advected off the shelf during fair-weather periods (hemipelagic laminated silts/organics, depending on the season), and during storms (silty/sandy graded beds with irregular order of internal structures).

1.2.2   Currents in submarine canyons

Current-meter data have been collected in submarine canyons to depths of over 4000 m (Shepard *et al.* 1979). Generally, the currents alternate directions, flowing up and down canyons with periodicities from 15 min to 24 h. The longest recorded unidirectional flows are five days down-canyon, off the Var River, France (Gennesseaux *et al.* 1971), and three days down-canyon in the Hudson Canyon off New York (Cacchione *et al.* 1978), in both cases with variable speeds.

Progressive vector plots of measured current data from many canyons tend to show a net down-canyon flow, although the results from canyons off the Eastern Seaboard of the United States show approximately equal durations of up- and down-canyon flow (Fig. 1.5). The time periods over which current speeds change vary considerably. The periodicity of most currents approximates to semi-diurnal tidal cycles at depths greater than about 200 m (e.g., Shepard *et al.* 1974). In canyons associated with small tidal ranges, such as off the west coast of Mexico, the length of a canyon-current cycle only approaches the tidal frequency at much greater depths. Shepard *et al.* (1979) summarised the relationship between the average cycle period of the up- and down-canyon alternating flows, the depth where data were recorded along each canyon axis and the local tidal range. In general, small tidal ranges and shallow depths tend to be associated with short average cycles, whereas large tidal ranges and/or deep water tend to be associated with long average cycles.

Although most currents flow up or down canyon, in some cases such as in Hueneme Canyon off the Santa Clara Delta, California, there is a considerable spread of flow directions. Hudson Canyon current data bear little or no relationship to the canyon orientation compared to the good agreement shown for Carmel Canyon off California. Currents that flow at an angle to the 'normal' up- or down-canyon direction are referred to as cross-canyon flows (Shepard & Marshall 1978). Cross-canyon flows are most common in wide canyons, for example in the Kaulakahi Channel off northwest Kauai, although the relatively narrow Hudson Canyon is the site of numerous cross-canyon flows. Strong cross-canyon flows tend to occur at low tide, possibly related to strong wind-driven currents becoming effective at slack low tide. In the Santa Barbara Channel, west of Santa Cruz Island, California, the cross-canyon bottom flows are mainly toward the east, similar to the direction of the surface currents in this area (Shepard & Marshall 1978). The origin of cross-canyon flows is poorly understood. One hypothesis of Shepard *et al.* (1979) is that these currents meander in wide canyons, in a similar manner to the way in which a small subaerial stream meanders in a wide valley.

Data from relatively shallow current-meter stations suggest a correlation between wind speed and the magnitude and direction of currents within canyons (Fig. 1.6). Pressure waves, preceding a storm, may be responsible for at least some, or part, of these current patterns. In other cases, however, there appears to be no correlation; for example, during a storm in La Jolla Canyon with 65 km h^{-1} onshore winds, maximum current speeds increased as wind speeds rose, although the up- and down-canyon periodicity did not vary until finally a large down-canyon surge up to 50 cm s^{-1} was recorded (Shepard & Marshall 1973a, b). Unfortunately, the current-meter was damaged during this surge and therefore any additional increases in speed that may have occurred went unrecorded – the meters were retrieved 0.5 km down-canyon, partially buried by sediments and kelp. Also, during this storm and probably during the current surge, a trough with walls 0.5 m high was excavated into the silty sand of the canyon
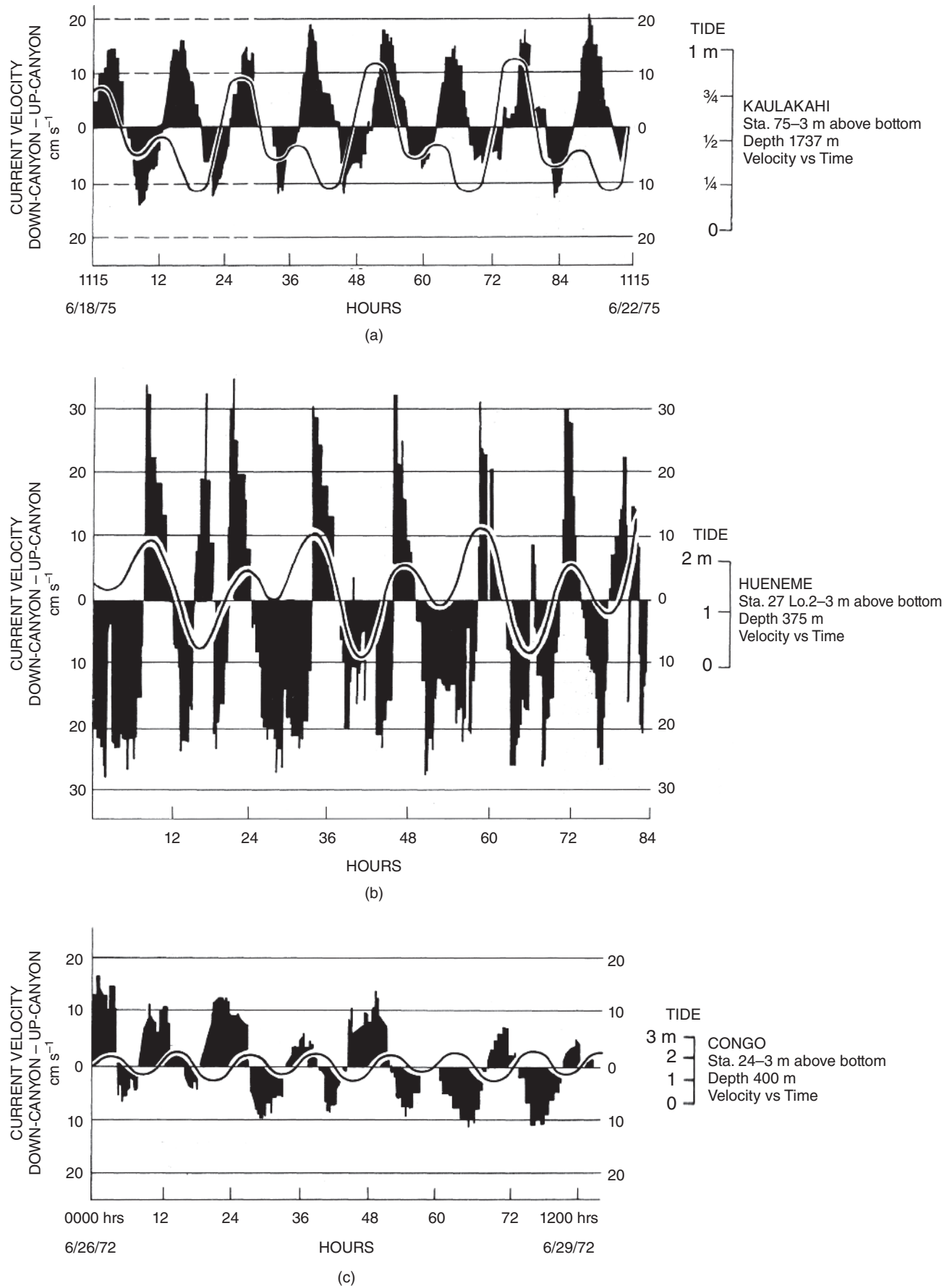
(a)

(b)

(c)

Fig. 1.5   Diagrams to show the periodicity of oscillating up- and down-canyon currents. Tide relationship obtained from the predicted tide at the nearest reference station. (a) Kaulakahi Canyon between Kauai and Niihau islands, Hawaii; (b) Hueneme Canyon, California; (c) Congo Canyon, west Africa. Redrawn from Shepard and Marshall (1978).
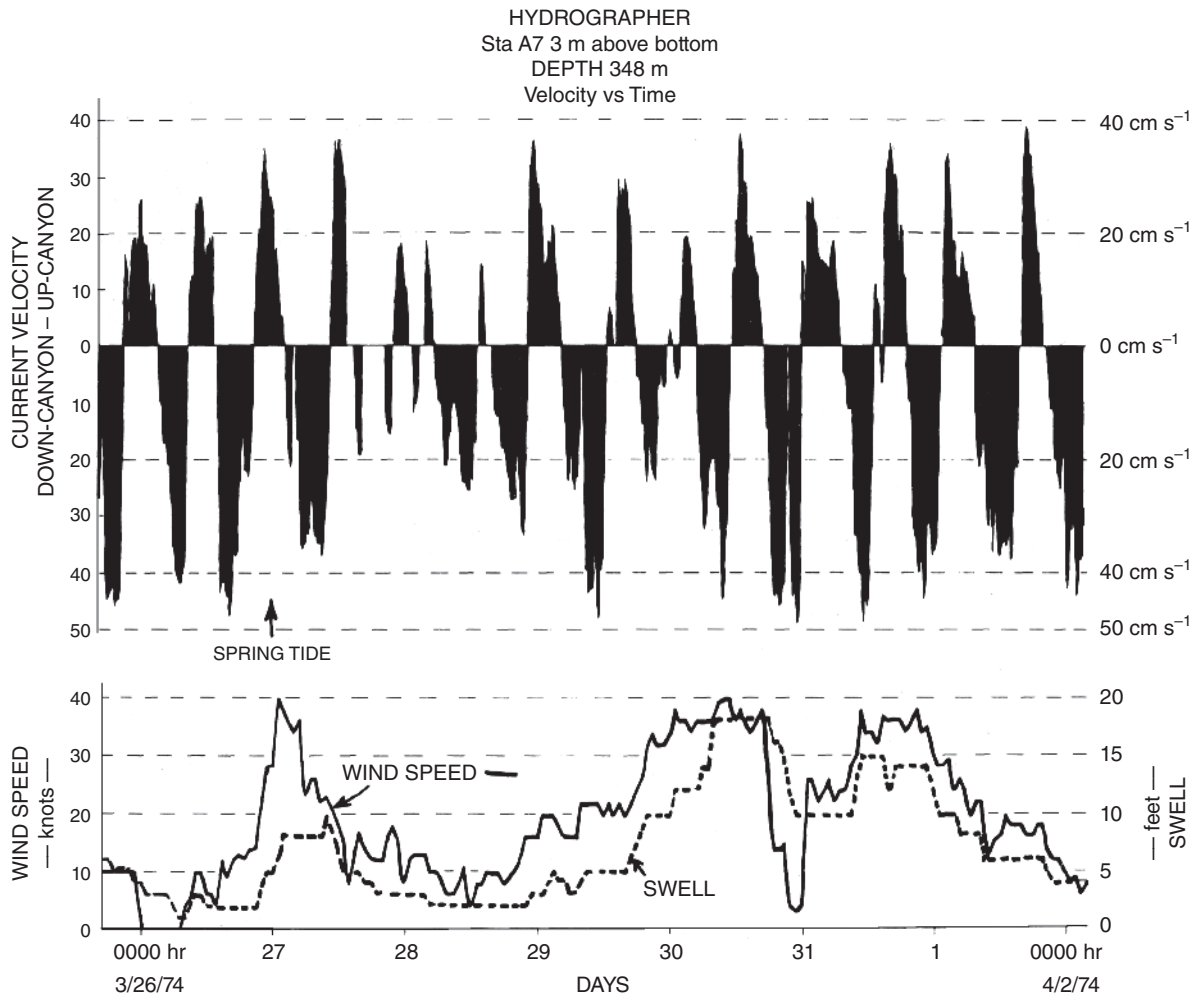
HYDROGRAPHER
Sta A7 3 m above bottom
DEPTH 348 m
Velocity vs Time

Fig. 1.6 Relationship of wind speed and swell height to the magnitude of up- and down-canyon currents during a storm period in Hydrographer Canyon, off Massachusetts. The slowest currents occurred during periods of reduced wind speeds and reduced swell. Redrawn from Shepard and Marshall (1978).

floor. Shepard and Marshall (1973a, b) ascribed the current surge and its associated erosional features to the passage of a storm-generated turbidity current flowing down-canyon. Similar down-canyon currents, with velocities up to 190 cm s^{-1}, have been reported from the head of Scripps Canyon during an onshore storm (Inman *et al.* 1976), and from other canyons (Gennesseaux *et al.* 1971; Reimnitz 1971; Shepard *et al.* 1975).

The measured current velocities are, at times, sufficient to transport sand. Shanmugam (2003) advocates that care be taken in interpreting the origin of tractional structures, such as current-ripple lamination, in canyon deposits, because some of this lamination might have been produced by tidal currents rather than turbidity currents.

The 'ambient' or 'normal' contemporary sedimentation within canyons appears to be mainly the deposition of finer grained suspended matter, presumably entrained by the periodic up- and down-canyon currents (Drake *et al.* 1978). In one recent monitoring study, however, an energetic SGF transported sand and gravel hundreds of metres down Monterey Canyon (Paull *et al.* 2003). The deposit from this event is at least 125 cm of porous sand and gravel, locally with a mud matrix and high water content. While sediment

transport by energetic SGFs appears to be unimportant in canyons at the present time, the ancient record suggests that this was not always the case (Chapter 8). The more energetic events might simply occur with such low frequency that they are rarely recorded in modern studies, or they might be largely restricted to times of lower sea level.

1.2.3 Internal waves

Internal waves form along density interfaces in stratified water masses. The surface of density change may be the temperature-dependent pycnocline or a contact between relatively fresh surface water (e.g., near a river delta) and underlying seawater. In continental-margin settings, the waves are associated with internal astronomical tides (diurnal or semi-diurnal) and are generated near the edge of the shelf (Wright 1995). The wave period depends on the vertical density gradient, and ranges from about 20 min at open-ocean thermoclines to somewhat less than 5 min where a freshwater plume overrides seawater. Amplitudes are of the order of 10 m. Many internal waves are solitons or groups of solitons with particularly large amplitudes and energies.
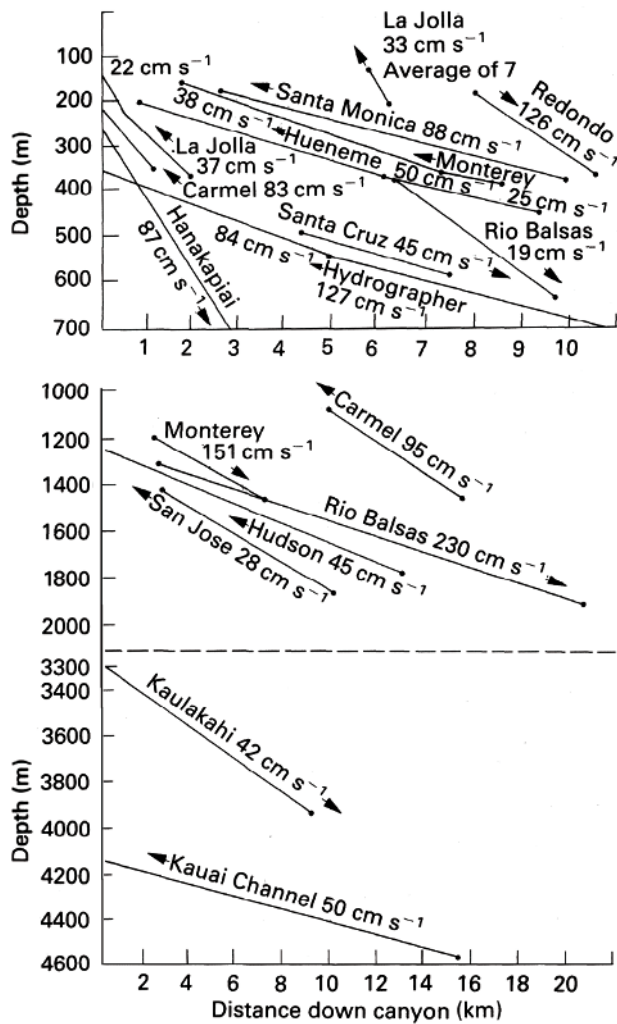
Fig. 1.7 Graphs to show the most likely direction and approximate speed of internal waves up and (less frequently) down the axes of various submarine canyons. The speed of wave advance is approximate because of errors in matching wave crests between current-meter stations, particularly in cases where the current appears to be up-canyon. Redrawn from Shepard and Marshall (1978).

Strong near-bed currents can develop where internal waves shoal as the pycnocline and seabed converge on a sloping shelf (Cacchione & Southard 1974; Wright 1995). The shoaling and breaking of solitons can generate intense turbulence (Kao et al. 1985) capable of suspending sediment that can subsequently move downslope under the influence of gravity. Internal waves are inferred to be active in submarine canyons. Similarities in time–velocity patterns for up- and down-canyon flows, when phase-shifted by the cycle length, point to the likely up-canyon advance of internal waves at depths shallower than 1000 m in many canyons, and at depths from 1000–2000 m in a few canyons (Fig. 1.7; Shepard & Marshall 1978). In other canyons, internal waves advance seaward. Shepard et al. (1979) ascribe the down-canyon advance of internal waves in Santa Cruz, Santa Barbara and Rio Balsas canyons to the introduction of moving water masses into the heads of the canyons.

1.2.4   Sediment slides and mass transport complexes (MTCs)

The downslope component of gravity can cause sediment masses previously deposited on a delta front or on the upper continental slope to move into deeper water, either by increments or during a single episode. Slow downslope movement without slip along a single detachment surface, that is without failure, is referred to as *creep*. No structures in ancient successions have been unambiguously attributed to creep, although features in seismic profiles have been interpreted to have been formed by this mechanism (Hill *et al.* 1982; Mulder & Cochonat 1996). More rapid downslope movements immediately following failure events generate sediment slides (Fig. 1.8) and submarine debris flows. Sediment slides can result in little-deformed to intensely folded, faulted and brecciated masses (Barnes & Lewis 1991) that have translated downslope from the original site of deposition. The head of the slide mass tends to display extensional features, whereas the toe suffers compression, folding and thrusting (Fig. 1.8). If the primary bedding is entirely destroyed by internal mixing, with soft muds and/or water mixed into the slide, then a slide may transform into a cohesive debris flow (Fig. 1.9).

According to the ISSMGE Technical Committee on landslides, submarine mass movements can be divided into slides (translational or rotational), topples, spreads, falls and flows (Locat 2001; *cf.* seismic examples described by Moscardelli *et al.* 2006; Moscardelli & Wood 2007). The various types of mass movements generate a spectrum of deposits which, when intimately associated with one another, are best referred to simply as *mass transport complexes* (MTCs). As defined by Pickering and Corregidor (2005):

> Mass transport complexes include chaotic deposits, typically with visco-plastically deformed rafts of disrupted bedding, cobble-pebble conglomerates, pebbly mudstones, mud-flake breccias, and pebbly sandstones. These deposits represent a range of processes, including slides, slumps, turbidity currents and debris flows.

We recommend that where a single event is believed to be responsible, the term '*mass transport deposit*' (MTD) be used, with MTC being reserved for stacked multiple events – accepting that in many cases such a distinction can prove difficult.

MTCs are common surficial sediments in the modern oceans and in ancient deep-water settings (e.g., Schipp *et al.* 2013; Shanmugam 2015). For example, Embley (1980) claims that 'at least 40% of the continental rise of eastern North America … is covered by a veneer of mass-flow deposits [slides] including debris flows'. On marine slopes, there is probably a complete gradation between coherent slides and thoroughly mixed cohesive debris flows. When sliding occurs, the movement occurs along a sharp or diffuse basal failure surface at some depth below the seafloor (Fig. 1.10). Along this surface, the shear stress produced by the sum of gravitational acceleration and cyclic accelerations due to seismic shocks (Morgenstern 1967) and passing surface waves (Lu *et al.* 1991) or internal waves exceeds the internal shear strength of the sediment. The shear strength depends on a variety of sediment properties like water content, texture, pore pressures and organic content.

Fine-grained sediment has a variety of geotechnical properties (Bennett & Nelson 1983) that are useful indicators of its physical state and that help determine under what conditions the sediment will fail and generate a slide. Conditions that favour initiation of
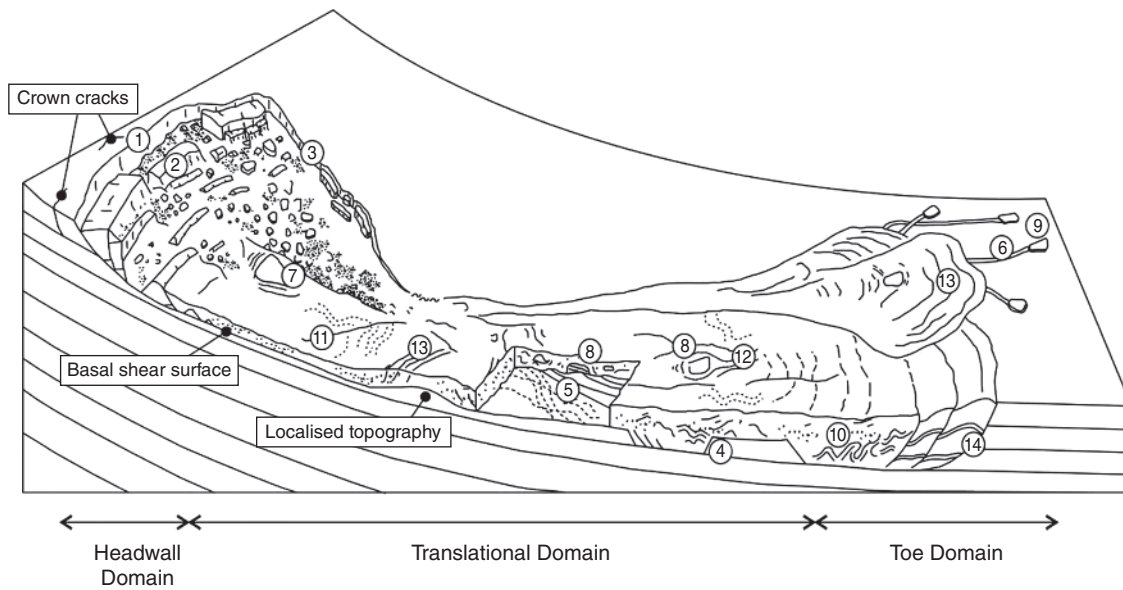
Fig. 1.8 Schematic representation of a sediment slide. Circled numbers show (1) headwall scarp, (2) extensional ridges and blocks, (3) lateral margins, (4) basal shear surface ramps and flats, (5) basal shear surface grooves, (6) basal shear surface striations, (7) remnant blocks, (8) translated blocks, (9) outrunner blocks, (10) folds, (11) longitudinal shears (= first-order flow fabric), (12) second-order flow fabric, (13) pressure ridges, (14) fold and thrust systems. From Bull *et al.* (2009).

slides in muddy terrigenous sediments are a function of (i) bottom slope (Moore 1961), (ii) sedimentation rates (Hein & Gorsline 1981) and (iii) the response of the sediment to cyclic stress produced by earthquake shaking (Morgenstern 1967). Sedimentation rates on basin-margin slopes vary widely, but Hein and Gorsline (1981) conclude that a rate of 30 mg cm^{-2} yr^{-1} must be attained before slope failures become common. For example, in the Santa Barbara Basin, California Borderland, sedimentation rates exceed 50 mg cm^{-2} yr^{-1}, and debris flows are widespread on slopes of <1° (Hein & Gorsline 1981). In many areas, sediment slides preferentially occur on very low slopes (Fig. 1.11), suggesting the involvement of water-rich, rapidly deposited sediments.

The sedimentation rate effectively determines the water content and shear strength, *S*, of the sediment, although shear strength is also a function of other variables such as content of organic matter (Keller 1982), generation of gas in the sediment by decay of organics or by gas-hydrate decomposition (Carpenter 1981), and binding by bacteria and fungi (Meadows *et al.* 1994). According to Keller (1982):

cohesive sediments with greater than about 4–5% organic carbon [have] … (1) unusually high water content, (2) very high liquid and plastic limits, (3) unusually low wet bulk density, (4) high undisturbed shear strength, (5) high sensitivity, (6) high degrees of apparent over consolidation, and (7) high potential for failure [by liquefaction] in situations of excess pore pressure.

The stability of sediments on a sloping bottom has traditionally been analysed using a static infinite slope model (Moore 1961; Morgenstern 1967). Consider a blanket of sediment on an inclined surface. Beneath the seabed, the shear stress increases downward in a linear fashion because of the cumulative weight of sediment. The sedimentary blanket will remain stable as long as the strength of the sediment increases downward at a faster rate than the rate of increase

in the shear stress. Strength is generated by internal friction, electrostatic cohesive forces and organic binding. In many natural situations, persistent high water contents (leading to elevated pore-fluid pressures) and gas evolution because of organic-matter decomposition prevent effective consolidation, and a depth is reached where the shear stress along an inclined bedding surface exceeds resisting forces. Slippage and therefore failure along this bedding surface is then inevitable. Of course the failure surface must, at its downslope end, cross bedding and rise upward to the seabed in order for the translating mass to glide freely into deeper water. Booth *et al.* (1985) developed the concept of a safety factor, *SF*, which is the ratio of resisting forces to shearing forces. For ψ = excess pore-fluid pressure, Z = depth measured vertically below the seabed, $\gamma' = \rho_s \, g'$, ρ_s = sediment density, reduced gravity $g' = g(\rho_s - \rho)/\rho_s$, ρ = density of seawater, g = gravitational acceleration, ϕ = angle of internal friction (a characteristic of the material), and α = slope angle,

$$SF = \left[1 - \frac{\psi}{\gamma' Z \cos^2 \alpha} \right] \left[\frac{\tan \phi}{\tan \alpha} \right] \qquad (1.1)$$

Case studies (Athanasiou-Grivas 1978) show that the probability of failure is low for *SF* >1.3, and that failure is a virtual certainty for *SF* <0.9. Notice that steadily increasing sediment density (because of normal consolidation) increases *SF*, whereas excess pore-fluid pressure has the opposite effect. Booth *et al.* (1985) provide a nomogram to determine *SF* under undrained conditions given sedimentation rate, coefficient of consolidation, sediment thickness, slope angle and angle of internal friction. Excess pore pressure is obtained from consolidation theory (Gibson 1958), under the assumption that these excess pressures are entirely the result of trapping of pore-water in compacting, fine-grained sediment of low permeability.

The infinite slope model can be extended to the case of superimposed ground accelerations due to earthquakes (Morgenstern 1967; Hampton *et al.* 1978). Horizontal peak accelerations, like earthquake
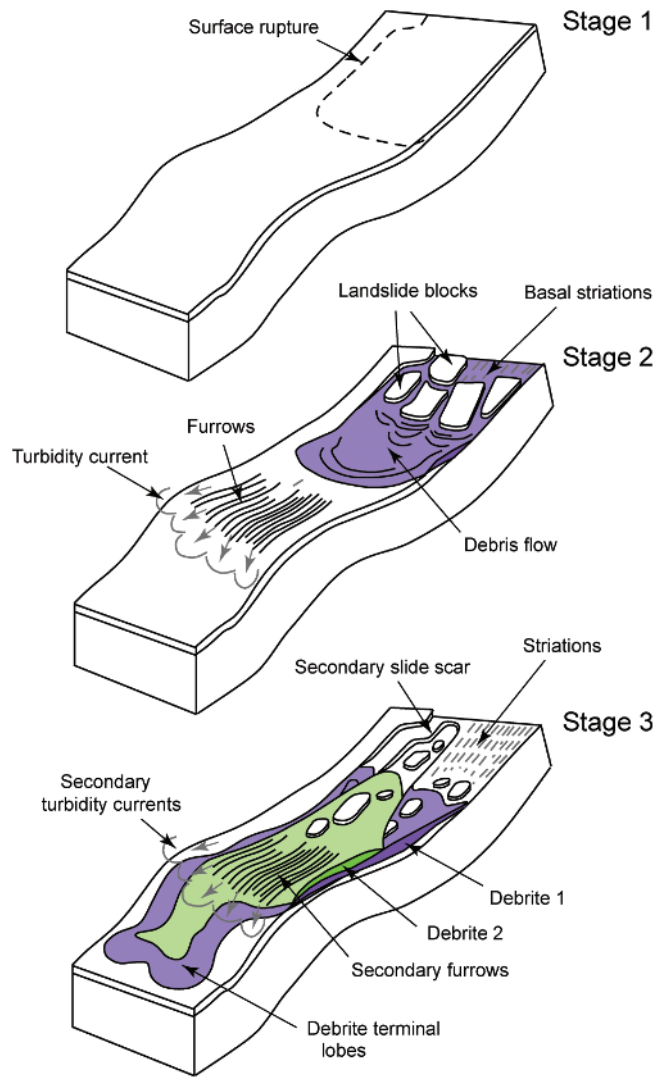
Fig. 1.9 Conceptual model of submarine slide evolution (Gee *et al*. 2006). Stage 1 shows seafloor rupture. Stage 2 shows tabular blocks, basal striations, debris flow and a turbidity current generated in the headwall area. Downslope of the headwall area, turbidity currents erode furrows in the seafloor. Stage 3 shows the development of secondary slide events within the headwall, triggering secondary debris flows and turbidity currents.

intensities, decrease away from the epicentre (Fig. 1.12). An earthquake safety factor, *ESF*, can be expressed as (Booth *et al*. 1985):

$$ESF = \frac{SF\gamma' \tan \alpha}{\gamma a_{\mathrm{X}} + \gamma' \tan \alpha} \tag{1.2}$$

where $\gamma = \rho g$. and $a_{\mathrm{x}} =$ horizontal acceleration coefficient expressed in terms of gravity (e.g., 0.1 g).

Figure 1.13 is taken from Booth *et al*. (1985), and allows estimation of the earthquake-induced horizontal ground acceleration required to reduce *ESF* to 1.0 for a wide range of slopes and safety factors, and a reasonable range of specific weights. The increase in excess pore pressures caused by ground shaking (Egan & Sangrey 1978) must be taken into account in estimating the safety factor. Clearly, 'even small earthquake-induced accelerations are very detrimental to the stability of a submarine slope' (Morgenstern 1967).

1.3   Deep, thermohaline, clear-water currents

Large parts of the deep ocean basins, especially the Atlantic Ocean, are characterised by geostrophic currents moving at mean speeds of 10–30 cm s^{-1} (McCave *et al*. 1980; Hollister & McCave 1984), with short 'gusts' reaching about 70 cm s^{-1} (Richardson *et al*. 1981). Deep circulation in the oceans is the result of thermohaline effects. In the North Atlantic Ocean, for example, dense cold water sinks off the coast of Greenland and in the Norwegian Sea and moves southward as a bottom current (Worthington 1976); in the South Atlantic, ice formation in the Weddell Sea causes an increase in salinity and hence density, the dense seawater sinks and flows northward along the bottom (Stommel & Arons 1961; Pond & Picard 1978: p.134). Other regions of the world's oceans that are characterised by spreading cold bottom water are outlined by Mantyla and Reid (1983). The deep ocean bottom currents are deflected to the right in the northern hemisphere and to the left in the southern hemisphere by the Coriolis effect, with the result that they are banked up against the continental slope and rise on the western sides of ocean basins, effectively flowing parallel to the bathymetric contours. Two examples are the *Western Boundary Undercurrent (WBU)*, which sweeps along the continental rise of eastern North America (Fig. 1.14) at depths of about 2000–3000 m and at peak velocities of about 25–70 cm s^{-1} (Stow & Lovell 1979), and the *Deep Western Boundary Current* (DWBC), which occupies the same region at depths of 4000–5000 m (Richardson *et al*. 1981). The WBU is derived from the Norwegian Sea, whereas the DWBC appears to be formed of Antarctic bottom water (Hogg 1983). These currents carry a dilute suspended load – generally <0.1–0.2 g m^{-3} – that forms the thick bottom *nepheloid* layer (Ewing & Thorndike 1965; Biscaye & Eittreim 1977). Concentrations may briefly reach values much higher, up to at least 12 g m^{-3} (Biscaye *et al*. 1980; Gardner *et al*. 1985). Most of the fine-grained suspended material is winnowed from the seafloor; the rest is probably added to the current by cascades of cold shelf water or lutite flows originating at the edge of the continental shelf (Postma 1969).

The WBU and DWBC are capable of long-distance transport of fine-grained sediments. According to Heezen and Hollister (1971), distinctive red mud derived from the weathering of Carboniferous and Triassic bedrock in the Gulf of St Lawrence area (eastern Canada, 45°N latitude) has been transported at least as far south as the Blake Plateau (30°N), a distance of about 2000 km. On the Newfoundland Rise (Carter & Schafer 1983), the high-velocity core flow of the WBU ($U \leq 35$ cm s^{-1}) intersects the bottom at depths of 2600–2800 m, and is capable of transporting sediment grains, of approximate diameter 0.1 mm, 1–15% of the time. The seabed beneath this core zone is sandy. Finer grains are effectively maintained in suspension as a nepheloid layer up to 800 m thick.

On the continental rise off Nova Scotia, the high-velocity core flow of the DWBC ($U \leq 70$ cm s^{-1}) is at depths of 4500–5000 m (Richardson *et al*. 1981; Bulfinch & Ledbetter 1984). Characteristics and effects of the DWBC were studied in great detail during the multidisciplinary 'High Energy Benthic Boundary Layer Experiment' (HEBBLE; for an excellent summary of findings, see Nowell & Hollister 1985; McCave & Hollister 1985; Hollister & Nowell 1991a,b). The bottom beneath the DWBC consists of coarse silts moulded into longitudinal ripples (Bulfinch & Ledbetter 1984; Swift *et al*. 1985;
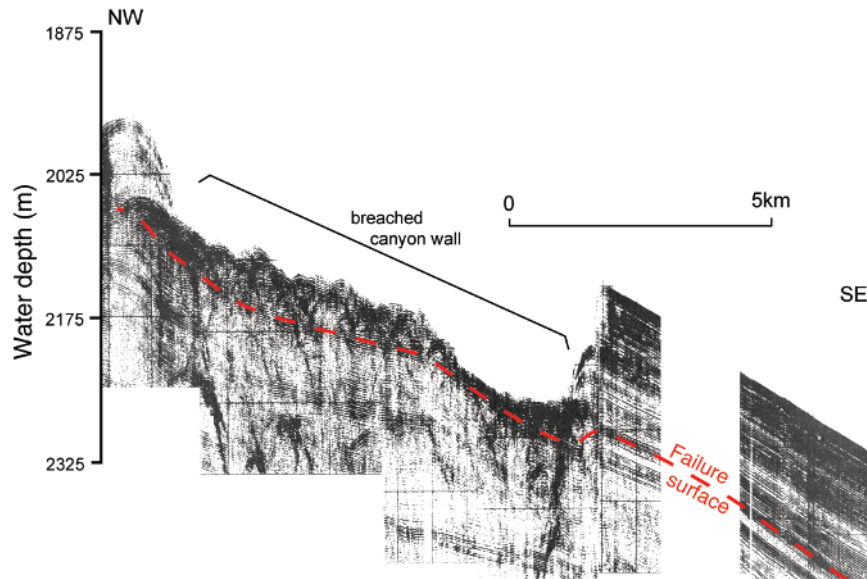
Fig. 1.10 Dip seismic-reflection profile through a failed part of the wall of Munson Canyon, US Atlantic coast. The failure surface is overlain by a chaotic MTC to the left, and is ~150 m below the seabed to the right. The apparent downward step in the failure surface at the edge of the depression is an artifact ('pullup') created by the differing acoustic travel-time in water and sediment. Modified from O'Leary (1993).
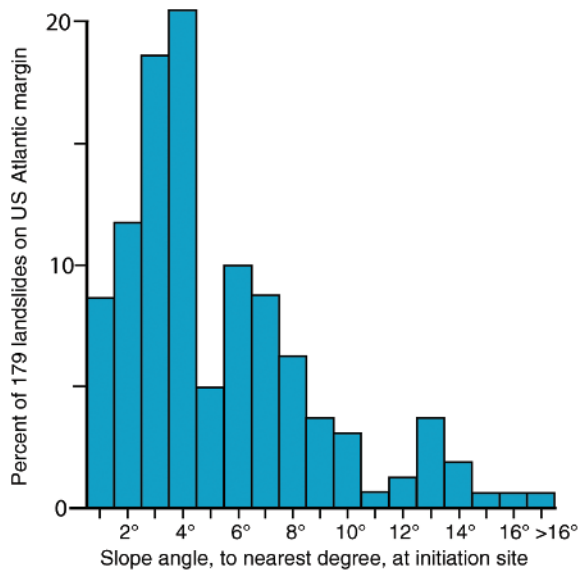

Fig. 1.11 Frequency distribution of submarine slides (MTCs) on the US Atlantic margin as a function of seabed slope at the site of initiation. Redrawn from Booth *et al.* (1993).

Fig. 1.12 Graph of the horizontal-component peak acceleration versus distance from the epicentre of the 1994 Northridge earthquake, California. The green envelope encloses >150 data points plotted by Mueller (1994). The curves represent the average peak acceleration (solid line) and the ±1 standard deviation accelerations (dashed lines) expected for a magnitude 6.7 earthquake. Redrawn from Mueller (1994).

Tucholke *et al.* 1985). The silt size fractions most affected by the core flow span 5–8 ϕ (where $\phi = -\log_2$[size in millimetres]). Net accumulation rates are not high (5.5 cm kyr^{-1}), but instantaneous rates can be, due to alternation of periods of rapid erosion and rapid deposition from a highly concentrated nepheloid layer (Hollister & McCave 1984). Temporal variations in the bottom flow are very complicated, and may involve significant variations in flow speed and reversals of flow direction. Times of strongest and most variable flow are called 'deep-sea storms' by Hollister and McCave (1984). The
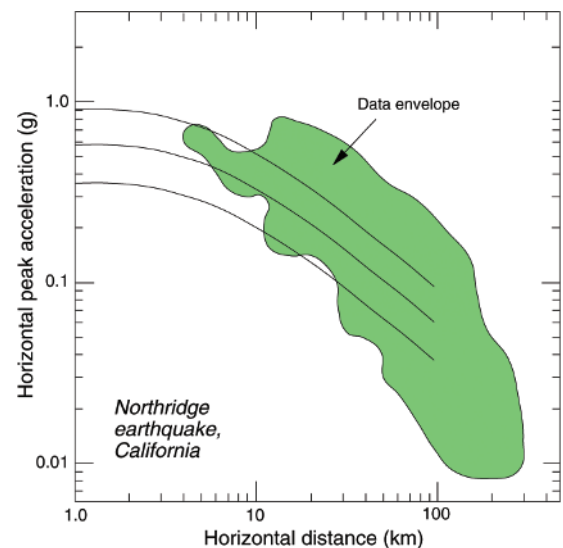
'storms' last from a few days to several weeks, are characterised by current speeds in excess of 20 cm s^{-1} and result in high concentrations of suspended sediment. The 'deep-sea storms' result from an interplay between the deep circulation and wind-driven currents in the surface layer of the ocean created by atmospheric storms passing overhead (Faugères & Mulder 2011). Based on a five-year record in the HEBBLE
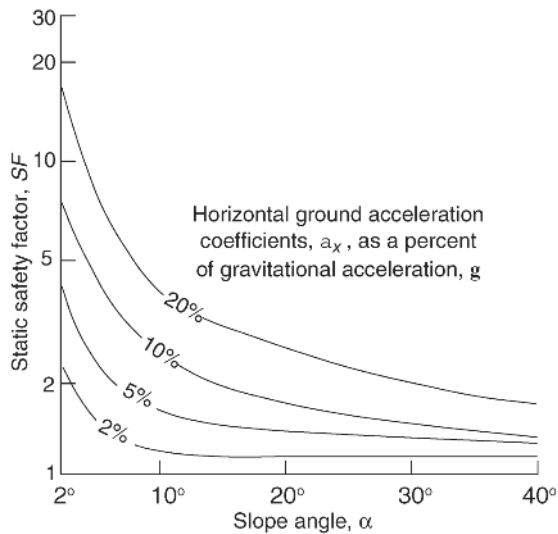
Fig. 1.13 Horizontal ground acceleration, a_x, required to reduce the static safety factor to a value of 1.0 for given slope angles and sediment density in the range 1.5–2.0 g cm^{-1} (simplified from Booth *et al*. (1985). For example, if $SF = 2.0$ and $\alpha = 10°$, ground accelerations of about 0.07 g or greater will reduce safety factor to 1.0 or less, and failure will be likely. On the same slope with $SF = 4.0$, accelerations of at least 0.2 g would be needed to cause failure. Note that SF is itself a function of bottom slope and excess pore pressure (Eq. 1.1).

area off the coast of Nova Scotia, about three such 'storms' occur each year, and occupy about 35% of the time (Hollister & McCave 1984).

Contour current deposits, or *contourites* (Hollister & Heezen 1972), may be treated as two end members: (i) muddy contourites and (ii) sandy contourites (see also Section 6.3). Muddy contourites are fine grained; mainly homogeneous and structureless; thoroughly bioturbated (McCave *et al*. 2002); and only rarely show irregular layering, lamination and lensing. They are poorly sorted silt- and clay-size sediments with up to 15% sand. They range from finer-grained homogeneous mud to coarser-grained mottled silt and mud, and their composition is most commonly mixed biogenic and terrigenous grains. According to Hollister and McCave (1984), short-term depositional rates of mud can be extremely high, about 17 cm yr^{-1}, followed by rapid biological reworking.

Sandy contourites comprise thin irregular layers (<5 cm) that are either structureless and thoroughly bioturbated, or may possess some primary parallel or cross-lamination which may be accentuated by heavy minerals or foraminiferal tests (Bouma & Hollister 1973; Stow & Faugères 2008). Grading may be normal or inverse, and bed contacts may be sharp or gradational. Grain size ranges from coarse silt to, rarely, medium sand, with poor to moderate sorting. The sandy facies is produced by winnowing of fines by stronger flows (Driscoll *et al*. 1985), and physical sedimentary structures only seem to be preserved where the currents are particularly focused and strong, as is the case where Mediterranean water flows out of the Strait of Gibralter into the Gulf of Cadiz (Stow & Faugères 2008), or where tidal or wind-driven currents are forced through constricted straits so that high velocities are maintained to hundreds of metres water depth (Colella & d'Alessandro 1988; Ikehara 1989).
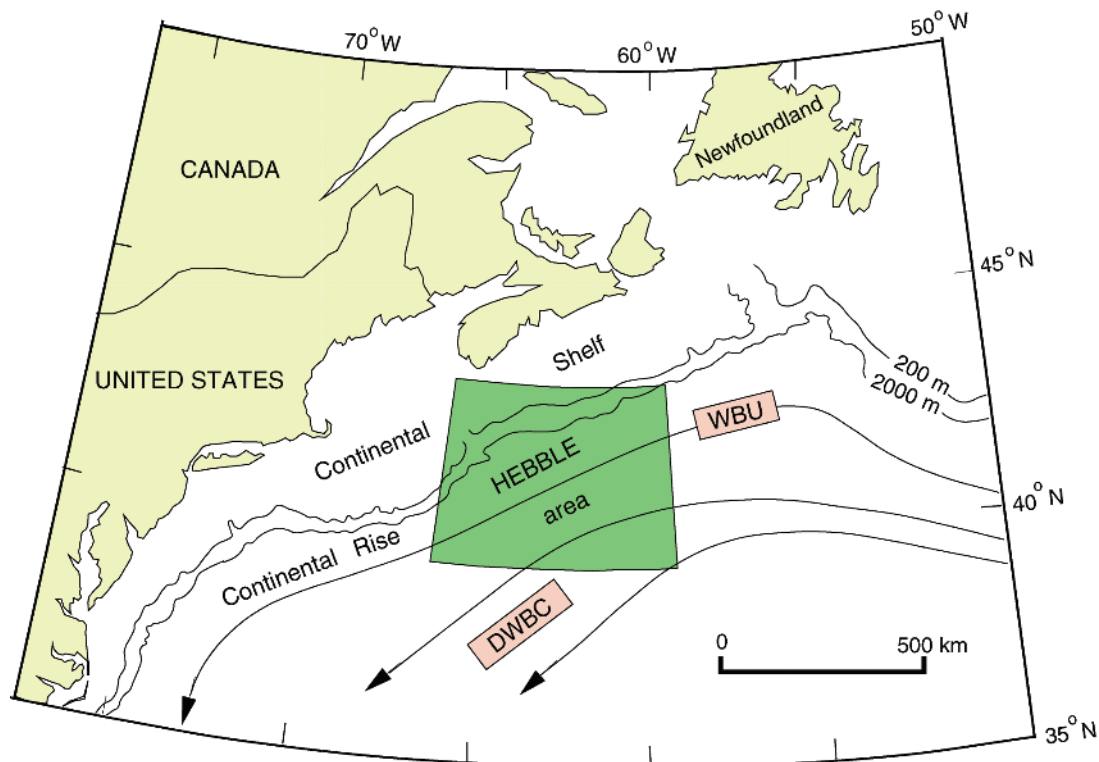

Fig. 1.14 Approximate tracks of Western Boundary Undercurrent (WBU) and Deep Western Boundary Current (DWBC) along the eastern continental margin of North America. The HEBBLE area was the site of detailed long-term measurements of bottom currents, and is an acronym for High Energy Benthic Boundary Layer Experiment. Redrawn from Hollister and McCave (1984).
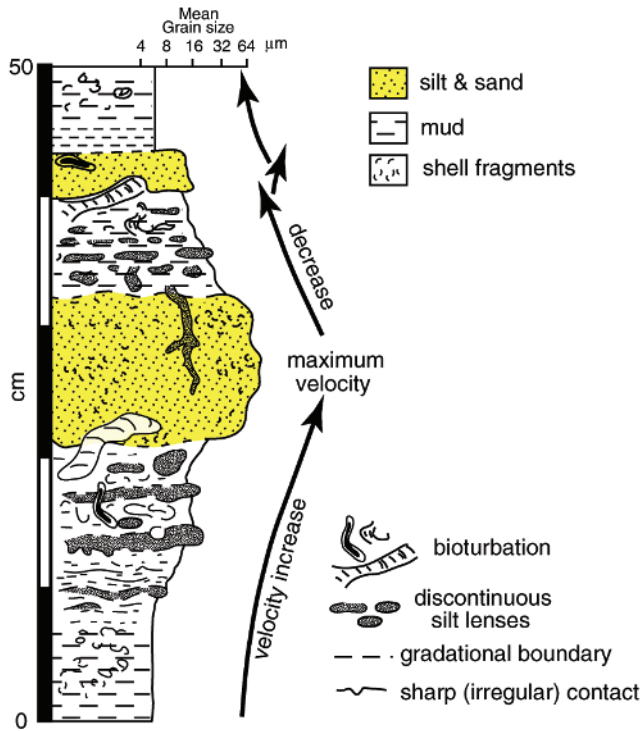
Fig. 1.15 Schematic model showing upward coarsening and fining of contourite facies from the Faro Drift, offshore southern Portugal. Redrawn from Gonthier *et al.* (1984).

Muddy and sandy contourites commonly occur together in upward-coarsening to upward-fining sequences (Faugères *et al.* 1984; Stow & Piper 1984b). A complete sequence shows inverse grading from a fine homogeneous mud, through a mottled silt and mud, to a fine-grained sandy contourite facies, and then normal grading back to a muddy contourite (Fig. 1.15). The changes in grain size, sedimentary structures and composition probably are related to long-term (1–30 kyr) fluctuations in the mean current velocity (Stow

& Piper 1984b). Stow and Faugères (2008) note that the time of maximum velocity (Fig. 1.15) might result in a hiatus and/or erosion if the currents become so strong that no accumulation is possible. In such cases, top cut-out motifs may occur if erosion cuts away the top of the idealised doubly graded profile, or base cut-out motifs may occur above the erosional unconformity.

In particular successions, it may be difficult to distinguish between mud turbidites and muddy contourites (Bouma 1972; Stow 1979). Also, the reworking of sand turbidites can result in bottom-current-modified turbidite sands, believed to be common on continental slopes and rises. In the central parts of ocean basins, bottom currents are known to construct large sediment drifts (Chapter 6) of almost pure biogenic material (McCave *et al.* 1980; Stow & Holbrook 1984). Such biogenic contourites may be indistinguishable from true pelagites.

Since the early 1990s, a number of authors have maintained that rythmically interbedded sands or large and well-sorted sand lenses in oilfields were emplaced, or largely reworked, by bottom currents (Mutti 1992: p. 19; Shanmugam *et al.* 1993a, b, 1995; Shanmugam 2008). Some of the supposed bottom-current deposits are coarse grained. The authors of this book doubt that such sands were deposited or largely reworked by bottom currents, because the required flow velocities and variability would be significantly greater than any known from the modern oceans. Features like sharp-topped ripple lenses and climbing ripple lamination are not diagnostic of bottom-current transport, as some have claimed (Shanmugam *et al.* 1995; Jordan *et al.* 1994; Shanmugam 2008). Sharp-topped ripples can form when turbidity currents bypass a part of the seafloor, perhaps because of flow unsteadiness (e.g., the 'depletive waxing flow' of Kneller 1995). Alternatively, the flow could leave sharp-topped ripples if it were deficient in silt sizes. Climbing ripples always require rapid deposition from suspension during ripple migration (Allen 1971; Jobe *et al.* 2012), consistent with deposition from turbidity currents (Fig. 1.16). The main reason, however, that the authors of this book dismiss the notion that sandy contourite deposits replete with stratification are the norm (Shanmugam 2008), is the meagre evidence for such stratified sands in modern bottom-current deposits because of widespread and thorough bioturbation except in very rare situations (Stow & Faugères 2008). We take the view
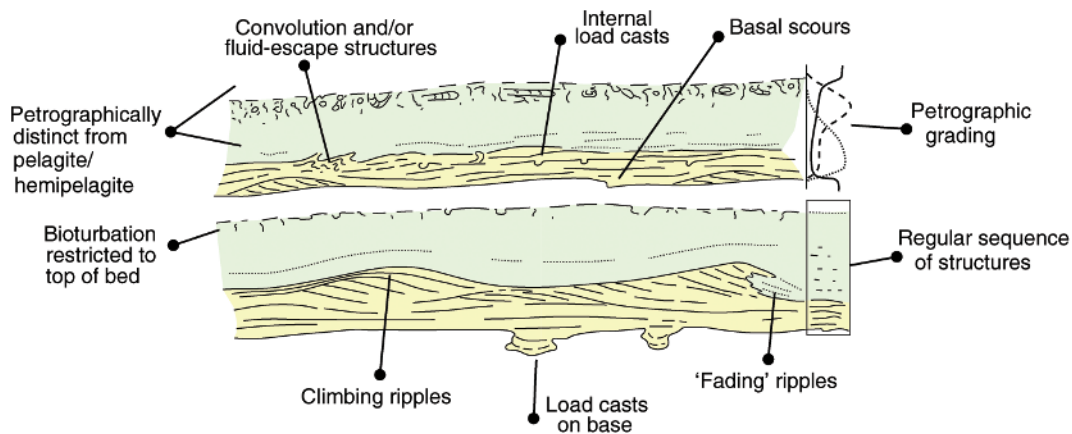

Fig. 1.16 Diagnostic criteria for the recognition of fine-grained turbidites. Rapid deposition from a decelerating SGF produces both wet-sediment deformation structures like load casts, and climbing ripples. Accumulation rates under thermohaline currents are much lower, preventing the development of these types of sedimentary structures. The co-occurrence of several of these structures is sufficient to rule out deposition by clear-water bottom currents (contour currents). Redrawn from Piper and Stow (1991).

that 'actualism' trumps arguments based on the presence of surficial bedforms in areas where bottom currents are active today. Apparently the stratification produced by the migration of these bedforms does not survive into the geological record because of intense sediment disturbance by burrowers under conditions of slow sediment accumulation. See Section 6.5 for additional discussion of this issue.

1.4 Density currents and sediment gravity flows

(1) A density current results when a more dense fluid or mobile plastic material moves beneath a less dense material under the influence of gravity. *Fluids* are materials like water and air that deform continuously when subjected to even the smallest shear stress. *Plastics* resist deformation until a critical level of shear stress is reached, after which they deform continuously unless the shear stress later declines below the critical value.

(2) The density contrast with the ambient fluid might result from compositional differences (e.g., oil flowing beneath water), from temperature differences (e.g., cold air entering a warm room), from the presence of suspended material (e.g., particulate gravity currents), or where there are strong salinity contrasts (e.g., laboratory saline currents and natural saline underflows as in the modern Black Sea – Di Iorio *et al.* 1999; Hiscott *et al.* 2013).

Dilute density currents consisting mainly of water or air are turbulent on even low slopes, unless they are extremely thin.

Natural turbulent density currents are widespread in the oceans and the atmosphere (Simpson 1982, 1997); they occur as powder snow avalanches (Hopfinger 1983), characterise many volcanic eruptions (Cas & Wright 1987), and carry suspended sediment from land areas into lakes and ocean basins. In the laboratory, turbulent density currents have been formed of both suspensions (e.g., Middleton 1966a, b) and saline solutions (e.g., Hallworth *et al.* 1996 – Fig. 1.17; Gladstone *et al.* 2004 – Fig. 1.18).

In sediment gravity flows (SGFs), particles and water move down slopes because the mixtures have a density greater than that of the
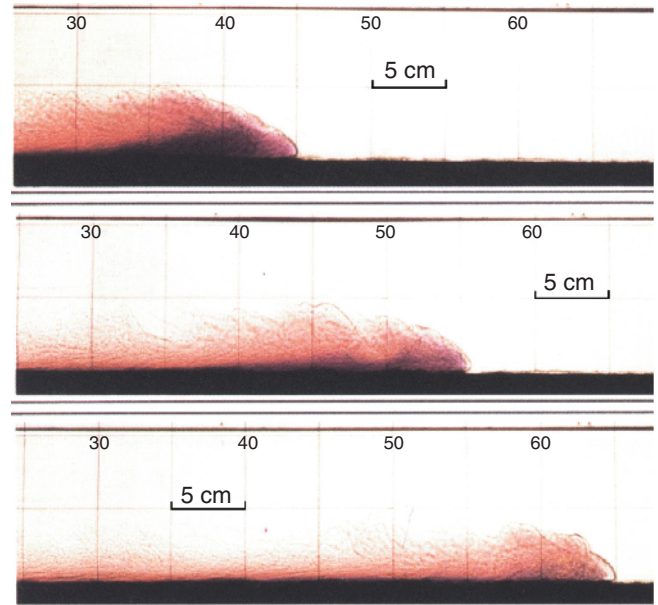

Fig. 1.17 Sequential development of a turbulent density current formed by release of an alkaline saline solution containing a pH indicator into an acidified freshwater ambient environment. The pH indicator stains the saline current purple, changing to red once mixing with the overlying ambient fluid results in a neutral pH. Mixing is strongly developed in the upper part of the flow and in the wake behind the head of the current. There, the visual contrast between red and colourless regions provides a detailed image of the shapes of the turbulent eddies. See Hallworth *et al.* (1996) for details.

ambient fluid, normally seawater. Initially, gravity acts solely on the solid particles in the mixture, inducing downslope flow; the admixed water is a passive partner in this process. Put another way, gravity pulls the grains, and the grains pull the water. If sufficient potential energy is converted into kinetic energy in the evolving flow, then the
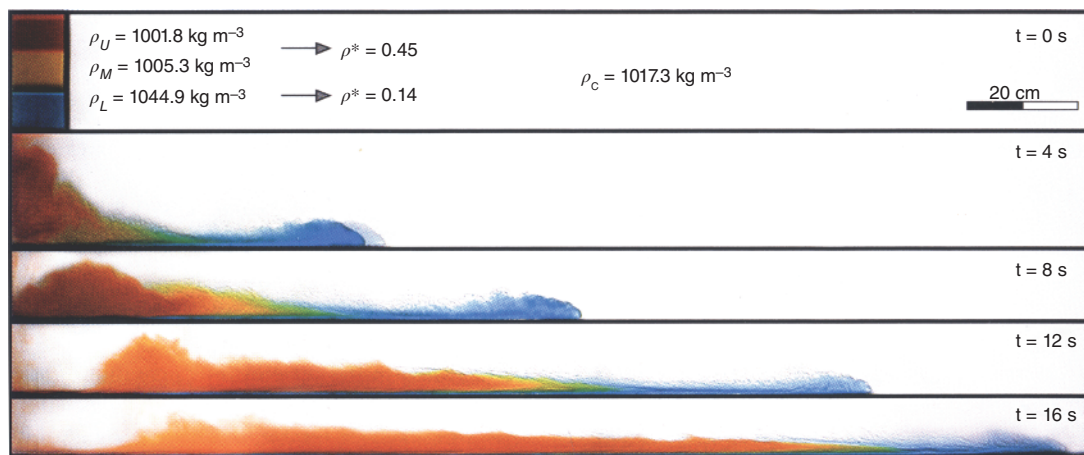

Fig. 1.18 Sequential development of a three-layered saline, turbulent density current in which the lower layer has the greatest density. $\rho* =$ density contrast between layers; $\rho_c =$ average flow density; $t =$ time after flow initiation. The three starting colours (red, yellow, blue) were created by artificial dyes, whereas transitional colours show the extent of fluid mixing during evolution of the flow (e.g., red+yellow = orange; blue+yellow = green). See Gladstone *et al.* (2004) for details.

flow may become turbulent and the eddies in the fluid phase then become fundamental to the maintenance of the suspension. The flow will continue to move if the following conditions are satisfied: (i) the shear stress generated by the downslope gravity component acting on the excess density of the mixture exceeds frictional resistance to flow; and (ii) the grains are inhibited from settling by one of several support mechanisms. Only a few support mechanisms are believed to be responsible for maintaining sediment in suspension on seafloor slopes of a few degrees or less.

(1) *Turbulence* characterises low-viscosity fluids in which inertial forces dominate viscous forces. Turbulence is the superimposition of swirling eddies and seemingly random velocity fluctuations on the average downstream velocity. The upward components of the velocity fluctuations diffuse sedimentary particles into the flow according to their settling velocity, so that the finest particles are evenly distributed throughout the flow, even though they are more dense than the turbulent fluid.

(2) *Buoyancy* is the support provided to an object by a dense surrounding fluid phase. If the surrounding fluid has the same density as the object, then the object has no immersed weight and seems to float aimlessly in the fluid. If the fluid is more dense, then buoyancy is positive and the object floats on its surface (e.g., dry wood floating in water). If the fluid is less dense than the object but more dense than water, then the downward gravitational forces on the object are reduced, and are equivalent to the gravitational forces on a much smaller object in clear water. Buoyancy permits relatively dense sediment–water mixtures like debris flows to carry large clasts even at low velocities.

(3) *Grain collisions and near-collisions* (also called *grain interaction*) transfer some of the downstream momentum of moving particles to an upwardly oriented dispersive pressure (Bagnold 1956) as faster moving grains ricochet off more slowly moving grains beneath them. The moving mass of grains dilates (expands), thus increasing the vertical spacing between the particles and reducing grain-to-grain friction. This support mechanism only operates at high particle concentrations and cannot alone maintain a SGF on low slopes.

(4) *Excess pore pressure* and *pore-fluid escape* result when a dispersion of grains settles too quickly to allow the interstitial pore-fluid to escape upwards. Instead, low permeability impedes the upward flow of escaping pore-water, causing fluid pressures in the pore spaces to significantly exceed the expected hydrostatic pressure. This excess pore pressure keeps the grains separated (as if separated by an inflated pillow) so that friction is reduced and the grains can continue to move relative to one another. In local areas, the pressured pore-fluid can escape rapidly along preferred channel-ways, potentially elutriating fine matrix material and forming porous fluid-escape pillars.

(5) *Matrix strength* is a property of concentrated mixtures of fine-grained or poorly sorted sediment and water. Small shear stresses do not cause such mixtures to flow because internal deformation is resisted by friction between adjacent grains (*frictional strength*) and electrostatic attraction between clay and silt particles (*cohesive strength*). This is different to the behaviour of Newtonian fluids, where the applied shear stress 'τ', is proportional to the fluid viscosity 'μ' x velocity gradient 'du/dy'. An example is water, which deforms (i.e., flows) no matter how small the applied shear stress. For materials with matrix strength, some critical shear stress must be applied before they will move – likewise, these materials will cease to move even on low slopes if the downslope component of gravity is not sufficient to generate the required shear stress along the basal surface of the flow. Once a material of this type is moving, matrix strength is believed to play a roll in reducing the tendency for large clasts to settle, because in order to do so they have to push cohesive and/or granular material out of the way, and overcome a certain amount of residual frictional and cohesive strength.

The relative importance of the various support mechanisms in the principal sediment gravity flows is summarised in Figure 1.19. The names of the flows in this figure are explained in Section 1.4.1 but for the moment it is probably sufficient to know that concentration increases to the right, from turbidity currents to cohesive flows.

A variety of late-stage depositional processes can leave their imprint on a deposit. Many of these depositional processes are not unique to a particular transport mechanism. For this reason, a clear distinction must be made between long-distance transport agents and local depositional mechanisms in explaining the origin of various deep-sea deposits. For example, Middleton and Hampton (1973, 1976) recognised grain-flow deposits as an end-member facies in the spectrum of SGF deposits. *Grain flows* derive their particle support entirely from the dilation induced by grain collisions and near collisions (Bagnold 1956). A familiar example of grain flow is the avalanching of sand down the front of a dune. However, pure grain flows cannot move on the gentle slopes that characterise ocean-basin margins, and instead require slopes of more than ~13° (Straub 2001). Because of this minimum slope requirement, many beds that have in the literature been referred to as 'grain-flow deposits' must instead have been deposited from decelerating *concentrated density flows* or *inflated sandflows* (Section 1.4.1) which can travel on slopes <1–2°. In concentrated density flows, turbulent suspension provides the long-distance particle support, but during rapid deceleration and grain settling, turbulence is increasingly replaced near the base of the flow by grain interaction effects resulting from particle collisions and near collisions above a bed under shear (Bagnold 1956; Rees 1968). Hence, the final deposit mainly or entirely records the effects of grain collisions and elevated particle concentrations (Fig. 1.19), leading to poor organisation, possible inverse-to-normal grading, and possible poorly developed lamination. This is in spite of the fact that long-distance transport might have been provided by a large turbulent flow. In inflated sandflows, a high concentration of clasts ranging in size from coarse silt to gravel guarantees that grain interaction effects are strongly recorded in the deposits (Fig. 1.19).

1.4.1 Classification

There has been a recent dramatic improvement in the understanding of characteristics and behaviour of SGFs (e.g., Talling *et al.* 2012). This has resulted from (i) improved hindcast analysis of recent SGFs in the oceans (a method for testing a mathematical model, where known or estimated inputs for past events are input into the model to see how well the output matches the known result); (ii) a post-1995 revitalisation of research into the flow dynamics and depositional mechanisms of such currents and (iii) completion of a number of relevant experiments on concentrated flows. New classifications of flow processes have resulted, with an interesting cross-fertilisation between those who study deep-marine SGFs and those who study the dispersal of volcaniclastic materials (e.g., Pierson & Costa 1987; Gladstone *et al.* 2004).
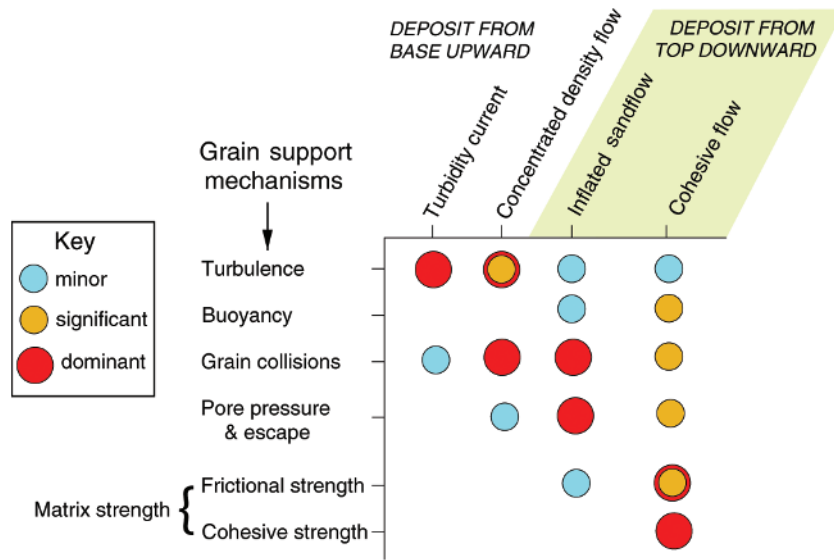
Fig. 1.19   Relative importance of particle-support mechanisms for the four varieties of SGF recognised in this book, and defined in Section 1.4.1. Where orange and red symbols are superimposed, the support varies from significant to dominant. See also Figure 1.22.

The most widely accepted approach to classification has been to attempt, even though difficult, to infer the likely dominant transport mechanism for the entire flow event from both the deposits and theory (Middleton & Hampton 1973; Lowe 1982; Middleton 1993; Hiscott *et al.* 1997a; Mulder & Alexander 2001; Talling *et al.* 2012). This approach has been challenged by G. Shanmugam and colleagues in numerous publications (Shanmugam 1996, 1997, 2000, 2002, 2003; Shanmugam & Moiola 1995; Shanmugam *et al.* 1994, 1995, 1997) who prefer to use different names for component parts of a single decelerating flow (e.g., the upper part is a turbidity current and the lower part a sandy debris flow) based on changing characteristics of the deposits (e.g., normally graded versus ungraded sand in a single event deposit). G. Shanmugam and colleagues advocate that nearly all traction-generated lamination (e.g., planar lamination, ripple lamination, climbing-ripple lamination) is formed by bottom currents, not SGFs. In addition, they insist that 'process terms [should] refer only to depositional mechanisms, not transport mechanisms' (Shanmugam 2000: p. 302). If pushed to the extreme, this approach might lead to the classification of all avalanche-generated foresets on current ripples and dunes as the deposits of grain flows! This is not our preferred approach. Instead, we seek to interpret long-distance transport processes and processes operating during the final stages of deposition from experimental datasets and inferences based on field examples of deep-water deposits.

Many of the classification pitfalls identified by G. Shanmugam and colleagues result from the fact that most large, natural, non-cohesive SGFs are vertically stratified in terms of their properties, so that the near-bed conditions are considerably different to conditions in the main part of the flow. Also, the final deposit is commonly much thinner than the full flow thickness, so that the imprint left by the near-bed processes is enhanced (Fig. 1.20). We see no merit, however, in mentally slicing such flows into separate components, and in assigning different names to these component parts of what is actually a single SGF. Instead, if a single SGF has a spectrum of support mechanisms from top to base, or from front to back, then in this book we will explicitly deal with this as a stratified or hybrid flow, not two or more different flows. As a cautionary note, however,
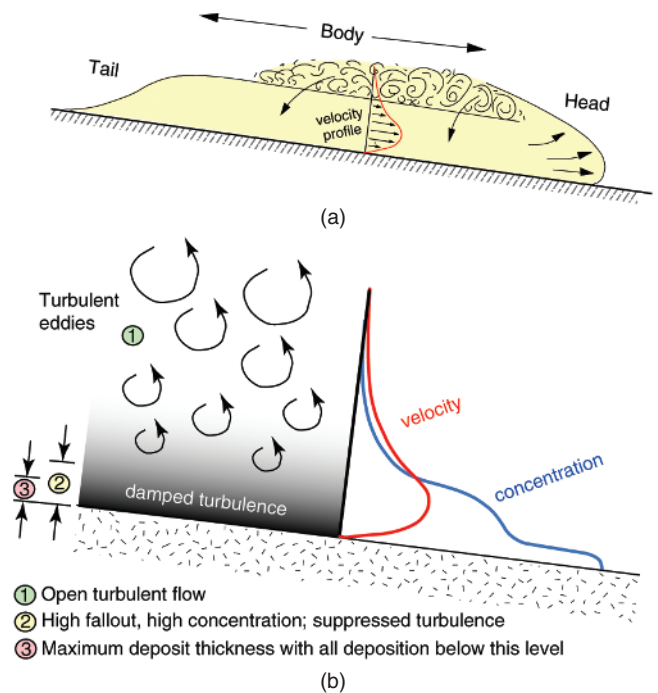

Fig. 1.20   (a) Simplified depiction of a turbidity current or concentrated density flow divided into head, body and tail regions. (b) Conceptual view of the vertical stratification of velocity and concentration expected in the body of such a flow. Rapid particle fallout during deposition can increase the near-bed concentration to the point that turbulence is damped, grain collisions become common, and deposits become poorly organised. The eventual deposit is much thinner than the flow that created it.
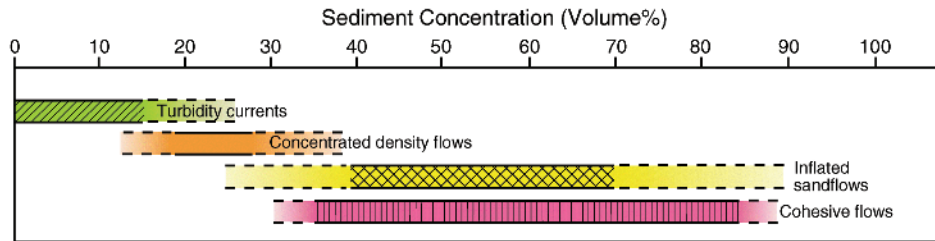
Fig. 1.21 Approximate solids concentrations typical of SGFs, modified from Mulder and Alexander (2001). Dashed lines show the possible extensions of sediment concentrations to lower and higher values than those deemed to be typical. Note the overlaps between different flow types, which result from the effects of flow stratification and different textures of the sediment load.
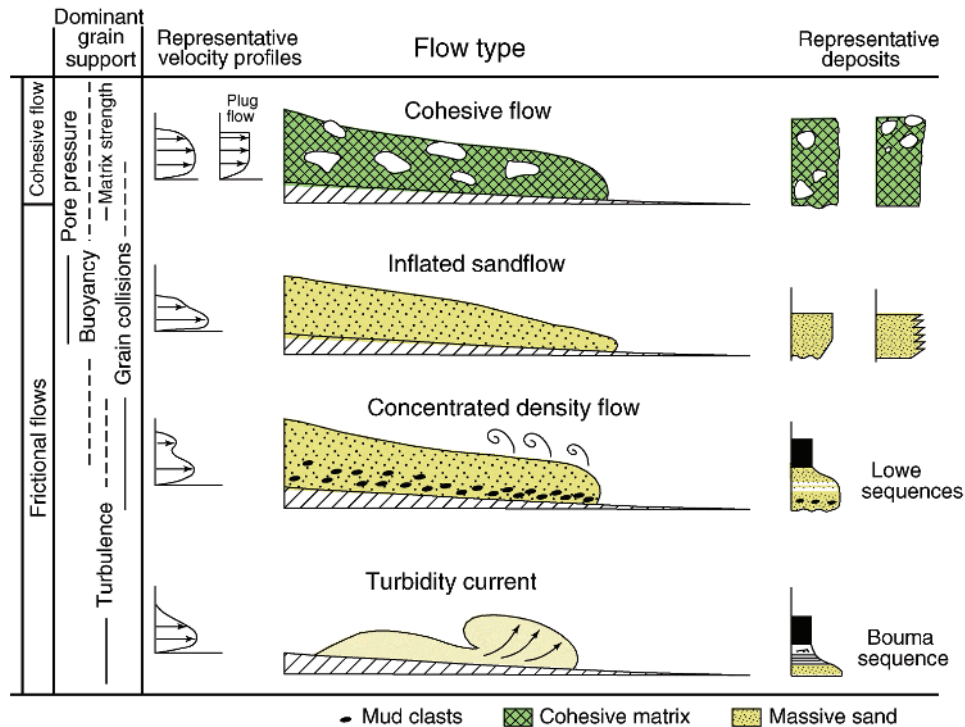

Fig. 1.22 Summary of flow characteristics, typical deposits, and grain-support mechanisms for cohesive and frictional (non-cohesive) SGFs, modified from Mulder and Alexander (2001).

G. Shanmugam is correct in his view that there is a formidable challenge in correctly interpreting the long-distance transport mechanism of many deep-marine sandy and gravelly deposits, because of the strong imprint of late-stage depositional effects.

We have elected to use an existing classification as the foundation for this and subsequent chapters, with some modification of terminology. The classification of Mulder and Alexander (2001) is based on sound theoretical understanding of flow rheology, supported by diverse research results from natural settings. The essence of this classification is outlined below. The reader is directed to the original paper for more extensive background and explanation.

SGFs are subdivided according to their rheological behaviour into predominantly *cohesive flows* and *frictional flows* (the latter called 'granular flows' by some researchers). Approximate ranges for the volume concentrations of solids are shown in Figure 1.21. Cohesive flows have matrix strength resulting from electrostatic attraction between fine particles in the mud fraction. They are differentiated

from all the other flows discussed in this section because they have a pseudoplastic rheology and, hence, do not tend to become diluted by either particle loss (via deposition) or entrainment of ambient water. In effect, cohesive flows tend to 'hold together'. In contrast, frictional (non-cohesive) flows are made up of discrete particles dispersed in water. The behaviour of frictional flows is related directly to the relative proportion of grains and water. In general, frictional flows are characterised by selective deposition, and cohesive flows by en masse deposition.

We recognise four types of sediment gravity flow: *cohesive flows*, *inflated sandflows*, *concentrated density flows* and *turbidity currents* (Fig. 1.22). The last three are frictional flows. Cohesive flows can be further subdivided into *debris flows* and *mudflows*. The solid fraction in mudflows consists of <5% gravel by volume and mud : sand >1 : 1. Mudflows transport little or no coarse sediment except for isolated large blocks. Debris flows consist of more poorly sorted sediment (>5% gravel with a variable sand proportion) and may transport

Table 1.1   Published names for SGFs compared to the classification used in this book. Two names set in bold are used by Mulder and Alexander (2001) but are not used in this book

This book	Approximately equivalent terms
(Cohesive) debris flow & mudflow	Debris flow & mudflow
Inflated sandflow	Liquefied flow (Middleton & Hampton 1976)
	Density-modified grain flow (Lowe 1976a)
	Cohesionless debris flow (Postma 1986)
	Sandflow (Nemec *et al*. 1988; Nemec 1990)
	Sandy debris flow (Shanmugam 1996)
	Hyperconcentrated density flow (Mulder & Alexander 2001)
Concentrated density flow	High-concentration turbidity current (Lowe 1982)
Turbidity current	Low-concentration turbidity current (Middleton & Hampton 1973)
	Turbidity flow (Mulder & Alexander 2001)

boulder-sized clasts of soft sediment or rock and very large rafts or olistoliths. In cases of very coarse-grained material and so little mud that cohesion is insignificant, the alternative terms *inflated sand/gravel flows*, or *inflated gravel flows* can be used.

The four flow types recognised here replace a number of other terms that Mulder and Alexander (2001) argue do not correctly accord with the physical behaviour of natural flows. Approximately equivalent terms are listed in Table 1.1. We also show the terms of Mulder and Alexander (2001) that appear in their original classification but that we have replaced in this book. For example, we have avoided their use of the term 'hyperconcentrated' because of its potentially ambiguous meaning (see below). We support the suggestion of Shanmugam (2000) that the general term 'sediment gravity flow' should be used whenever the transport and depositional processes are unconstrained.

We have elected to replace two of the names proposed by Mulder and Alexander (2001), but otherwise retain the essence of their classification. Other authors (including Mulder & Alexander 2001) use the term 'turbidity flow', but we avoid this for essentially the same reason that we would not refer to a debris flow as a 'debris current'. The terms 'turbidity current' and 'debris flow' have clear precedence in literature extending back to the early part of the twentieth century. We also avoid the name 'hyperconcentrated density flow' (Mulder & Alexander 2001) because the name 'hyperconcentrated flow' has been used in variable ways to describe the more fluid pulses of stream flow associated with certain volcanic debris-flow events (Beverage & Culbertson 1964; Pierson & Costa 1987). To avoid confusion with this type of stream flow, we instead use the term 'inflated sandflow' (with variants of 'inflated sand/gravel flow' and 'inflated gravel flow'). This term builds on the use of the term 'sandflow' by Stanley *et al*. (1978), Nemec *et al*. (1988) and Nemec (1990) for laminar sand-laden flows characterised by strong grain interactions and liquefaction. The adjective 'inflated' is used because the term 'sandflow' alone invites confusion with the rather precisely defined process called 'grain flow' (Bagnold 1956), in which particles are mostly in collisional contact (or near contact) with one another, as is the case when grains avalanche down the face of a dune. Unlike grain flow, the process envisaged by Mulder and Alexander (2001), Nemec *et al*. (1988) and the authors of this book involves particles which are more dispersed than in a grain flow, kept apart by both grain collisions and elevated pore-fluid pressures and capable of moving on very low slopes.

In describing processes and deposits in this chapter, we have incorporated observations from the literature using the equivalencies provided above (plus others outlined by Mulder & Alexander 2001). Original authors might not support the licence we have taken with their work, but otherwise the chapter (and reader) would be burdened by an unworkable number of overlapping and different terminologies. In a textbook, rather than review article, we are comfortable with ensuring consistent and simple terminology for the reader.

All four flow types recognised in this chapter are capable of long-distance transport of particulate sediments into the deep sea on relatively gentle slopes (<5°). Cohesive-flow deposits and inferred inflated sandflow deposits are common on slopes less than 1° (Prior & Coleman 1982; Damuth & Flood 1984; Simm & Kidd 1984; Thornton 1984; Nelson *et al*. 1992; Aksu & Hiscott 1992; Masson *et al*. 1993; Schwab *et al*. 1996); the flows are capable of travelling for hundreds of kilometres from upper continental slopes to abyssal plains (Embley 1980). Turbidity currents can flow long distances on flat basin floors or even upslope (Komar 1977; Elmore *et al*. 1979; Hiscott & Pickering 1984; Pickering & Hiscott 1985; Underwood & Norville 1986; Lucchi & Camerlenghi 1993). For example, Pleistocene turbidity currents carried distinctive coal fragments at least 1800 km from the eastern Canadian continental margin to the Sohm Abyssal Plain (Hacquebard *et al*. 1981), and Chough and Hesse (1976) suggest that turbidity currents flow for 4000 km in the Northwest Atlantic Mid-Ocean Channel. Concentrated density currents travel onto the middle parts of even large submarine fans where the gradients are extremely low (Pirmez *et al*. 1997).

Mulder and Alexander (2001) carefully distinguish between dominant particle support mechanisms and depositional mechanisms (Fig. 1.23). The utility of this distinction can be demonstrated with reference to the contentious issue of the origin of so-called 'massive sands' (Stow & Johansson 2000). In the case of inflated sandflow deposits, en masse deposition by frictional 'freezing' leads to a chaotic grain fabric (Hiscott & Middleton 1980), whereas macroscopically similar, unstratified deposits of concentrated density flows have a strong *a*-axis fabric with a high imbrication angle throughout much of the deposit (Hiscott & Middleton 1980). This results because concentrated density flows deposit their load from suspension, and the strong shear near the aggrading bed strongly aligns the particles. Similarly, structureless T_a divisions of turbidity-current deposits can form whenever the suspension fallout rate is too high to allow sufficient grain traction to form lamination (Lowe 1988; Arnott & Hand 1989; Allen 1991; Hiscott *et al*. 1997a), but the grain fabric of such deposits is characteristically well organised with *a*-axes of elongate grains parallel to flow and imbricated upflow ~10–15°. As advocated by Hiscott *et al*. (1997a), careful grain-fabric studies can be a powerful aid in distinguishing the transport mechanisms for structureless (also referred to as 'massive') sands.
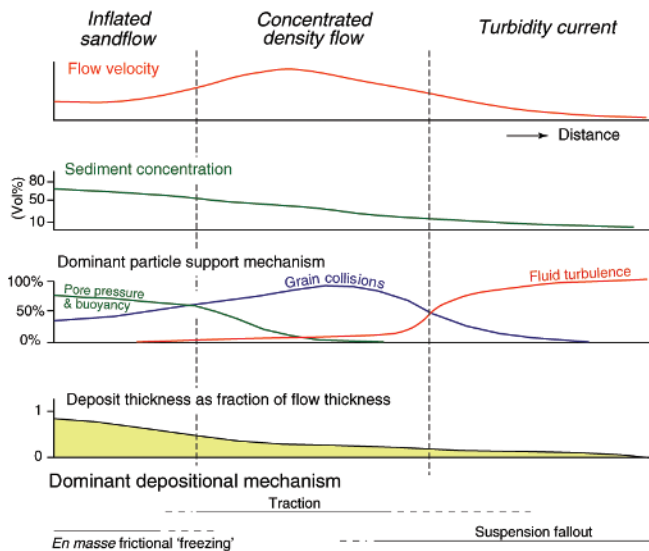
Fig. 1.23 The gradual transition in grain-support mechanisms between inflated sandflows, concentrated density currents and turbidity currents. Cross-overs in the relative importance of these mechanisms are used to define these SGFs. As is the case for cohesive flows, the thickness of the deposit of an inflated sandflow is similar to the thickness of the flow itself. Turbidites, in contrast, are much thinner than the associated turbidity current. Modified from Mulder and Alexander (2001).

1.4.2 Transformations between flow types

It has been proposed that density currents might become stratified, with discontinuities in concentration (Fig. 1.24), or might change their character dramatically while moving downslope as a result of *flow transformations*. Four varieties of flow transformation are recognised:

(1) As defined by Fisher (1983), *body transformations* involve down-current changes between turbulent and laminar flow, or between a coherent slide and a debris flow as seawater is incorporated (e.g., as interpreted for ancient examples by McCave & Jones 1988; Jones *et al.* 1992; Talling *et al.* 2004; Pickering & Corregidor 2005; Strachan 2008; Haughton *et al.* 2009; Talling *et al.* 2010).

(2) *Gravity transformations* involve gravitational segregation into a lower, laminar, highly concentrated part and an upper, turbulent, less concentrated part (e.g., as studied experimentally by Postma *et al.* 1988).

(3) *Surface transformations* occur where the front or top of a highly concentrated flow is eroded by shear beneath the overlying ambient fluid, creating a more dilute, turbulent daughter current (e.g., as described from experiments by Hampton 1972 and Talling *et al.* 2002, and inferred for an ancient deposit by Strachan 2008).

(4) *Fluidisation transformations* occur mainly above highly concentrated pyroclastic flows as a dilute cloud of elutriated material forms a secondary, less concentrated, and turbulent flow (elutriation = the upward flushing out of fine particles by escaping fluids).

The stratified flows produced by gravity, surface and fluidisation transformations might deposit composite beds with abrupt grain-size or textural breaks (Gladstone & Sparks 2002; Talling *et al.* 2004; Pickering & Corregidor 2005; Amy & Talling 2006; Strachan 2008; Haughton *et al.* 2009; Talling *et al.* 2010; Fig. 1.25), or the two parts of the flow might ultimately take different paths or travel different distances, thus forming spatially separate deposits.

It is very difficult in ancient deposits to determine whether a composite bed formed by a flow transformation, or whether there might have been two (or more) separate flows that contributed to what seems to be a single deposit. Amy and Talling (2006) discuss this dilemma in relation to intimately interbedded turbidites and debrites in the Apennines, with the debrites having much more limited extent than the possibly co-genetic turbidites (Fig. 1.26). Haughton *et al.*
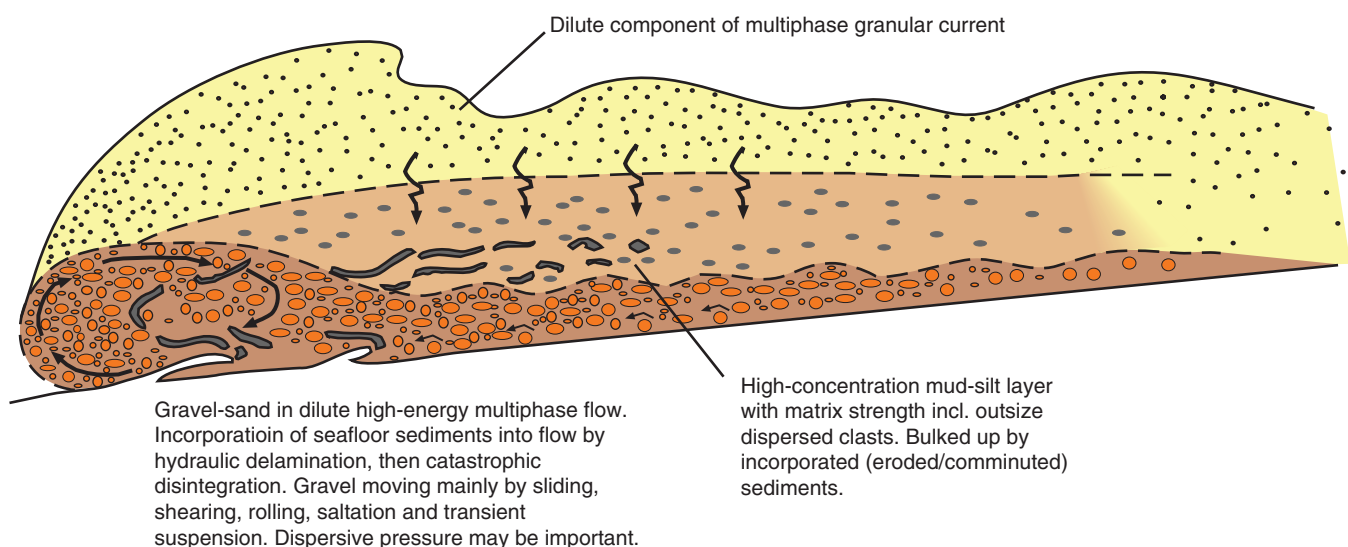

Fig. 1.24 Multiphase hybrid SGF proposed by Pickering and Corregidor (2005) to explain certain disorganised beds in the Ainsa Basin, southern Pyrenees.
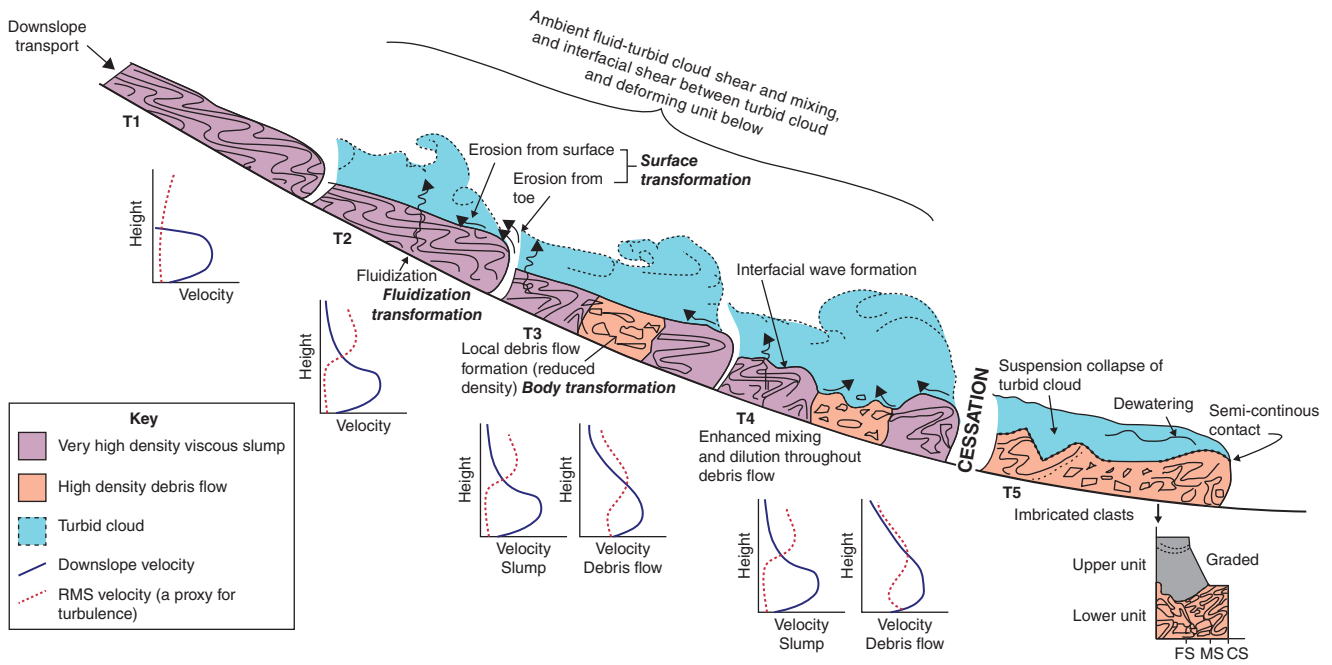
Fig. 1.25 Schematic drawing of the Little Manly Slump flow transformation model from Strachan (2008). T1 to T4 represent progressive development of transformation with time. Vertical velocity profiles for T1 to T4 are indicated and, where two are present, indicate the differences between slump and debris flow vertical velocity profiles. T5 shows deposition of units following slump cessation, together with a log showing a vertical profile. Surface and body transformations are inferred during T2 and T3. (FS = fine sand; MS = medium sand; CS = coarse sand.)
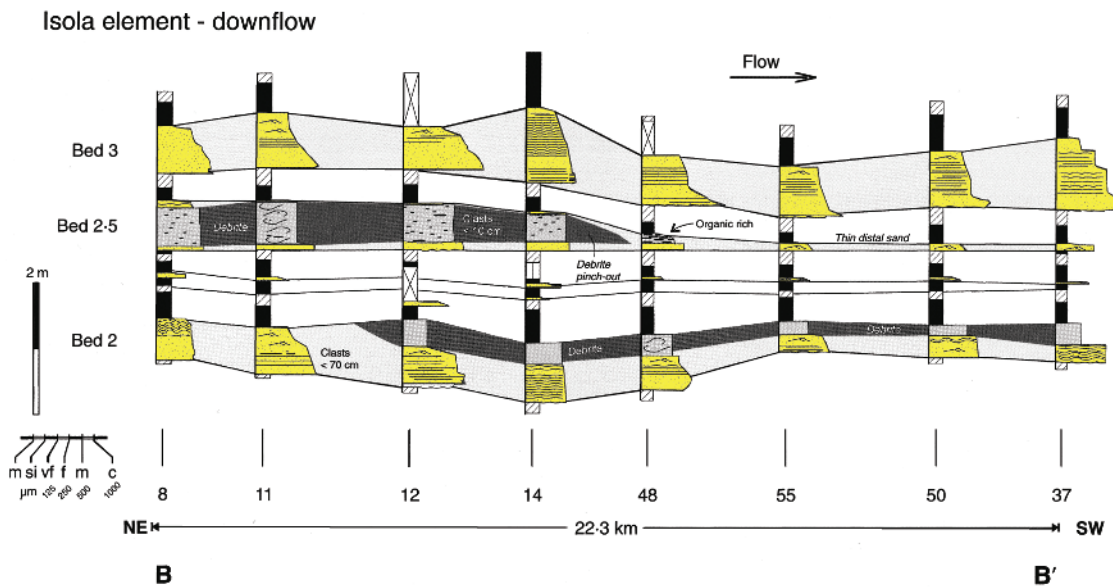

Fig. 1.26 Limited distribution of debrite units when compared with associated turbidites within tri-partite beds in the Marnoso arenacea, Italy. From Amy and Talling (2006).

(2003) concluded that 'linked' debrites in Jurassic deep-water deposits in the North Sea (Fig. 1.27) formed from separate flows that were triggered at the same time as sand-load concentrated density flows, but eventually came to rest on top of the freshly accumulated sand. In this case, two separate flows with different rheology were apparently generated by the same failure event, leading to bi-partite beds with sharp textural discontinuities.

Talling *et al.* (2007) have studied an enormous sediment slide and its runout deposits (debris flow and turbidite) from the Agadir Basin, and the Seine and Madeira abyssal plains, located offshore northwest
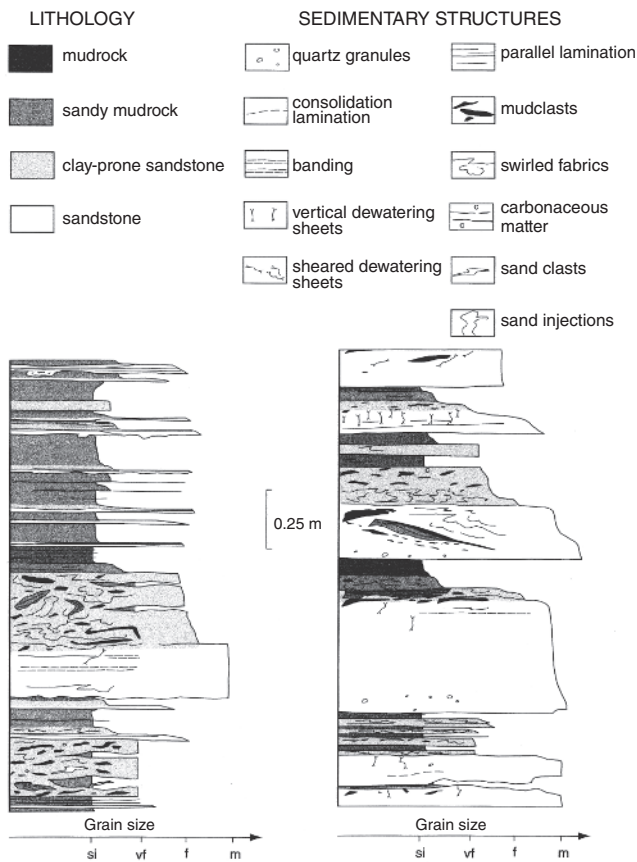
LITHOLOGY

- ■ mudrock
- ▨ sandy mudrock
- ▦ clay-prone sandstone
- □ sandstone

SEDIMENTARY STRUCTURES

- quartz granules
- consolidation lamination
- banding
- vertical dewatering sheets
- sheared dewatering sheets
- parallel lamination
- mudclasts
- swirled fabrics
- carbonaceous matter
- sand clasts
- sand injections

0.25 m

Grain size
si vf f m

Grain size
si vf f m

Fig. 1.27 Examples of linked debrites and Facies Class B sandstones (see Section 2.4) from the fringe of a Jurassic sand-prone fan in the subsurface of the North Sea. From Haughton *et al.* (2003).

Africa. Beyond the base of the continental slope, a mostly >1 m thick bed consists of a lower stratified sand and a middle muddy sand that is interpreted as a co-genetic debrite. The debrite is overlain by the graded mud top of the turbidite. The total volume of this linked turbidite and muddy debrite is ~125 km^3 assuming a bulk density of 1.8 g cm^{-3}, which is about ten times the annual discharge of all rivers to the world ocean. Their work shows that extensive debrites can form downflow from abrupt slope breaks and areas of significant seafloor erosion. The 'linked' debrite forms the centre of the deposit and is encased within turbidite sandstone and mudstone.

Based on a detailed study of 1–10 m-thick muddy SGF deposits from the Madeira Abyssal Plain, McCave and Jones (1988) and Jones *et al.* (1992) proposed their deposition from dense ($\Delta\rho = 5$–100 kg m^{-3}), non-turbulent flows. The deposits are ungraded, structureless mud. The proposed density contrast with seawater is equivalent to a volume concentration of less than ~6 volume%; non-turbulent mud-laden flows of this character have been produced experimentally by Baas and Best (2002) at velocities of ~0.33 m s^{-1}. McCave and Jones (1988) and Jones *et al.* (1992) believe that a fully turbulent flow decelerated, went through a body transformation to form an essentially laminar and viscous SGF. With turbulence severely damped, the suspension consolidated into a cohesive layer with inter-particle forces preventing the differential settling of coarser grains. Consideration by Masson (1994) of the small cross-sections of the channels through which the muddy SGFs passed en route to

the Madeira Abyssal Plain, and the lack of prominent levées along these channels (suggesting little overspill), supports the notion of high flow densities.

Gravity flows that undergo transformations along their path have been termed *composite flows* by Haughton *et al.* (2009), with the deposits referred to as *hybrid event beds*. These authors propose a classification (Fig. 1.28a) that includes such composite flows and their deposits. Contrary to the better-understood case of gradual flow dilution and deposition of progressively more organised and finer-grained deposits in the downdip direction (Fig. 1.28b1), composite flows increase in concentration distally and transform, in part, into mudflows or debris flows (Fig. 1.28b2). Three processes can force an increase in concentration and suppression of turbulence (Haughton *et al.* 2010; Fig. 1.29): (i) deceleration of a clay-rich flow so that viscous effects become dominant; (ii) segregation of clay components into trailing and lateral parts of a flow so that turbulence intensity is damped; and (iii) addition of clay to the suspension by disintegration of soft clasts eroded along the travel path – a process referred to as 'bulking'. The first of these processes has been studied experimentally by Sumner *et al.* (2009) and Baas *et al.* (2011). With rapid deceleration of a flow carrying ~10% suspended clay, silt and sand, Baas *et al.* (2011) hypothesise that a basal relatively clean sand division can accumulate rapidly because of a sharp drop in the total transport capacity for sand. This drop results from a decline in turbulence support that occurs more quickly than the parallel increase in cohesive support.

An alternative way to produce a hybrid event bed is for synchronously triggered debris flows and concentrated density flows to deposit one after the other, with the latter flow outrunning its more viscous partner (Fig. 1.29d).
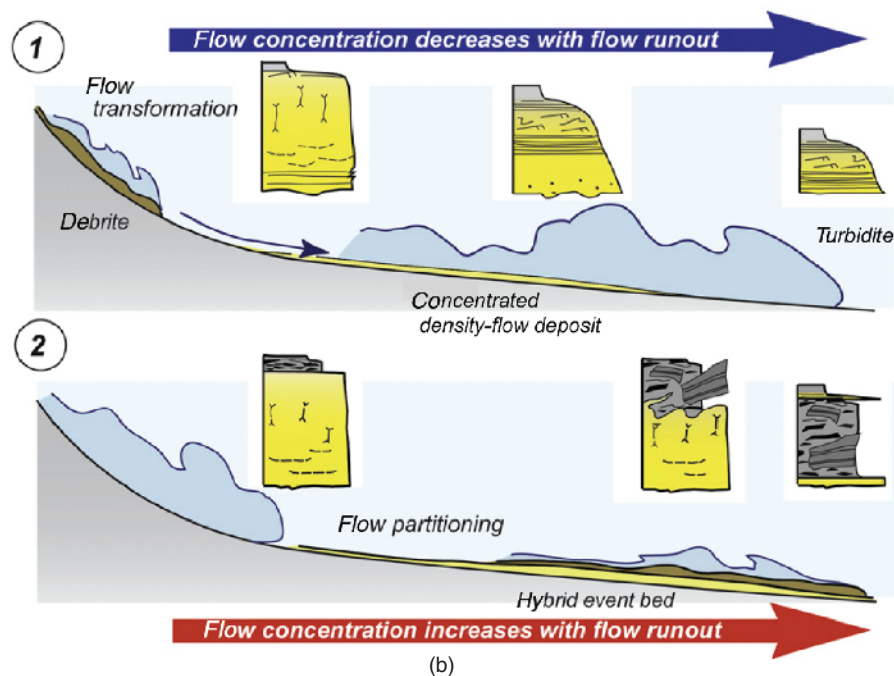
1.5 Turbidity currents and turbidites

1.5.1 Definition and equations of flow

Turbidity currents are density currents in which the denser fluid is a grain suspension, with particles supported largely by the upward velocity fluctuations associated with turbulent eddies (Bagnold 1966; Leeder 1983). Entrained sediment diffuses throughout the flow thickness, but the highest particle concentrations are at the base of the flow (Stacey & Bowen 1988; Middleton 1993; Felix 2001). As with open-channel flows in flumes and rivers (Rouse 1937), the coarsest size fractions are also carried toward the lower part of the flow. Depending on the manner in which the flow was initiated, the turbidity current may be (i) relatively short, quickly passing an observation point on the seafloor (surge-type flow); or (ii) relatively long with steady discharge due to prolonged input from a long-lived source (steady and uniform discharge – generally river-fed as 'hyperpycnal' flows) (Mulder & Syvitski 1995; Mulder *et al.* 2001, 2003; Alexander & Mulder 2002; Felix *et al.* 2006). *Hyperpycnal flow* is the term used to describe river discharge which, because of a high suspended load, is more dense than seawater so travels down the delta front as an underflow.

Talling *et al.* (2012) provide an historical reminder that Ph. Kuenen and co-workers coined the term 'turbidity current' because the density currents they were investigating were 'turbid' (murky because of suspended solids) rather than because they were turbulent. However, it is now rather common practice to associate this term with turbulent flows. We therefore follow Mulder and Alexander (2001) in restricting

(a)

(b)

Fig. 1.28   (a) Haughton *et al*. (2009) classification scheme for event beds emplaced by subaqueous sediment gravity flows. (b1) Debrites, concentrated density-flow deposits and turbidites dominate the record of many deep-water systems and record increasing downdip dilution of the flow (debrites passing to concentrated density-flow deposits and eventually turbidites). (b2) In some systems there is instead a downdip progression from non-cohesive flows (depositing concentrated density-flow deposits and turbidites) to flows transformed into components with radically different rheology, with the deposits of the cohesive flow components increasingly dominant distally. From Haughton *et al*. (2009) who used 'high- and low-density turbidity currents' instead of 'concentrated density-flows and turbidity currents'.
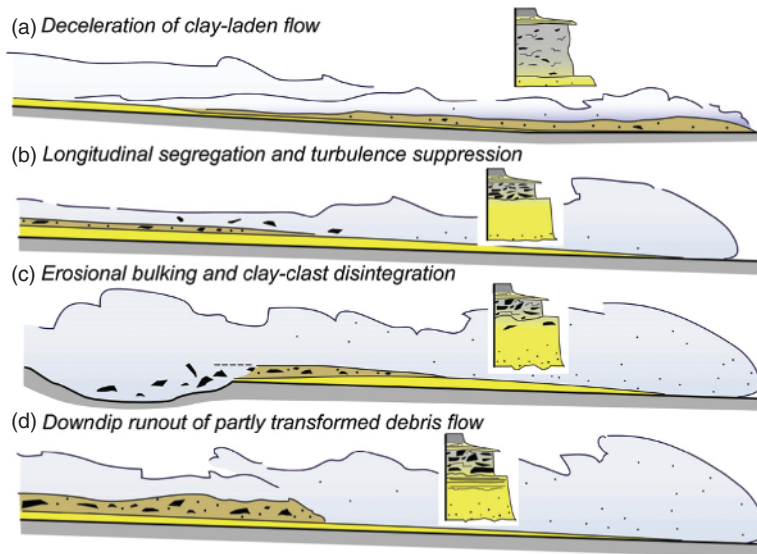
Fig. 1.29 Summary of depositional origin for hybrid event beds as a result of (a) loss of turbulence and deceleration of a clay-rich flow, (b) longitudinal segregation of clays and clay flakes to suppress turbulence in the rear and margins of an otherwise turbulent flow, (c) bulking and disintegration of clay clasts to release clay near-bed in an otherwise turbulent flow and (d) downdip runout of a flow that was either synchronously triggered with a concentrated density flow, or that partially transformed to generate a forerunning concentrated density flow. From Haughton *et al.* (2010).

the term 'turbidity current' to flows in which turbulence is the dominant support mechanisms (Figs. 1.19 and 1.23). The concentration of solids in the lower part of such flows can exceed the Bagnold (1962) limit of 9% by volume (Fig. 1.21), beyond which grain-to-grain interaction begins to occur. Natural flows with a mixture of sediment sizes are stratified according to density and other properties, so that two flows of identical average density might have quite different near-bed concentrations. Since it is the near-bed concentration that controls settling rates, the intensity of turbulence and the formation of sedimentary structures, it is unavoidable that the deposits of some turbidity currents might resemble those of the more dilute concentrated density flows. For example, basal structureless divisions in some turbidites likely imply more about the rate of deposition from suspension than the absolute concentration (Lowe 1988; Arnott & Hand 1989; Allen 1991). The rate of suspension fallout will vary with the rate of flow deceleration, so that two turbidity currents with exactly the same average concentration and turbulence intensity might deposit structureless sand at one locality (rapid deposition) and laminated sand at a different locality (protracted deposition).

Concentration has a bearing on flow velocity and therefore competence on basin margin slopes. On gentle slopes, coarse sands and gravels are likely to be transported by inflated sandflows or concentrated density flows rather than turbidity currents. Concentration influences flow density and viscosity, but has little effect on the flow mechanics of a turbidity current until particle concentrations become so high that (i) interparticle collisions become an important component of grain support even well above the bed (Fig. 1.23), or (ii) turbulence, particularly near the bed, becomes damped (Fig. 1.30).

Modelling of deposition from surge-type turbidity currents is difficult because equilibrium velocities and sediment concentrations may never be attained, and because of scaling problems in small-scale experiments (Middleton 1993). Experimental modelling of density surges by Laval *et al.* (1988) shows that the velocity of the surge is effectively proportional to the square root of the initial

volume, and that surge velocity increases with increasing initial density of the flow, being proportional to the square root of the ratio of the excess density to the density of the ambient fluid. These results are corroborated by the numerical simulations of Zeng and Lowe (1997a, b).

Dade *et al.* (1994) and Dade and Huppert (1995) developed mathematical models to explain flow evolution and deposition from turbidity currents. On slopes, the primary cause of decreasing flow concentration is entrainment of ambient seawater (Dade *et al.* 1994). On horizontal surfaces like basin plains or the very low slopes on distal submarine fans, flows gradually become less concentrated as their suspended load is deposited (Dade & Huppert 1995); seawater entrainment is much less significant than on slopes (Stacey & Bowen 1988). For deep-water gravity currents travelling across horizontal surfaces (flow thickness <0.075 water depth), the box model of Dade and Huppert (1995) predicts a maximum deposit thickness of about three times the average deposit thickness, located 1/5 of the way between the most proximal deposit and the most distal deposit. The run-out distance, measured from the point of arrival onto the basin plain, is proportional to the initial reduced gravity and volume of the surge, and is inversely proportional to the average particle settling velocity. Sorting is predicted to improve in the downcurrent direction for mixed-load currents.

On uniform slopes, the model of Dade *et al.* (1994) predicts deposit thickness and texture, evolution of flow velocity and Froude number, and depositional runout distance. Critical parameters that control evolving flow properties are the rates of sediment loss through deposition, and dilution of the suspension through seawater entrainment. When applied to a hypothetical natural surge travelling about 300 km, this model predicts growth in flow thickness from 100 m to >1 km, and in length from 1 km to >10 km, solely because of seawater entrainment.

Sophisticated numerical simulations, tested against natural data from a fjord setting (Bute Inlet), have been formulated by Zeng and
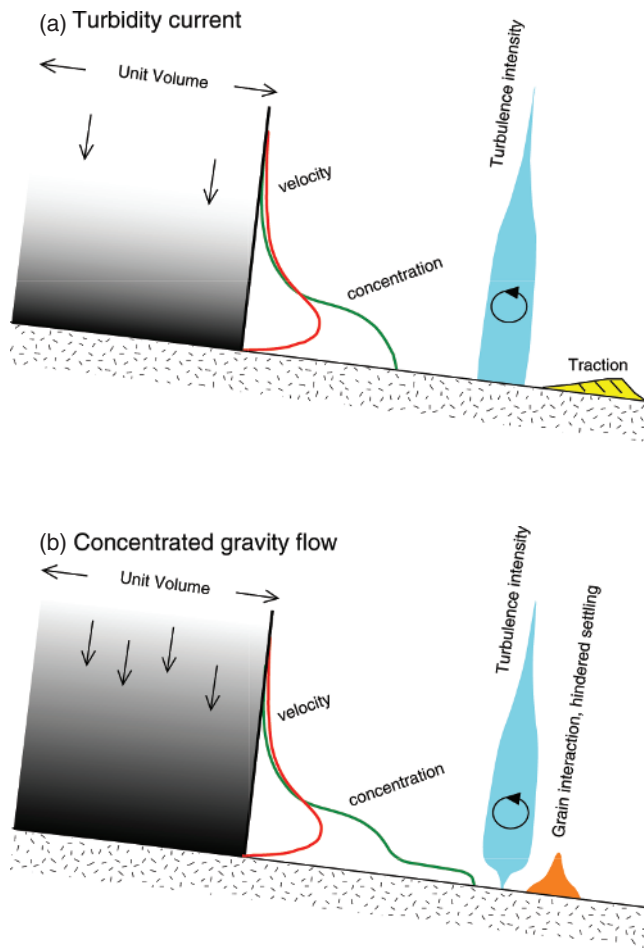
(a) Turbidity current

(b) Concentrated gravity flow

Fig. 1.30 Contrasting near-bed grain support between a turbidity current and a concentrated density flow. Although both types of SGF are turbulent away from the sedimentation surface, the latter has strong grain interaction at the aggrading bed, and turbulence is sufficiently damped to prevent the development of tractional sedimentary structures.

Lowe (1997a, b). The simulated flows have prominent grain-size stratification and relatively low concentration. The simulated deposits show good distribution grading like that observed in natural turbidites. For initial boundary conditions of higher concentration, the predicted grading is poorer and limited to the coarsest parts of the size spectrum (coarse-tail grading). These simulated flows compare best with the smallest of the natural flows that have been observed in Bute Inlet.

For continuously-fed flows or unusually large-scale surge-type flows on a constant slope, a condition of effective flow steadiness (i.e., $\partial U_B / \partial t = 0$; U_B = body velocity) may exist in the long body of the current. The maximum velocity is in the lower part of the body of the current (Fig. 1.31) and is ∼1.6 times the mean velocity (Felix 2004). The finest grain sizes have an essentially uniform concentration throughout the flow, whereas the coarsest grain sizes are most concentrated near the base of the flow (Rouse 1937; Hiscott 1994a). Because the time-averaged velocity is lower near the base of the flow than in the vicinity of the velocity maximum, coarse size fractions lag behind fine fractions; this differential transport rate may lead to basal

inverse grading in the deposits of turbidity currents (Hand & Ellison 1985; Hand 1997).

The flow steadiness described above is at best an average condition, because velocity fluctuations are superimposed on the body of the flow by the passing of interfacial waves along internal density boundaries and along the top of the current (Simpson 1997; Baas & Best 2002), and by longer-period pulsing described from natural currents by Best *et al.* (2005) but still poorly understood.

Experiments of Gladstone *et al.* (2004) provide insight into how vertical and streamwise stratification might affect grading and textures of deposits. These authors demonstrate that strong vertical grain-size stratification inevitably leads to downflow lateral grading in the flow (Fig. 1.18). In most cases, the lower part of the flow will contain coarser sediment. If it also has a higher concentration, then the coarse fractions may outpace the upper part of the same flow with its finer sediment load (opposite to the predictions of Hand 1997). Sequential deposition as the flow passes will produce a graded bed, with the smoothness of the grading (or the degree of step-wise grading) depending on the initial density structure of the flow.

A comprehensive mathematical model for flow evolution and deposition from turbidity currents is presented by Pratson *et al.* (2000). In this book, we provide simpler equations for homogeneous, non-erosional and non-depositing flows, primarily to clarify what factors control velocity and thickness of turbidity currents. For more sophisticated treatments, the reader is referred to Pratson *et al.* (2000), Stacey and Bowen (1988) and other references in preceding paragraphs.

As shown by Middleton (1966b), the velocity of the body of a turbidity current is given by a Chezy-type equation,

$$U_B{}^2 = \left[\frac{8g}{f_o + f_i} \right] \left[\frac{\Delta\rho}{\rho + \Delta\rho} \right] d_B \tan\alpha \tag{1.3}$$

where $\Delta\rho$ = density difference between the flow and seawater, ρ = density of seawater, d_B = body thickness, α = bottom slope in degrees, f_o = dimensionless Darcy–Weisbach friction coefficient for bed friction, and f_i = dimensionless friction coefficient for interfacial friction at the top of the flow. Friction coefficients have been determined empirically for rivers and in flumes, but turbidity currents differ from rivers in that there is also friction between the flow and the overlying water. According to Middleton and Southard (1984), $f_o + f_i$ for large natural turbidity currents is likely to be about 0.01. For subcritical flow conditions (Froude number, $F < 1.0$), $f_o \gg f_i$, but for supercritical flows ($F > 1.0$), $f_i > f_o$ due to intense mixing at the upper interface of the flow.

The velocity of the head of the current, U_H, does not appear to depend significantly on the bottom slope for turbidity currents moving over low slopes; Middleton (1966a) gives:

$$U_H{}^2 = 0.56g\, d_H \left[\frac{\Delta\rho}{\rho + \Delta\rho} \right] \tag{1.4}$$

On steeper slopes, from perhaps 2–10°, a more general result (Hay 1983a) includes a dependence of head velocity on the bottom slope:

$$U_H{}^2 = g\, d_H \left[\frac{\Delta\rho}{\rho + \Delta\rho} \right] (0.50\cos\alpha + t\sin\alpha) \tag{1.5}$$

Experiments with small surges suggest that the empirical factor t is in the range 1.6–4.0 (Hay 1983a). Note that for $\alpha = 1°$ and $t = 3.3$, Equation 1.5 reduces to Equation 1.4, but for $\alpha = 10°$, the numerical
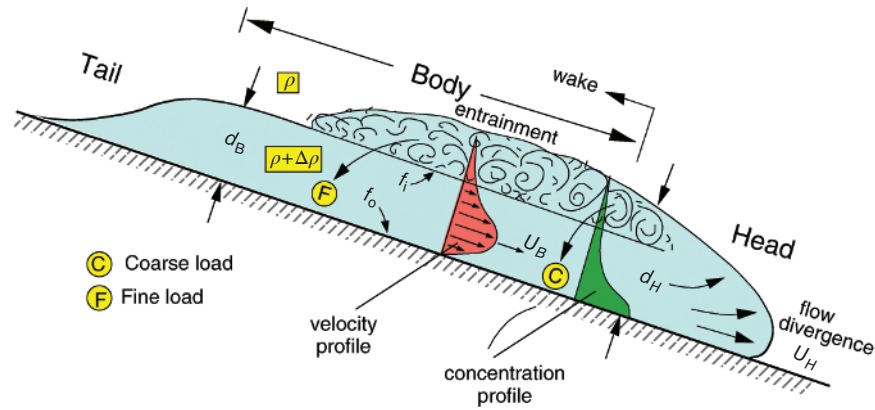
Fig. 1.31 Idealised streamwise cross-section of a turbidity current, divided into head, body and tail regions. Settling from the wake behind the head produces a lateral size grading in the flow.

constant in Equation 1.4 would be 1.1, not 0.56. The ratio of the head velocity to the body velocity (U_H/U_B) is approximately 1.0 on gentle slopes but <1.0 on steeper slopes (Fig. 1.32). The head does not grow unchecked as suspension from the body of the current overtakes it. Instead, an equilibrium is developed. The rate of body flow into the head region is balanced by loss of suspension from a region of intense turbulence and flow separation at the back of the head (Simpson 1982, 1997; Fig. 1.31). This ejected material settles back into the flow top according to fall velocity, with the coarsest grains returning to the body nearest the head and the finest grains returning far behind the head. This process amplifies the lateral size grading that might result from density stratification in the flow (Gladstone *et al.* 2004). The result is a coarser suspension near the head and a finer suspension near the tail (Walker 1965).

Equations 1.3 through 1.5 can only provide guidance as to the behaviour of a turbidity current at a single location along its flow path, because flow concentrations and thicknesses evolve downcurrent as seawater is entrained into the suspension and as deposition removes suspended load. A special case in which flow thickness is partly regulated over long flow distances occurs in deep-sea levéed channels.
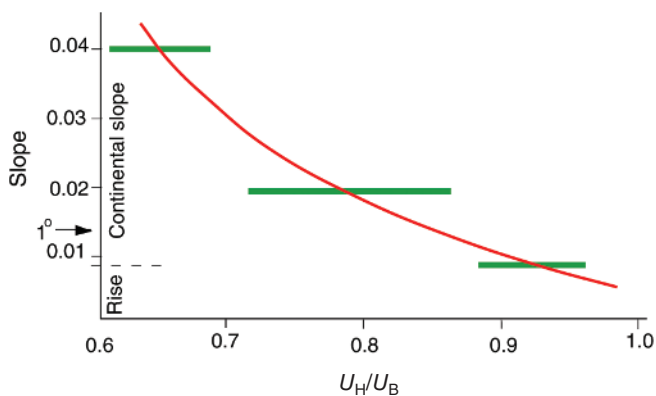

Fig. 1.32 Ratio of head velocity to body velocity plotted against bottom slope for experimental turbidity currents (5-m flume) of Middleton (1966a). Horizontal bars show extent of scatter in the data. Ranges of bottom slope for continental margins are superimposed.

Here, dramatic flow thickening is counteracted by overspill across the levées. Such channelised flows may also have their sediment concentration regulated by flow shortening through time, as the rear part of the body (travelling on steeper slopes) progressively catches up with the frontal part of the body (travelling on gentler slopes) (Hiscott *et al.* 1997b). As a result, turbidity currents are able to maintain their fundamental properties and travel long distances through such levéed channels (e.g., Chough & Hesse 1976).

1.5.2 Natural variations and triggering processes

Initially, the theory of flow and deposition of turbidity-currents was based mainly on observations from simple, small-scale experiments (Middleton 1993), leading to predicted facies characteristics simpler than those encountered in nature. Natural currents, however, are strongly stratified (Gladstone *et al.* 2004) and typically encounter irregular seabed topography, opposing slopes, or are confined within meandering channels, all of which modify flow behaviour and direction. The result may be structurally complex beds or beds showing step-wise grading and a complex repetition of structures (e.g., Pickering & Hiscott 1985; Marjanac 1990; Pickering *et al.* 1992, 1993a; Edwards 1993; Edwards *et al.* 1994; Haughton 1994; Gladstone *et al.* 2004). The influences of basin topography and density layering of the ambient fluid (Figs 1.17 and 1.18) have only recently been studied experimentally (e.g., Kneller *et al.* 1991; Alexander & Morris 1994; Kneller 1995; Rimoldi *et al.* 1996; Gladstone *et al.* 2004). It will be challenging to extrapolate these results to large natural scales, but it is critical that complex topography and special oceanographic conditions be taken into account when interpreting ancient successions.

Natural marine turbidity currents have been studied only superficially because of the inherent difficulties in devising and deploying monitoring systems. More has been published on turbidity currents in lakes and reservoirs (see review in Middleton 1993). Human-made marine turbidity currents formed by the dumping of mine tailings have been studied by Normark and Dickson (1976), Hay (1987a, b; see also Hay *et al.* 1982), and Normark (1989). Nascent turbidity currents in Scripps Submarine Canyon have been monitored up to the point at which current-meters were lost, giving minimum flow speeds of 1.9 m s^{-1} (Inman *et al.* 1976). Natural delta-fed turbidity currents in a protected fjord were monitored (Fig. 1.33) and their deposits studied and later numerically modelled by Zeng *et al.* (1991, 1997a, b). Larger
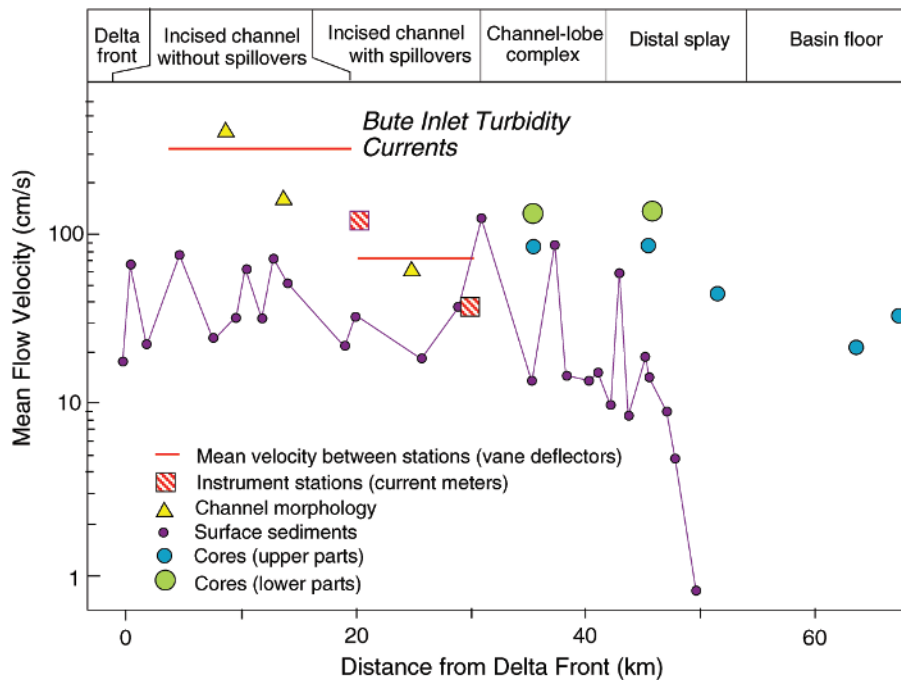
Fig. 1.33 Measured flow velocities of turbidity currents in Bute Inlet compared with velocity estimates inferred from the texture of turbidites along the flow path. Redrawn from Zeng *et al.* (1991).

natural flows have only been studied indirectly, by examining records of submarine cable breaks or displacements of instrument packages (Heezen & Ewing 1952; Heezen *et al.* 1954; Gennesseaux *et al.* 1980; Normark *et al.* 1993b), variation in levée heights of submarine channels at channel bends (Komar 1969; Pirmez 1994), and the height of flow deposits and deposit characteristics (Bowen *et al.* 1984; Piper & Savoye 1993). Quantitative results of some of these studies are summarised in Table 1.2.

The best documented large natural flow was generated by a 7.2 magnitude earthquake in the Laurentian Channel, eastern Canada, in 1929. The so-called '1929 Grand Banks turbidity current' broke a succession of submarine cables and deposited a graded fine sand to silt layer about l m thick (Fig. 1.34) in a water depth of about 5200 m (Heezen & Ewing 1952; Heezen *et al.* 1954; Fruth 1965). According to Piper *et al.* (1988), the turbidity current carried about 200 km^3 of sediment. Calculated maximum velocity and flow depth are 19 m s^{-1} and about 400 m. In order to carry sufficient sediment through the valleys of the Laurentian Fan to account for the volume of the turbidite on the Sohm Abyssal Plain, the 1929 turbidity current must have taken 2–3 hours to flow past a point along one of the fan valleys. Piper *et al.* (1988) and Hughes Clarke *et al.* (1990) initially attributed the formation of large gravel bedforms with wavelengths of 10–70 m in the Laurentian Fan valleys (Fig. 1.35) to the 1929 turbidity current. Now, the gravel transport and reworking into large bedforms is interpreted to have taken place during a Pleistocene glacial-lake outburst event which formed a powerful hyperpycnal gravity flow (D.J.W. Piper, in Wynn *et al.* 2002b).

Triggering mechanisms for natural turbidity currents include the following processes (Normark & Piper 1991; Van den Berg *et al.* 2002): (i) hyperpycnal flow from rivers and glacial meltwater (Heezen *et al.* 1964); (ii) sand liquefaction (Seed & Lee 1966; Andresen & Bjerrum

1967) in canyon heads, triggered by storms, earthquakes or local failures, followed by water entrainment and acceleration; (iii) breach failure which results from gradual back-sapping (retrogression) of an over-steepened slope in cohesionless material after an initial failure (Van den Berg *et al.* 2002; Mastbergen & Van den Berg 2003); (iv) erosion of the front of a moving debris flow (Hampton 1972; Talling *et al.* 2002) or thickening and dilution of a debris flow as it undergoes an hydraulic jump (Weirich 1988); (v) dilution of sediment slides (Ricci Lucchi 1975b; Cita *et al.* 1984; Hughes Clarke *et al.* 1990); (vi) suspension of sediments in canyon heads by edge waves associated with storms (Inman *et al.* 1976, Fukushima *et al.* 1985); (vii) ignitive flow of shelf suspensions that descend a basin slope and (viii) ignitive flow of ash from pyroclastic falls. *Hyperpycnal flow* is the term used to describe river discharge which, because of a high suspended load, is more dense than seawater so travels along the seabed as an underflow. The term *ignition* (Parker 1982) refers to a state in which an accelerating density current entrains more sediment along its path, which causes it to continue to accelerate and grow in size. According to Normark and Piper (1991), ignition is favoured by initial volume concentrations of particles of about 0.01, initial velocities of about 1 m s^{-1} (fine-grained sand) to 1.2 m s^{-1} (medium-grained sand), and slopes exceeding 3° (Fig. 1.36). Pratson *et al.* (2000) instead explain that ignition is most effective on slopes of ~2–2.5°; below this range the turbidity current will decelerate and die, whereas on higher slopes the quantity of entrained sediment is less and the turbidity current smaller.

Earthquakes are commonly called upon as prospective triggers for turbidity currents (Hiscott *et al.* 1993; Beattie & Dade 1996). Earthquake recurrence intervals follow a power law, as do many turbidite bed thicknesses (Hiscott *et al.* 1993; Rothman *et al.* 1994; Drummond & Wilkinson 1996). According to Kuribayashi and Tatsuoka

Table 1.2 Estimates of mean flow parameters for natural turbidity currents, using a seawater density of 1030 kg m^{-3} (unless given). Highest velocities at top of table

| Location	M=measured C=calculated H=hindcast	Basis of calculations	Density contrast (kg m^{-3})	Body velocity (m s^{-1})	Comments	Source
Laurentian Fan, 1929 event	C, H	Cable breaks, seabed features, theory	~95	19	Gravel waves now believed older (Wynn et al. 2002b)	Piper et al. (1988)
Monterey Fan, California	C	Levee height differences, theory		20–4		Komar (1969)
Var middle and lower valley	C, H	Sand distribution and size, theory	~95–25	~10–2	Proximal to distal ranges given	Piper & Savoye (1993)
Var Canyon and Valley	C, H	Cable breaks, seabed features, theory	25–8	~8–3	Turbidity current 'plume' only; concentration assumed	Mulder et al. (1997)
Labrador Sea (NAMOC)	C, H	Grain size	87	8	Base of in-channel flows	Klaucke et al. (1997)
Bute Inlet, Canada	M, C	Current-meters, grain-size of deposits	26–2	3.3–0.5	Sea-water density 1023 kg m^{-3}	Zeng et al. (1991)
Scripps Canyon, California	M	Current-meters		1.9		Inman et al. (1976)
Rupert Inlet, Canada	C	Channel geometry, tailings discharge rate	100	~1.3	Surge-type turbidity currents	Hay (1987b)
Zaïre submarine valley	M	Current meters, sediment traps		1.2	Coarse sand 40 m above floor; velocity for 150 m elevation	Khripounoff et al. (2003)
Labrador Sea (NAMOC)	C	Channel geometry	12–1	0.86–0.05	Proximal to distal ranges given	Klaucke et al. (1997)
Navy Fan, California	C, H	Grain size, channel geometry, theory		0.8–0.1		Bowen et al. (1984)
Labrador Sea (NAMOC)	C, H	Grain size	4	0.45	Top of in-channel flows	Klaucke et al. (1997)
Rupert Inlet, Canada	C	Channel geometry, tailings discharge rate	30	0.4	Continuous-flow of mine-tailings discharge	Hay (1987)
Reserve Fan, Lake Superior	M	Current meters and water samples	0.05	0.12–0.08		Normark (1989)
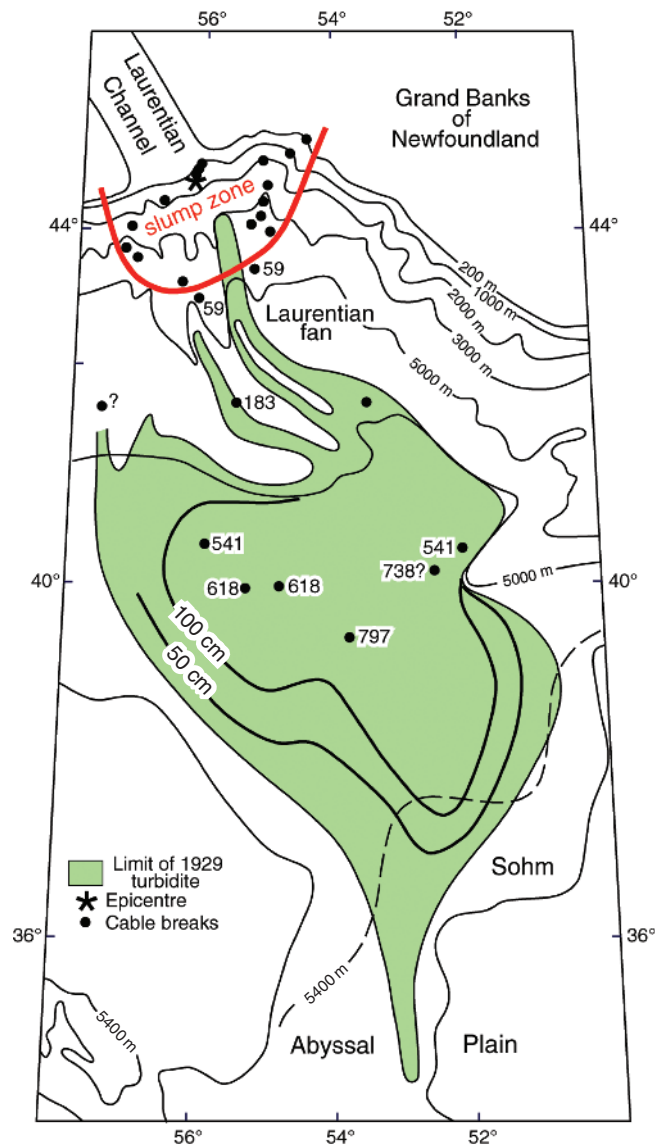
Fig. 1.34 Distribution of the sand turbidite generated by the 1929 Grand Banks earthquake. Numbers beside cable break positions are the time of each break, in minutes, after the earthquake. Bathymetric contours are in metres. Turbidite thickness is contoured in centimetres. Redrawn from Piper *et al*. (1988).

(1977) and Keefer (1984), only earthquakes with magnitudes greater than about 5.0 can cause significant sand liquefaction and, as the distance from the epicentre increases, so does the minimum magnitude required for liquefaction. Their data indicate, for example, that a magnitude 7.0 shock can liquefy sediment as far as about 100 km from the epicentre. Using historical records for the period 1905–64, Duda (1965) determined a recurrence interval, for those earthquakes stronger than magnitude 7, of 0.063 yr (23 days) for the entire length of the circum-Pacific convergent margins, about 40 500 km. For each 100 km segment of trench, therefore, the average recurrence interval is about 25 yr, in general agreement with more recent data around Japan (Mogi 1990). These frequent earthquakes would be capable of liquefying sediment and triggering sediment gravity flows over a wide area (Keefer 1984).

Hyperpycnal flows originate where sediment-laden river water attains a greater density than seawater, so that it is able to descend directly to the seabed at the river mouth and flow seaward as a turbidity current. Mulder and Syvitski (1995) explained the requirements for hyperpycnal flow and demonstrated the likelihood of such flows in modern oceans, particularly seaward of certain Asian rivers with high sediment loads. They concluded that sediment concentrations of at least 40 kg m^{-3} are needed to initiate hyperpycnal flow. In a groundbreaking re-evaluation of these ideas, Parsons *et al*. (2001) showed experimentally that sediment concentrations could instead be as low as ~1 kg m^{-3} because of *finger convection* between the warm, fresh, sediment-laden overflow exiting a river mouth, and an underlying colder, saline ambient water mass. The convection triggers instability and the removal of large amounts of suspension by a bottom-hugging hyperpycnal flow. The key to this process is the presence of a downward-increasing dominant gradient in salinity, and an upward-increasing gradient in temperature. Instead of only 9 of 147 rivers predicted to generate hyperpycnal flows annually (Mulder and Syvitski 1995), Parsons *et al*. (2001) predict that 61 of the rivers should show this behaviour. These particular 61 rivers 'produce 53% of the world's oceanic sediment load and are therefore responsible for a significant portion of the [modern] sediment record' (Parsons *et al*. 2001: p. 477).

The reader might take issue with calling the experimental flows of Parsons *et al*. (2001) 'hyperpycnal', because they did not exit directly from the proxy river channel, but rather developed through convection-driven collapse of a surface hypopycnal plume. However, this collapse occurred (and in nature is predicted to occur) very close to the river mouth, so that the resulting SGF effectively has the same close link with river input that characterises true hyperpycnal flows. The situation is not unlike the seaward gravity-driven flow of mud-laden suspensions produced where delta-derived mud is kept in suspension, and concentrated, by wave stirring through a process called 'frontal trapping' (Geyer *et al*. 2004). High mud concentrations in the wave boundary layer are able to initiate what Geyer *et al*. (2004) also call hyperpycnal flows, because suspended mud builds up near the seabed adjacent to the river mouth, and because the wave-induced mixing of seawater with fresh river water ensures that the suspension eventually exceeds the density of fully marine water. In some cases, the mud concentration in the zone of 'frontal trapping' can reach that of so-called 'fluid mud' (>10 000 mg litre^{-1}; Geyer *et al*. 2004).

A somewhat different approach was taken by Felix *et al*. (2006), who looked more carefully at the effects of density stratification and estuarine mixing, and concluded that hyperpycnal flows can be generated even when the density difference between the ocean and the particulate suspension is only a few tenths of 1 kg m^{-3}, much lower than advocated by Mulder and Syvitski (1995) and lower than proposed by Parsons *et al*. (2001).

In a study offshore of the Var River, France, Mulder *et al*. (1997) demonstrated that day-long hyperpycnal flows would occur each 5–21 years, and Mulder *et al*. (2001) showed that deposits from such flows are inverse-to-normally graded (Fig. 1.37). The number of turbidites in the geological record that were emplaced by hyperpycnal flows is still unknown, but the dominance of normal rather than inverse-to-normal grading in ancient deposits suggests that the deposits of hyperpycnal flows might not be as common as predicted by Parsons *et al*. (2001) and Felix *et al*. (2006). There are ancient examples, however, that possess the attributes expected for deposits from hyperpycnal flows (Soyinka & Slatt 2008). Additional data from modern natural settings will be needed to assess the true importance of hyperpycnal flow as an initiating mechanism for turbidity currents.
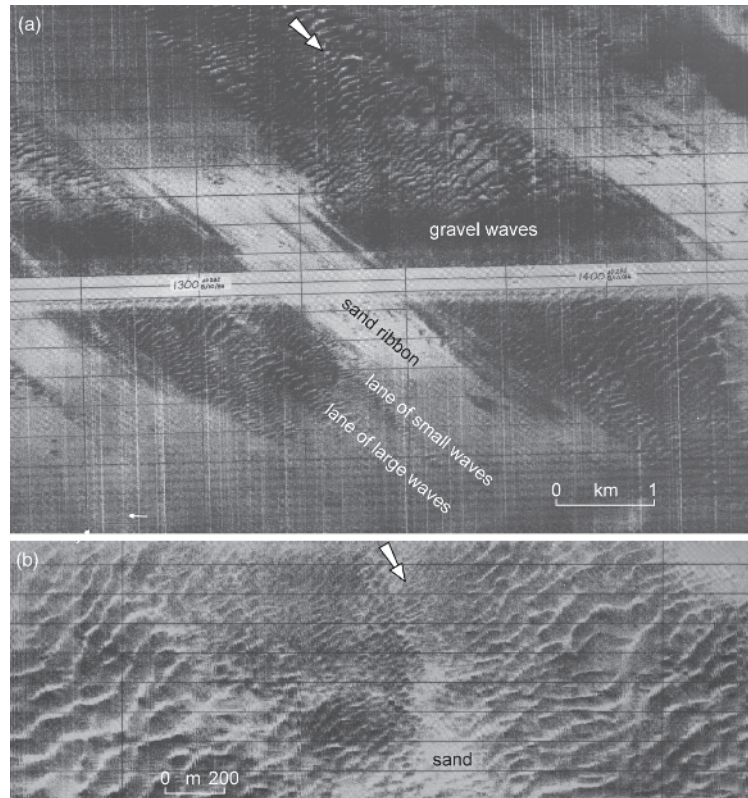
Fig. 1.35 Giant gravel waves in the Eastern Valley of the Laurentian Fan, likely formed under a hyperpycnal flow produced by an outburst flood during decay of continental ice sheets. (a) Fields of gravel-rich waves in lanes of larger and smaller waves, buried by sand ribbons. (b) Detail of rather sinuous gravel-rich waves of various sizes, locally covered by sand patches, using 1-km swath system. From Wynn *et al.* (2002b). Copies of original graphics courtesy of D.J.W. Piper, Geological Survey of Canada.
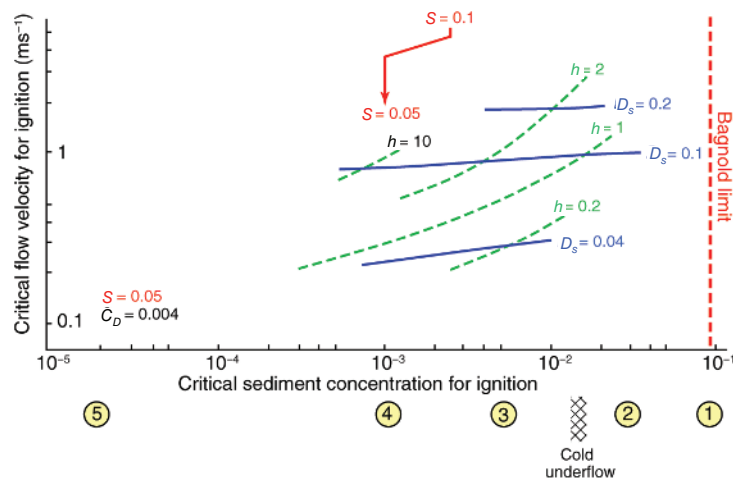

Fig. 1.36 Optimum conditions for ignition of turbidity currents, from Normark and Piper (1991). The plot shows critical velocity and critical concentration for various flow thicknesses (h, metres) and representative grain sizes (D_s, mm) on a slope of $S = 0.05$, assuming a drag coefficient of $C_D = 0.004$ (based on four-equation model results of Parker *et al.* (1986)). Also shown is the approximate offset in the concentration scale resulting from an increase in S to 0.1. Circled numbers are measured suspended-sediment concentrations from a number of settings: 1 = Huanghe River, China, in flood (Wright *et al.* 1988); 2 = Sustina River, Alaska, in flood (Hoskin & Burrell 1972); 3 = maximum measured discharge into Glacier Bay, Alaska (Hoskin & Burrell 1972); 4 = ignitive condition for sand in the head of La Jolla Canyon (Fukushima *et al.* 1985); 5 = nearshore sediment concentration after flood of Santa Clara River (Drake *et al.* 1972). The 'cold underflow' is the approximate sediment concentration in cold river water required to produce a marine underflow (Gilbert 1983).
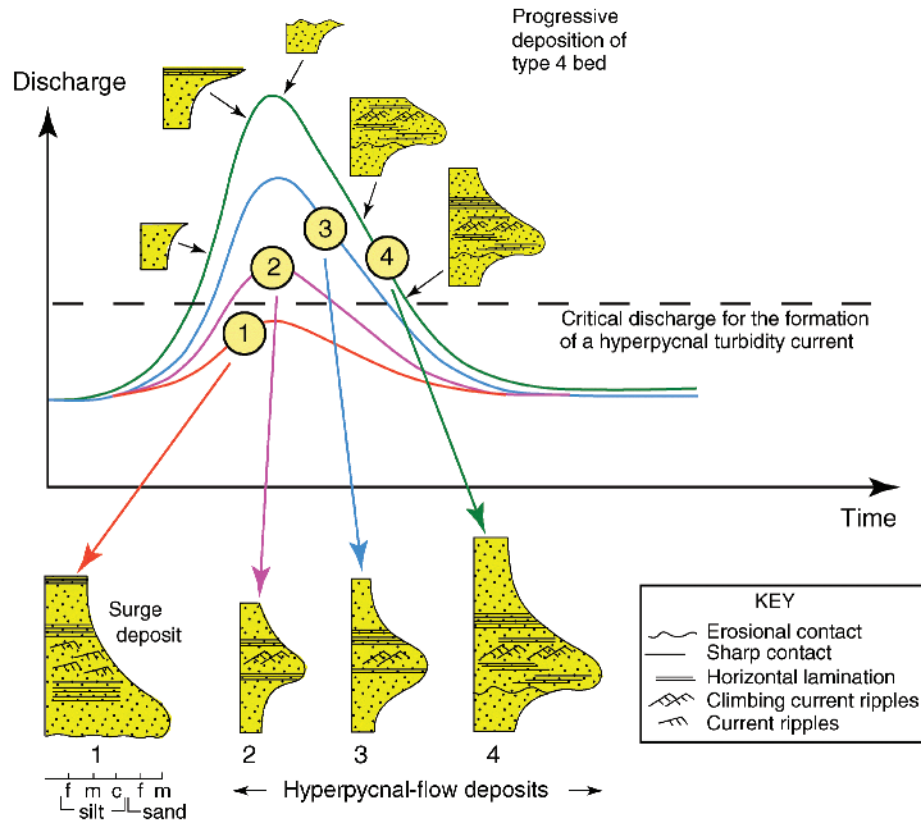
Fig. 1.37 Comparison of normally graded surge-generated turbidites and inverse-to-normally graded hyperpycnal-flow deposits produced by the rising and then falling flood stage of a river. The grain size scale below column 1 has divisions of fine (f), medium (m) and coarse (c) silt, and fine (f) and medium (m) sand. Redrawn from Mulder *et al.* (2001).

Table 1.3   Typical gradients of submarine fans and basin-margin slopes

Location	Bottom gradient	Source
Upper passive-margin slope	3–6°	Heezen *et al.* (1959)
Lower passive-margin slope	1.5–3°	Heezen *et al.* (1959)
Passive-margin rise	0.1–1°	Heezen *et al.* (1959)
Transform-margin scarps	10–30°	Aksu *et al.* (2000)
Forearc basin flanks	6–12°	Tappin *et al.* (2007)
Accretionary prism lower slope	>8°	Tappin *et al.* (2007)
Submarine canyons	1–3°	Nelson & Kulm (1973)
Upper fan channels	0.2–0.5°	Barnes & Normark (1984)
Suprafan lobes	0.1–0.4°	Barnes & Normark (1984)
Lower fan	0.1–0.2°	Barnes & Normark (1984)
Carbonate bank slopes	4–40°	Mullins & Neumann (1979)

1.5.3   Supercritical flow of turbidity currents

A fundamental distinction can be made between turbidity currents that are subcritical (Froude Number, F <1.0) and those that are supercritical (F > 1.0), where

$$F^2 = \frac{U_B^2}{\left(\frac{\Delta\rho}{\rho+\Delta\rho}\right)gd_B} \tag{1.6}$$

For dilute flows with $\Delta\rho/(\rho+\Delta\rho) \approx \Delta\rho/\rho$, Equation 1.6 reduces to

$$F^2 = \frac{U_B^2}{RCgd_B} \tag{1.7}$$

where R is the submerged weight of the grains ($\sim$1.65 g cm^{-3} for quartz) and C is the volume fraction of grains. This formulation for the Froude number is only valid for dilute turbidity currents, but is useful when trying to understand the relationship between flow concentration and the transition to supercritical flow. Clearly, the most dilute

currents ($C \ll 1.0$) will be supercritical even at low velocities (but see Huang *et al.* (2009) for caution regarding determination of the critical densimetric Froude number for transitions from supercritical to subcritical flow).

For a reasonable friction factor, $f = 0.02$, Komar (1971) concluded that turbidity currents would be supercritical on slopes $>0.5°$, a value exceeded on many basin-margin slopes and on the upper parts of submarine fans (Table 1.3; *cf.* Section 4.13). The transition to subcritical flow occurs as the bottom gradient declines, and may involve a hydraulic jump with intense turbulence and flow homogenisation (Middleton 1970; Komar 1971), as well as creation of an upcurrent-migrating bore in confined mini-basins (Toniolo *et al.* 2006). Hydraulic jumps have considerable effect on the formation of widespread scours and lenticular deposits of all scales (Mutti & Normark 1987, 1991; Garcia & Parker 1989; Alexander & Morris 1994; Vicente Bravo & Robles 1995).

1.5.4 Autosuspension in turbidity currents

It is frequently claimed that turbidity currents can effectively carry sand-sized detritus across basin-margin slopes without leaving a deposit: there may even be net erosion in these areas (i.e., flow *ignition*). Weaver (1994) demonstrated slope bypassing by large mud-rich turbidity currents entering the Madeira Abyssal Plain (*cf.* Stevenson *et al.* 2013) by examining their reworked coccolith assemblages. Such 'bypassing' requires that the turbidity current be at the least self-sustaining on the slope, or while flowing through slope channels. This process of 'self maintenance' (Southard & Mackintosh 1981) was named *autosuspension* by Bagnold (1962), and is summarised in Figure 1.38. In words, the excess density of the grain suspension, combined with the downslope component of gravitational acceleration, induces basinward flow. The turbulence generated by the flow maintains the grains in suspension (Middleton 1976; Leeder 1983; Eggenhuisen & McCaffrey 2012), and the suspension maintains its density contrast with the overlying seawater, allowing continued flow, turbulence generation and effective grain suspension. According to Middleton (1966c), Allen (1982: II, p. 399) and Pantin (1979), true autosuspension is probably not common in nature, except for thick turbidity currents carrying fine particles on steep slopes. For all other cases, some of the suspended load settles through the flow and is deposited.

Southard and Mackintosh (1981) and Middleton and Southard (1984) claim that Bagnold's (1962) mathematical formulation of the autosuspension criterion fails to find support in experiments. This shortcoming is ascribed to flaws in Bagnold's (1962) energy-balance equation, resulting in a 'fallacious system of energy bookkeeping' (Paola & Southard 1983). As outlined by Middleton and Southard (1984), Bagnold's (1962) equations do not account for the fact that only a small percentage of a flow's power, about 2%, is available to suspend sediment, the rest being expended to overcome frictional resistance at flow boundaries and to produce turbulence and heat, most of which does not contribute to grain suspension. This over-estimation of available power by Bagnold (1962) was remedied by Pantin (1979), who introduced an efficiency factor, e, into the formulation of an autosuspension criterion. This criterion is:

$$e\alpha U_s > w \tag{1.8}$$

where α = slope angle, U_s = transport velocity of the suspended sediment and w = grain settling velocity. In a worked example, Pantin
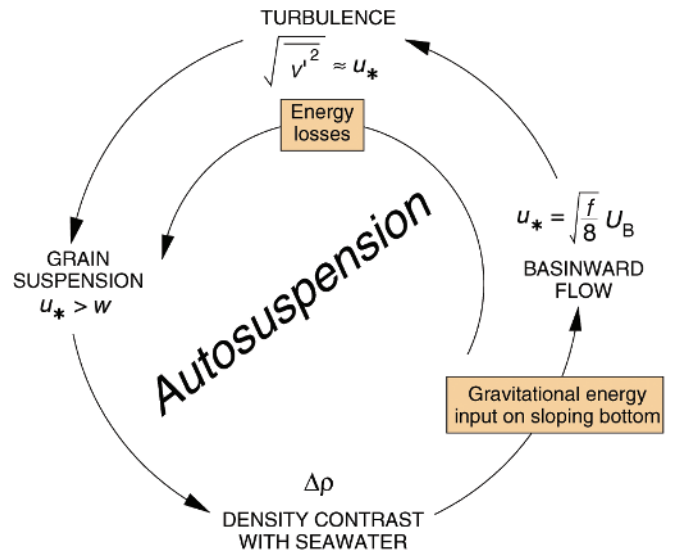

Fig. 1.38 Conceptual diagram to explain autosuspension. If gravitational energy input = energy losses, the flow will be self maintaining, and grains with settling velocity w will be kept in suspension by vertical velocity fluctuations of average strength $\sqrt{\overline{v'^2}}$, approximated by u_*.

(1979) sets $e = 0.01$. In general, Pantin (1979) shows that flow density is the main control on whether autosuspension will occur. Below a critical density, which varies with slope, flow thickness, grain size and drag coefficient, a turbidity current will 'subside' and deposit its sediment. Above the critical density, the flow will 'explode' (i.e., ignite) and will achieve autosuspension. This latter condition is only predicted for sediment finer than fine sand. Autosuspension has been achieved in small-scale laboratory experiments by Pantin (2001). Application of the theory of Pantin (1979) and Parker (1982) to conditions for initiation of erosive turbidity currents in Scripps Submarine Canyon, California, suggests that ignition of turbidity currents will occur for initial down-channel velocities in excess of about 0.5 m s^{-1} (Fukushima *et al.* 1985), in general agreement with field observations on the conditions required for initiation of flows in this canyon by Inman *et al.* (1976).

1.5.5 Effects of obstacles in the flow path

In natural settings, turbidity currents must flow over or around obstacles. In extreme cases, the obstacle is insurmountable and the turbidity current is reflected back on itself, leading to peculiar deposits with internal flow reversals and grain-size breaks created by successive passes of the depositing flow over the same site (Pickering & Hiscott 1985; Haughton 1994). More commonly, the flow is deflected, or perhaps is forced to decelerate in order to climb over the obstacle. The deviation from the original flow path is greatest when the height of the obstacle is comparable to the flow thickness. Laboratory-scale experiments have been used to study the effects of different obstacle heights and geometries (Kneller *et al.* 1991; Alexander & Morris 1994; Kneller 1995; Morris & Alexander 2003). Deposits are predictably thin over the top of obstacles, but can also thicken abruptly in front of barriers oriented oblique to flow because of hydraulic jumps created by the flow perturbation at the obstruction (Fig. 1.39).
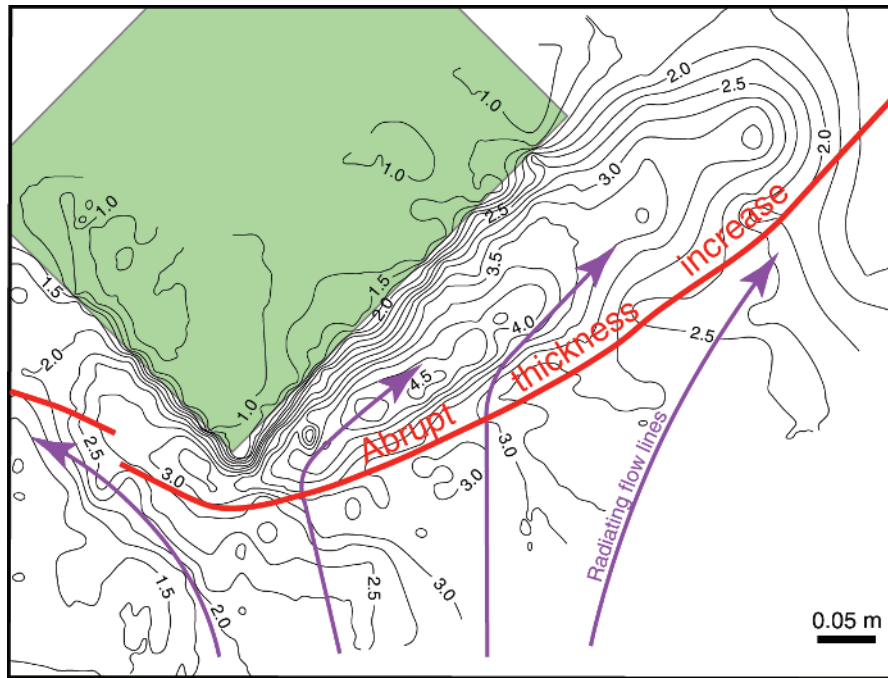
Fig. 1.39 Thickness of the sedimentary deposit in an experimental tank in the presence of an obstacle oriented oblique to the radiating flow. Contours are in millimetres of thickness. The spreading turbidity current (purple vectors) came from the bottom of this map. The obstacle (green) is a wedge with leading edge 2.4 cm high. Initial suspension density was 1.222 g cm^{-3} (10%), maximum head velocity was 24 cm s^{-1}, and grain size was 80 μm. The obstacle induced a hydraulic jump. Downflow of this jump, flow expansion caused a velocity drop and enhanced deposition (beyond the red line marked 'abrupt thickness increase'). Flow vectors (purple) changed sharply at the position of the jump. Redrawn from Morris and Alexander (2003).

1.5.6   Turbidites

Deposits of turbidity currents are called *turbidites*. They show evidence of grain-by-grain deposition from evolved currents (i.e., those in which particles are sufficiently mobile that they can become size-sorted either vertically or laterally in the flow). Such evidence includes size grading, presence of lamination, or organised grain fabric with moderate to low angles of imbrication (Hiscott & Middleton 1980; Arnott & Hand 1989). As explained by Mulder and Alexander (2001), the imprint of fluid turbulence and grain-by-grain behaviour should be stronger in these deposits than the imprint of grain-to-grain interactions (Fig. 1.22). The character of turbidites depends as much on the mode of deposition as on the long-distance transport mechanism (Fig. 1.1). Depositional process is mainly a function of (i) flow concentration near the sediment bed and (ii) rate of deposition. Rate of deposition is dependent on the rate of decrease of both flow *competence* – the coarsest particle that can be transported, and flow *capacity* – the sediment discharge, in units of volume or mass per unit time, integrated over the cross-section of the flow. Competence and capacity both decrease as mean velocity decreases (Hiscott 1994a). Velocity may decrease for any of the following reasons: (i) decreasing bottom slope; (ii) flow divergence; (iii) increased bed friction; (iv) increased particle interaction (intergranular friction); (v) decreasing flow density due to deposition; or (vi) deflection of slow, mud-rich flows by contour currents or by the Coriolis effect so that they are constrained to move roughly parallel to the slope contours rather than down the slope (Hill 1984a). Van Andel and Komar (1969) provide mathematical expressions for the momentum losses in a turbidity current due to grain-to-grain friction, bottom and interfacial friction,

and sediment loss due to deposition. Flows with a high proportion of suspended mud can flow for a greater distance than mud-poor flows without suffering a crippling degree of sediment loss, even on quite gentle slopes (Salaheldin *et al.* 2000). Such flows are therefore more 'efficient' in moving both their mud- and sand-size loads into the basin. The relative 'efficiencies' of turbidity currents have been used by some workers to characterise types of submarine fans (Chapter 7).

The slowing of a turbidity current with velocity u can be expressed mathematically as $du/dt < 0$, where t is time and $du/dt = \partial u/\partial t + u \cdot \partial u/\partial x$. The slowing can be one of, or a combination of, (i) a temporal deceleration at a fixed observation point (non-steady flow with $\partial u/\partial t < 0$, called *waning flow*), or (ii) a spatial deceleration along the flow path (non-uniform flow with $u \cdot \partial u/\partial x < 0$, called *depletive flow* by Kneller 1995 and Kneller & Branney 1995). Deposition is assured by a combination of depletive and waning flow, but other combinations are possible (Fig. 1.40). Five combinations of spatial and temporal deceleration and acceleration (the latter called *accumulative flow* and *waxing flow* by Kneller 1995) may generate deposits with distinctive grading profiles or structural sequences (Fig. 1.41). Accumulative and/or waxing flows can cause erosion and sediment entrainment (e.g., flow ignition), whereas flows with no net acceleration or deceleration (i.e., $\partial u/\partial t + u \cdot \partial u/\partial x = 0$) will bypass, leaving little if any record. The determination of a velocity/time/distance history for a turbidity current (Fig. 1.42) is an instructive way to understand the progress of deposition.

Komar (1985) attempted to use the median size of eleven samples through a mainly laminated and cross-laminated Miocene turbidite to infer the velocity history of the waning turbidity current. He found serious discrepancies between the velocity estimates based on grain
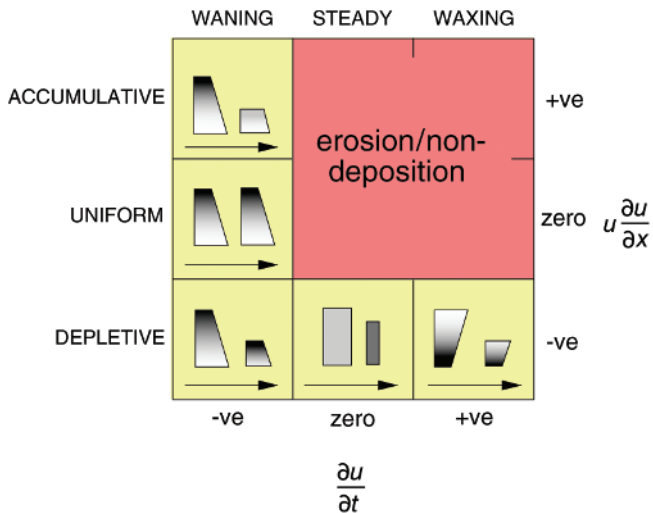
Fig. 1.40 Definition diagram for spatially and temporally accelerating and decelerating turbidity currents. The former accumulate or deplete, whereas the latter wax and wane. Arrows point downflow. Predicted grading profiles are shown, with white = sand and black = mud. Redrawn from Kneller (1995).
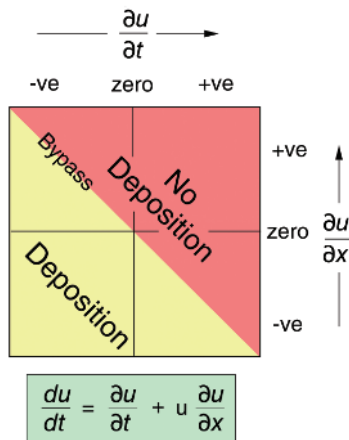

Fig. 1.42 Graphical representation of the velocity history of a turbidity current (arrow) as it changes with time (*t*) and distance along the flow path (*x*). Redrawn from Kneller (1995).

$$\frac{du}{dt} = \frac{\partial u}{\partial t} + u\,\frac{\partial u}{\partial x}$$

Fig. 1.41 Subdivision of acceleration space into fields characterised by deposition, non-deposition (or erosion) and bypass. Redrawn from Kneller (1995).

size and an estimate based on the transition from upper to lower flow regime conditions. Hiscott (1994a) showed that this discrepancy might be the result of an unjustified assumption that turbidity currents deposit their suspended load because they become incompetent to carry some of that load. Instead, Hiscott (1994a) argued that the fundamental control on deposition is the progressive loss of the *capacity* to maintain a particular sediment discharge as turbulence intensity decreases (see also Leeder *et al.* 2005). Even at velocities considerably higher than those needed to suspend individual particles of a particular size, a turbidity current that is at its full capacity must lose some of this load through deposition if the flow velocity decreases.

As an example, consider a turbidity current carrying a maximum particle size of 1 mm. Using the suspension criterion of $u_* > w$, a flow with shear velocity greater than about 12 cm s^{-1} would be competent
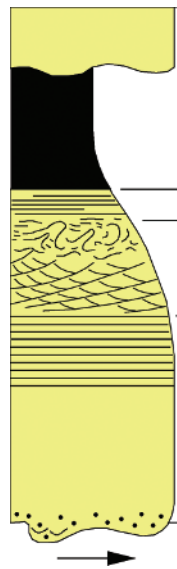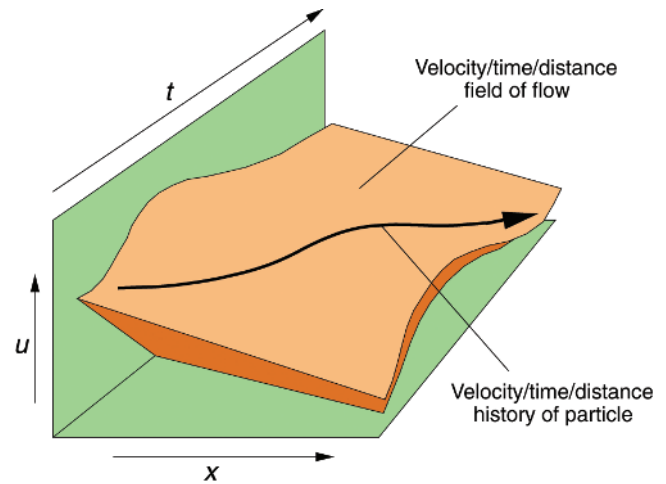
to suspend the coarsest grains (Blatt *et al.* 1980: p. 65). Nevertheless, a flow at full capacity (i.e., holding as much suspended load as turbulence intensity allows), carrying a maximum size of 1 mm, and decelerating from shear velocities of 50 → 20 cm s^{-1} (mean velocities about ~15 → 5.5 m s^{-1}) would drop about 85% of its suspended load (including essentially all of the 1 mm particles). This deposition would not occur immediately, because of a lag between the time of the onset of grain settling and the time at which a particle arrives at the bed. Nevertheless, a large fraction of the original suspended load could be deposited by such a flow, even though it would be at all times competent to carry even the largest grains in suspension. What controls deposition is the natural limit on the *amount* of suspended load that can be carried (i.e., sediment discharge), rather than the limit on the size of the largest particle that can be suspended in a clear flow of the same velocity. Clearly, flow velocities calculated using competence considerations can only provide minimum estimates – a turbidity current might be travelling much faster than such an estimate based solely on competence, yet still deposit a wide range of suspended particles.

Experimental monitoring of deposition from turbidity currents has only rarely been attempted. These laboratory studies are inadequate analogues for deposition from much larger natural flows, but provide some insight into depositional processes. Middleton (1967) monitored deposition of graded beds from both low- and high-concentration flows (i.e., from turbidity currents and concentrated density flows). Low-concentration flows deposited beds with good distribution grading; because of the nature of the experiments, no traction transport took place, and no lamination nor bedforms were generated. Lüthi (1981) studied deposition from unconfined turbidity currents that were free to expand laterally after leaving a narrow entry slot. With increasing distance from the entry slot, velocity and grain size both decreased, and sedimentary structures changed from parallel lamination, to climbing-ripple lamination, to fine parallel lamination. These structures are the same as in vertical sections through ancient turbidites, and correspond respectively to the Bouma (1962) divisions T_b, T_c and T_d.

By far the most detailed observations of the internal characteristics of turbidites come from study of ancient sediments. The Bouma

Fig. 1.43 Ideal sequence of sedimentary structures in a turbidite bed (from Bouma 1962, with interpretation from Harms & Fahnestock 1965; Walker 1965; Middleton 1967; Walton 1967; Stow & Bowen 1980).

(1962) sequence (Fig. 1.43) represents a summary of the transitions observed in 1061 beds in the Grès de Peïra-Cava in the Maritime Alps of southern France. In a complete Bouma-type turbidite, the T_a division was probably deposited during a phase of rapid fallout from suspension, without traction. Other divisions have been interpreted in relation to the progression of bedforms observed during deceleration of flow in flumes (Harms & Fahnestock 1965; Walker 1965), but with omission of dunes. Most natural turbidites do not contain all five Bouma divisions, but instead are missing one or more basal division. Beds lacking upper divisions and dominated by structureless sand are more likely the deposits of concentrated density flows (see Section 1.6). The Bouma sequence is a good model for medium-grained deposits of many surge-type turbidity currents (Mulder & Alexander 2001), but is too general for fine-grained turbidites that consist entirely of Bouma's T_d and T_e divisions.

For a completely contrary opinion on the genesis of the Bouma (1962) divisions T_b–T_d, readers are directed to Shanmugam (2000, 2008), who attributes the laminated nature of these divisions to reworking of the tops of sand beds by deep-water bottom currents generated by thermohaline circulation, ocean tides, shoaling internal waves or atmospheric winds. In his view, the original sand beds are more likely to have been deposited by sandy debris flows (our inflated sandflows) than by turbidity currents. Shanmugam (2000) only ascribes the normally graded parts of a basal T_a division to direct accumulation beneath a turbidity current. As one argument, Shanmugam (2000) points to the uncommon occurrence of complete Bouma sequences in nature, and extends this argument further to suggest that if turbidity currents are responsible for the lamination, then there should be documented examples of beds possessing all 16 divisions of the Lowe (1982), Bouma (1962) and Stow and Shanmugam (1980; Fig. 1.47) idealised structural sequences, which those authors have attributed to accumulation beneath decelerating turbulent density currents. To quote: 'The absence of a complete turbidite bed with 16 divisions in the geologic record suggests that the ideal turbidite facies models are wrong' (Shanmugam 2000: p. 316). We dismiss this suggestion because it presupposes that the deceleration of a SGF takes place at a single point, so that the

entire range of sediment grain sizes and the entire spectrum of sedimentary structures might be found in a single core or outcrop. Instead, let us consider a SGF that descends the upper slope as an inflated sandflow, transforming through water entrainment and dilution into first a concentrated density flow and then a turbidity current. The first deposits would consist of the coarsest grain-size fractions, either structureless because of the high rate of fallout, or with structures indicative of particle interaction (e.g., spaced stratification of Hiscott 1994b). This material would be left behind, perhaps covered by a thin veneer of fine fallout of sediment from a residual dilute cloud (likely later eroded by subsequent flows), and the remainder of the flow would bypass this area and move farther downslope to deposit finer sediment with different sedimentary structures and different structural divisions. Hence, Shanmugam (2000) might be theoretically correct that a single SGF could deposit all 16 structural divisions if it had a sufficiently broad range of grain sizes in suspension, but these divisions would logically be strung out for tens to hundreds (or even thousands) of kilometres along the track of the evolving flow, and so would never be found at a single locality. More specific arguments against the interpretation of the laminated Bouma divisions as bottom-current deposits are found in Section 6.3 of this book.

1.5.7 Cross-stratification in turbidites

The general absence of dune-scale cross-stratification in Bouma-type turbidites can be explained in at least five ways.

- Walker (1965) suggested that deposition from turbidity currents is too rapid for bedforms to equilibrate with the decelerating flow. The result is that dunes, which require a significant time to develop because of their size, only begin to form by the time that velocity decreases to values consistent with ripple, not dune, stability. Allen (1969) used a similar argument (Fig. 1.44), that is, for grain sizes available in most turbidity currents 'the range of flow power appropriate to these forms was traversed too quickly, being narrow, to permit their growth' (Allen 1982: II, p. 414).
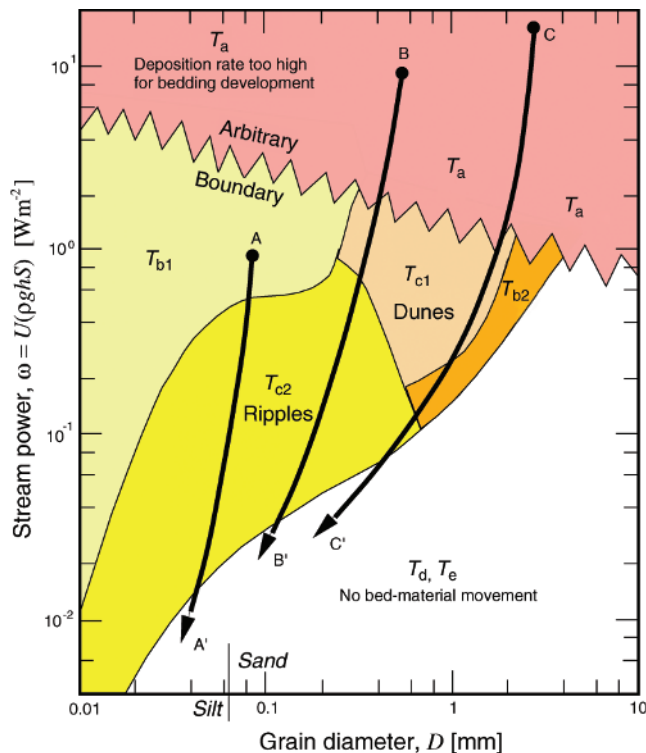
Fig. 1.44 Explanation of Allen (1969, 1982) for the absence of dune-scale cross-stratification in most turbidites. Once the rate of grain fallout declines sufficiently for tractional bedforms to develop, the stability field for dunes has either been bypassed, or there is not enough time for dunes to grow before current ripples become the stable bedform.

This is exacerbated by the fact that high rates of sediment fall-out during the early phases of deposition prevent the formation of lamination (see also Arnott & Hand 1989).

- Walker (1965) suggested that many turbidity currents may be too thin to allow formation of dunes, which only form if the ratio of flow depth to bedform height is about 5 : 1. For natural flows with velocity maxima below the flow top, and perhaps with strong internal density stratification, Walker (1965) suggested that flow thicknesses of 5–10 m might be necessary for the growth of dunes 50 cm high.
- For the appropriate flow conditions, most turbidity currents are depositing sediment too fine for production of dunes (Fig. 1.44 path AA′; Walton 1967; Allen 1982: II, p. 414). Experiments show that dunes are absent in sediment finer than 0.1 mm (Allen 1982: I, p. 339). This explanation gains strong support from the observation that coarse-grained bioclastic turbidites differ from generally finer grained terrigenous turbidites in that they may contain dune cross-stratification in association with the Bouma T_b division (Hubert 1966a; Thompson & Thomasson 1969; Allen 1970).
- Cross-stratification might be absent due to the occurrence of a hydraulic jump between deposition of the Bouma T_b and T_c divisions. Although upper flow regime planar lamination does not necessarily indicate supercritical flow, it may do so. Even long-wavelength antidune lamination (Hand *et al.* 1972) may be so subdued as to appear flat. Downstream of a hydraulic jump,

flow depth increases and velocity decreases sharply. This rapid velocity drop could cause complete omission of the dune stability field. Upstream migration of the hydraulic jump would result in superposition of ripples on a previously flat sediment bed. This mechanism is restricted to submarine slopes or the upper parts of submarine fans, where hydraulic jumps are believed to occur (Komar 1971).
- High suspended sediment concentrations in depositing currents might extend the conditions for stability of upper flow regime plane beds to lower velocities, so that the eventual transition to the lower flow regime would occur within the stability range for ripples, not dunes (Lowe 1988).

There are no data on the mechanics of deposition from large natural turbidity currents, but it is not improbable that all five explanations for lack of dunes in turbidites are valid in particular cases. It is interesting that increasingly numerous side-scan sonar surveys of submarine fan channels and channel-termination areas have documented the presence of large sand and gravel bedforms (Fig. 1.35), both transverse and parallel to flow (Piper *et al.* 1988; Malinverno *et al.* 1988; Hughes Clarke *et al.* 1990; Wynn *et al.* 2002b). To date, there is no evidence that these bedforms contain cross-stratification like that recognised in outcrops or cores (Piper & Kontopoulos 1994).

1.5.8   Antidunes in turbidites

It is unclear whether supercritical turbidity currents ($F > 1.0$) deposit any diagnostic sedimentary structures. In rivers and flumes, supercritical flows mould antidunes on the bed. These antidunes may migrate either upcurrent or downcurrent to produce internal lamination with low angles of dip (Middleton 1965). Skipper (1971) and Skipper and Bhattacharjee (1978) described cross-bed sets with wavy upper profiles at the base of some thick turbidites in the Ordovician Cloridorme Formation of Quebec, Canada, and interpreted these bedforms as short-wavelength antidunes (wavelength ~65 cm), based primarily on the observation that the foreset dip directions opposed the local palaeoflow as deduced from flutes. The hydrodynamic interpretation of these bedforms proved to be difficult (Hand *et al.* 1972), because antidune wavelength beneath turbidity currents should be of the order of 12 times the flow depth. Pickering and Hiscott (1985) have re-interpreted this part of the Cloridorme Formation as a basin-floor sequence deposited in a constricted foreland basin, in which large turbidity currents were repeatedly reflected and deflected from marginal slopes. Many individual graded beds have sole markings and divisions of cross-stratification or ripple lamination indicating flow reversals during deposition. Grain fabric data obtained by Pickering and Hiscott (1985) from the bedforms described by Skipper (1971) indicate that the depositing current flowed in a direction opposite to that indicated by most flutes in the sequence. These fabric results are supported by experiments of Yagishita and Taira (1989). The bedforms are therefore not antidunes, but instead record the migration of dunes under subcritical flow conditions (Fig. 1.45).

Prave and Duke (1990) and Yagishita (1994) described wavy bedforms with lengths of about 1 m from turbidites, and interpreted these as antidunes. The lamination within the structures described by Yagishita (1994) is *spaced stratification*, which we argue below is produced beneath vigorous unsteady flows. Both of these interpretations have the same problem as the original Skipper (1971) interpretation, in that the bedform wavelength is unreasonably short for antidunes beneath turbidity currents, unless the turbidity currents were strongly stratified. Although the jury is still out on this issue, we suspect that
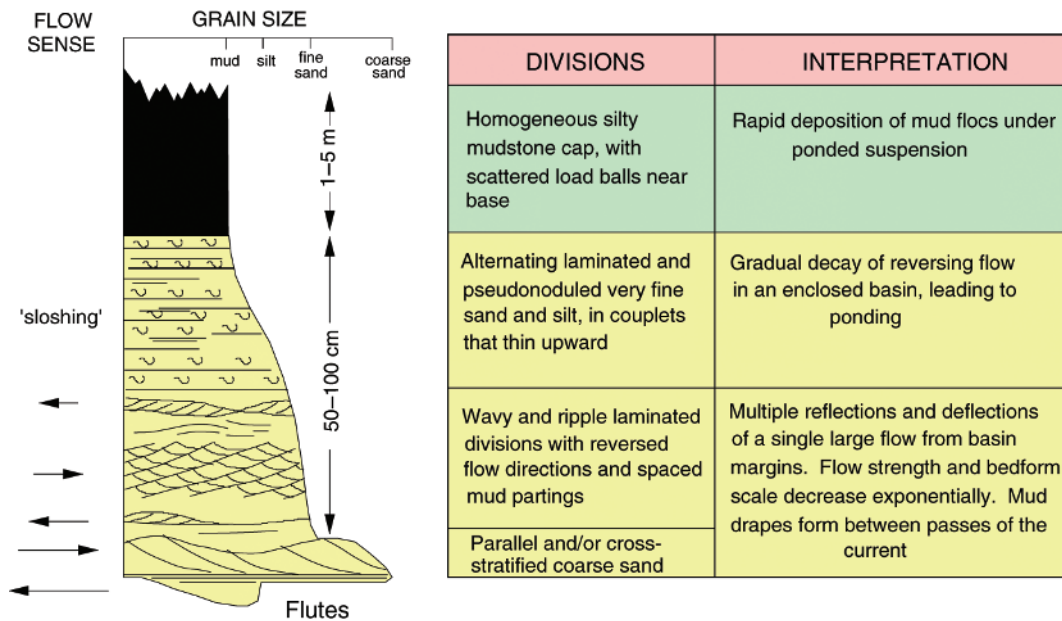
Fig. 1.45 Generalised sequence of internal structures produced beneath large reflected turbidity currents (Pickering & Hiscott 1985). The thick mud cap is deposited after the flow becomes ponded within a confined basin. Single beds of this type may be >10 m thick.

true antidune lamination is either exceedingly rare or is not discernable in deposits because of its long wavelength and low amplitude in turbidites.

Some exceedingly large mud waves on the levées of the Monterey Fan (Fig. 1.46; wave height 2–37 m, wavelength 0.3–2.1 km) have been interpreted as antidunes formed beneath low-concentration, low-velocity turbidity currents ($u \sim 10$ cm s^{-1}) ~ 100–800 m thick (Normark *et al.* 1980). Other levée systems and some unconfined slopes are characterised by long-wavelength mud waves that are interpreted to have been initiated as antidunes (Ercilla *et al.* 2002, Normark *et al.* 2002). The layering in these mud waves would appear flat in both deep-sea cores and outcrops. Younger fine-grained turbidites and hemipelagic sediments may drape the wave forms and maintain their morphology, well after conditions of supercritical flow cease to occur.

1.5.9   Turbidites from low-concentration flows

The deposits of low-concentration, mud-load turbidity currents have been described by Piper (1978), Stow (1979), Stow and Bowen (1980), Stow and Shanmugam (1980) and Stow and Piper (1984b). The Bouma (1962) divisions for sandy turbidites are too general for mud turbidites; many beds contain only Bouma's T_d and T_e divisions. Several schemes to further subdivide mud turbidites have been proposed, and are outlined in Figure 1.47. Stow and Shanmugam (1980) recognised nine divisions, numbered T_0 to T_8. The physical structures in these nine divisions are believed to result from suspension fall-out and traction (T_0–T_2), shear sorting of silt grains and clay floccules in the bottom boundary layer (T_3–T_5) and suspension fall-out with no traction (T_6–T_8). Division T_0 corresponds to Bouma's division T_c. As with Bouma-type turbidites, complete structure sequences are unusual; top-absent, base-absent and middle-absent sequences are common (Stow & Piper 1984b). The very thin, regular laminations of division T_3 have been attributed to shear sorting near the base of the flow and then alternating deposition of silt grains and clay particles by settling through the viscous sublayer (Stow & Bowen 1980; Kranck 1984). According to this model, as the silt grains and clay floccules fall toward the bed, the increased shear in the boundary layer causes the clay flocs to break up (Fig. 1.48a). The silt grains then settle through the viscous sublayer to form a silt lamina (Fig. 1.48b). As more sediment is supplied to the top of the boundary layer, the mud concentration builds up, and some reflocculation may occur (Fig. 1.48c). At some critical concentration, the clays are able to form sufficiently large aggregates that they escape disaggregation by shear stresses and are able to settle rapidly through the viscous sublayer to form a mud lamina (Fig. 1.48d). The cycle of silt and mud deposition is then repeated for successively finer grain sizes.

A second interpretation for fine-scale lamination in fine-grained turbidites has been proposed by Hesse and Chough (1980). The silt-rich laminae are believed to form during periods when bursts and sweeps repeatedly disturb the viscous sublayer of the flow, resulting in transport of clay-sized particles away from the boundary. The composite nature of individual silt laminae is used as support for this model. Clay-rich laminae are attributed to periods when bursts and sweeps are suppressed, perhaps by passage of large eddies. Alternatively, flow pulsing (Best *et al.* 2005) might account for the fluctuations in the viscous sublayer.

Stow *et al.* (1990) has proposed the term *hemiturbidite* for subtly banded, largely bioturbated muds on the distal Bengal Fan. He interprets these muds to represent deposition during the waning stages of turbidity current flow, probably over time periods from a few weeks to a few months for a 1 m-thick unit. *Flow lofting* (that is, detachment of the final dilute suspension from the seafloor because of positive buoyancy) produces the final cloud of suspended clay and mud that settles to produce the uppermost mud layer. On the Amazon Fan, Damuth and Kumar (1975a) described grey 'hemipelagic' muds that were interpreted to have been derived from dilute, thick, mud-laden turbidity currents spreading over the entire
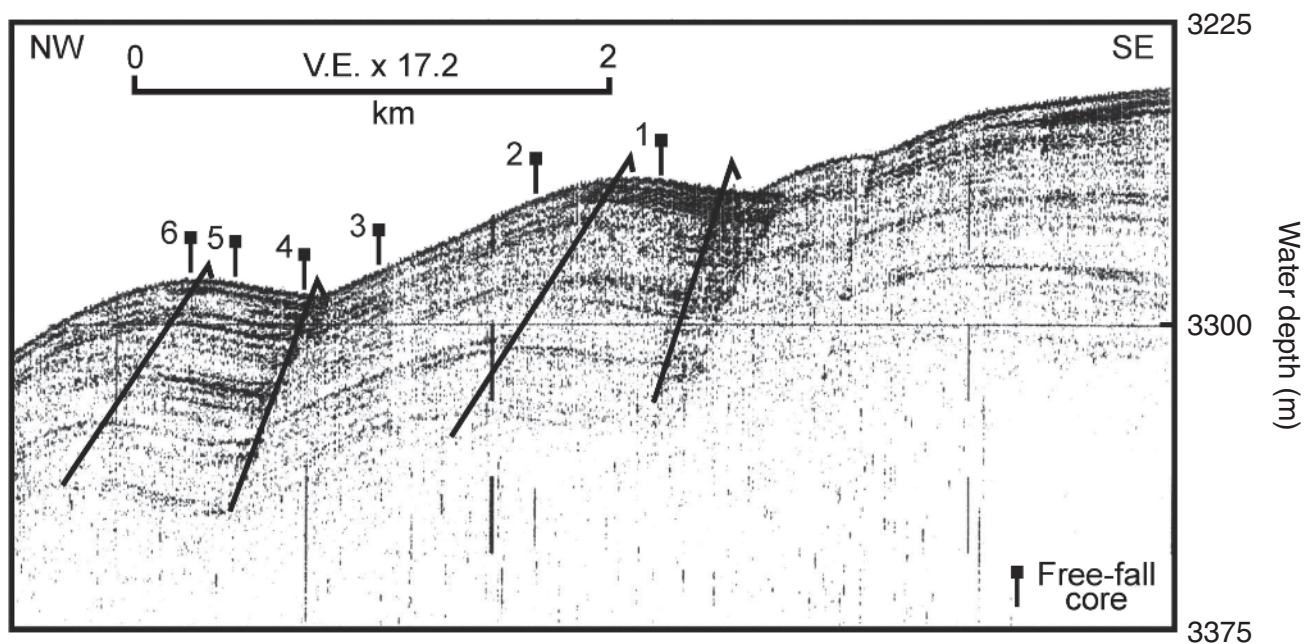
Fig. 1.46 3.5-kHz profile of sediment waves on western levée of Monterey Fan valley. The levée crest is 20 km to the right. Arrows show migration of sediment-wave crests and troughs. From Normark *et al.* (2002).
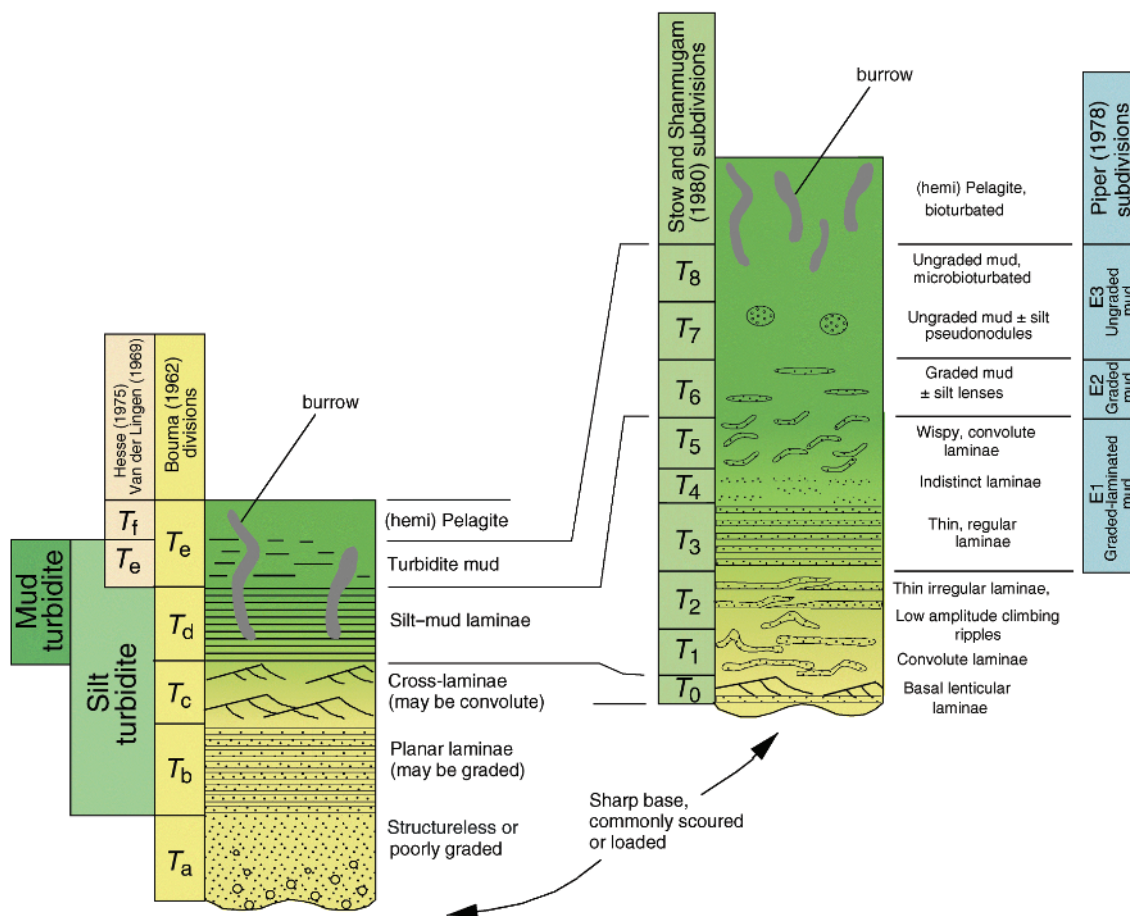

Fig. 1.47 Summary of schemes for subdivision of fine-grained turbidites, based on Hesse (1975), Piper (1978), van der Lingen (1969) and Stow and Shanmugam (1980).
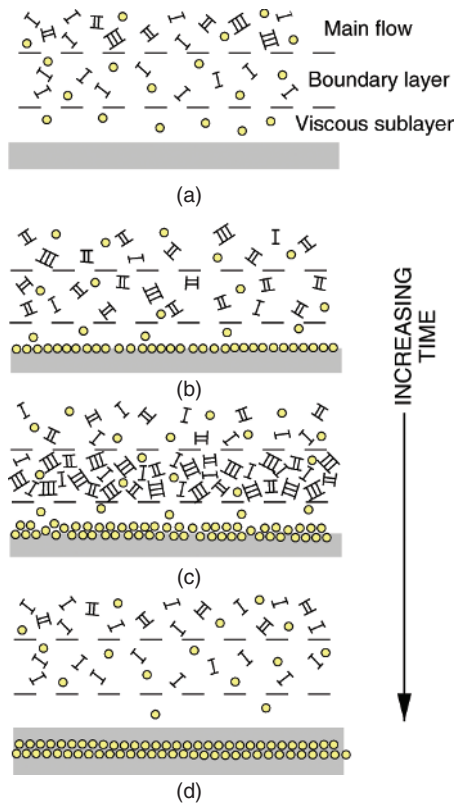
Fig. 1.48 (a–d)Schematic representation of the four stages of silt and mud deposition through the boundary layer of a turbidity current to form silt and mud laminae. From Stow and Bowen (1980).

fan. These muds are probably analogous to the hemiturbidites of Stow *et al.* (1990).

1.5.10   Downcurrent grain size – bed thickness trends in turbidites

Turbidites derived from a single source with a consistent range of grain sizes have been shown to exhibit a well-defined relationship between bed thickness and grain size (Fig. 1.49) (Sadler 1982). Sadler's curves indicate a downslope trend from (i) proximal, relatively thin, medium-grained beds, to (ii) intermediate, relatively thick, somewhat coarser grained beds, to (iii) progressively finer-grained and thinner beds with increasing distal transport. The 'distal limb' of this trend is relatively easy to explain. Sadler (1982) calculated that 'for a given flow density and slope and with a uniform grain-size distribution, bed thickness becomes proportional to the square root of bed shear stress cubed'. Hence the decrease of both competence and capacity as turbidity currents decelerate leads to a related decrease of both grain size and bed thickness. The 'proximal limb' of the trend involves a temporary downslope increase in both grain size and bed thickness, and requires a special explanation. Sadler points to experiments of Kuenen (1951) that show a longitudinal decline of density and competence from the head to the tail of a turbidity current. As a flow that is in a state of autosuspension decelerates, deposition will begin beneath the tail of the current where competence and flow density are relatively low. 'The most proximal part of the deposit will therefore thicken and coarsen downcurrent until the point at which all of the flow, except a small region near the head, will be depositing sediment' (Sadler 1982: p. 48).

Dade and Huppert (1995) also predicted that deposit thickness first increases and then decreases for beds laid down on basin plains. They give a different explanation than Sadler (1982) for this geometry: 'At early times, the rapidly moving body of the turbidity current passes over a point very quickly and so little mass is laid down despite high rates of deposition … At large times, duration of passage of the surge over a fixed point is much longer, but the slowly moving current has relatively little to deposit.'

Dade *et al.* (1994) developed a mathematical model that relates deposit thickness for turbidites laid down on slopes to flow velocity,

$$BT = \frac{U_B w_s \cos \alpha}{kF^2 g'_b} \tag{1.9}$$

where w_s = average settling velocity, BT = bed thickness, $g'_b = g\phi_b[(\rho_{clasts}-\rho)/\rho]$, ρ = seawater density, ϕ_b = volume fraction of solids in the bed, α = slope gradient, U_B = surge velocity, k = (surge height)/(surge length) and F = Froude number (nearly constant except near the distal point of deposition). In this case, BT is proportional to the square root of bed shear stress (because $\tau_o \propto [U_B^2]$), not $\tau_o^{3/2}$ (Sadler 1982).

1.5.11   Time scales for turbidite deposition

Time scales for deposition can be looked at in three ways:

(1) the time taken to deposit a turbidite at one location on the seafloor;

(2) the total time that it takes for a turbidity current to travel from the place where it was initiated to the place downslope where it loses its identity;

(3) recurrence intervals (or frequencies) of turbidite emplacement.

The time taken to deposit a turbidite at one location on the seafloor is similar to, but potentially less than, the time taken for the turbidity current responsible for the deposit to pass a particular cross-section. If the head and frontal part of a turbidity current are erosional or non-depositional, then the deposit might form only during a short part of the total transit time. At the extreme, it might take several weeks for the cloud of fine-grained suspension to dissipate after passage of a large turbidity current, particularly in confined basin plains (Pickering & Hiscott 1985). This recovery phase for the return of the local water column to its pre-flow condition is not generally considered when evaluating the time to deposit turbidites at a single site. Instead, accumulation times for sand/silt divisions, commonly Bouma divisions T_a through T_d, are assessed. Arnott and Hand (1989) studied the development of sedimentary structures and fabric under experimental conditions of a steady rain of suspended sediment to the bed. They determined a linear relationship between imbrication angle in degrees, β, and the bed aggradation rate in cm min^{-1}, x; that is

$$\beta = 10.7 + 1.36x \tag{1.10}$$

For some Ordovician turbidites from the Appalachians, this relationship gives aggradation rates of 7–12 cm min^{-1}, and a requirement of 1.25 h to deposit a 9.1 m-thick sand bed described by Hiscott and Middleton (1980). Allen (1991) used aggradation rates published for
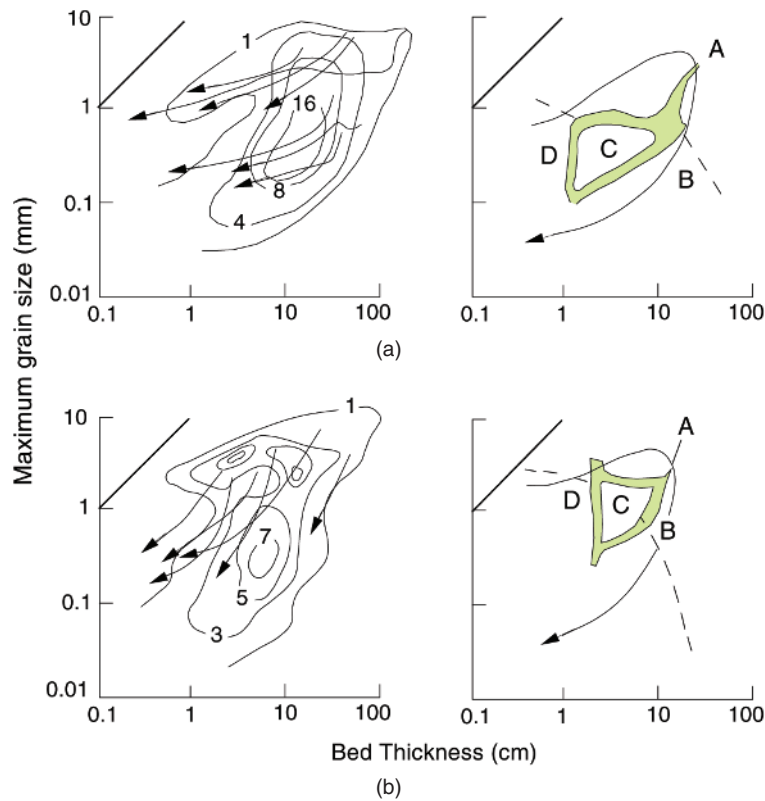
Fig. 1.49 Maximum grain size plotted against bed thickness for Lower Carboniferous turbidites of (a) the Rhenaer Kalk (498 beds), and (b) the Posidonienkalk (235 beds), from Sadler (1982). The left-hand diagrams show contours of density of data points representing total bed thickness and corresponding maximum grain size. Arrows are selected vertical grading curves using the x-axis scale as a 'distance to top of bed'. The right-hand diagrams show fields for Bouma divisions T_a through T_d found at the base of the beds for which maximum size was determined. Green zones = overlap of fields for divisions T_b, T_c and T_d. Dashed line = lower limit of field for division T_a, which has extensive overlap with the other fields. Arrow = modal horizontal grading curve, based on contour pattern in left-hand diagram.

the transition from divisions T_a to T_b (Arnott & Hand 1989) and the transition from division T_b to climbing ripple lamination of division T_c (Allen 1971) to estimate a few tens of minutes for deposition of the 27 cm-thick turbidite described by Komar (1985). Piper *et al.* (1988), using deposit volume and channel discharge estimates for the 1929 Grand Banks event, concluded that the turbidity current must have taken 2–3 h to pass a particular channel cross-section on its way to the Sohm Abyssal Plain. Jobe *et al.* (2012) calculated sedimentation rate and accumulation time for 44 climbing-ripple cross-laminated intervals from three field areas using TDURE (a mathematical model developed by Baas *et al.* (2000)). For T_c divisions and T_{bc} beds averaging 26 cm and 37 cm thick, respectively, average climbing-ripple cross-lamination and whole-bed sedimentation rates were 0.15 mm s^{-1} and 0.26 mm s^{-1} and average accumulation times were 27 min and 35 min, respectively.

For relatively compact surge-type flows, the time required for a turbidity current to travel from the place where it was initiated to the place downslope where it loses its identity because nearly all sediment has been deposited is approximately the total path length divided by the time-averaged head velocity. Time scales for large natural currents are a few days (e.g., Dade & Huppert 1995 for the Black Shell turbidite). Timing of cable breaks indicates that the 1929 Grand Banks turbidity current took about one day to reach about 34°N on the Sohm Abyssal Plain (Doxsee 1948; Piper *et al.* 1988).

Turbidity currents transiting the ~800 km-long Amazon Channel crossing the Amazon Submarine Fan (Chapter 7) at average speeds of about 1 m s^{-1} (Pirmez 1994) would take about 9 days to complete their journey. A slow-moving mud-load turbidity current crossing the Navy Fan in the California borderland flowed for about 6 days (Bowen *et al.* 1984). Some turbidity currents are believed to be semi-continuous events, either during extended periods of peak river discharge for hyperpycnal flows, or when industries discharge suspensions over a period of weeks to months (Hay 1987b).

The frequency of turbidity currents can be estimated by dividing the age of a stratigraphic column by the number of turbidites it contains. This procedure requires that there has been no seafloor erosion. Only those turbidity currents which reached the site and deposited sediment there can be included, so this procedure underestimates the total number of turbidity currents generated by upslope failures, many of which might have followed a path leading away from the sampling site. In successions containing beds of different thicknesses, the frequencies of deposits of different thickness can be evaluated separately, although the small number of some beds can make frequency calculations untrustworthy.

There is a wide reported range of recurrence intervals, dependent both on variable rates of sediment supply and triggering mechanisms for initial failures. For example, thin Pleistocene turbidites forming colour-banded muds in the levées of the Amazon Fan,

which accumulated at rates as high as 25 m kyr^{-1}, are potentially near-annual in their frequency (Hiscott *et al.* 1997b). Piper and Normark (1983) estimated recurrence frequencies of 1–1000 yr for turbidity currents reaching different parts of the Navy submarine fan. Simm *et al.* (1991) determined a frequency of about 25 kyr for large fine-grained turbidity currents reaching the Madeira Abyssal Plain during the past 127 kyr. For seven bed-thickness classes from 1–3000 cm in an Oligocene forearc-basin succession from the western Pacific, Hiscott *et al.* (1993) determined turbidity-current recurrence intervals of 3–1000 yr.

1.6   Concentrated density flows and their deposits

Experimental and theoretical understanding of concentrated density flows lags far behind the understanding of turbidity currents. The high concentrations (∼15–40% by volume, Fig. 1.21) that lead to distinctive deposits might be limited to the lower parts of stratified flows which, farther above the bed, are less dense and more turbulent. The features seen in the deposits of these flows certainly demonstrate significant grain-to-grain interaction and imply a suppression of turbulence near the sediment bed (Fig. 1.20). According to Mulder and Alexander (2001) and others, depositional processes include: (i) rapid en masse deposition of a quick bed (Middleton 1967) due to an increase of intergranular friction; (ii) generation of inverse grading at the base of the flow because of grain collisions and dispersive pressure; (iii) formation of *spaced stratification* (formerly called *traction carpets*) under unsteady flows (Hiscott & Middleton 1979, 1980; Hiscott 1994b; Sohn 1997); (iv) grain-by-grain deposition with little subsequent traction transport (Arnott & Hand 1989); (v) alternate deposition of bedload and suspended load (Walker 1975a); (vi) deposition of mudclasts well above the base of the bed and (vii) expulsion of pore-fluids when the primary, unstable, open-grain packing collapses, generating fluid-escape structures (Lowe & LoPiccolo 1974).

Because the transition between a turbidity current and a concentrated density flow depends on the relative importance of fluid turbulence and other mechanisms in providing particle support, it is possible for a single current to undergo one or more transition between these flow types during its history. This might occur if an undulatory seabed, or variable amount of flow confinement, leads to alternating increases and decreases in speed along the flow path (Kneller & Branney 1995; Fig. 1.42). Sharp decreases in speed would induce higher rates of particle fallout and intensified grain-to-grain interactions in the lower part of the flow. If these alternative support mechanisms dominate the depositional phase, then the deposits will reveal structures characteristic of deposition from a concentrated density flow rather than a turbidity current. Hence, it should always be remembered that these two flow types might be transitional when making interpretations about depositional environment and deposit distribution.

1.6.1   Deposits from concentrated density flows

In experiments on deposition from high-concentration flows, Middleton (1967) demonstrated rapid, en masse deposition leading to the formation of a 'quick bed' that was easily deformed by Helmholtz waves at the top of the deposit. The deposit was characterised by coarse-tail grading. Field studies have revealed sedimentary structures not present in the Bouma (1962) sequence for turbidites. One of these was initially called traction-carpet stratification, but has since been renamed *spaced stratification* by Hiscott (1994b). The term *traction carpet* (Dzulynski & Sanders 1962: p. 88; Lowe 1982 division S2) was used to describe generally 5–10 cm-thick, inversely graded stratification found in some concentrated density-flow deposits (Fig. 1.50). As originally envisioned, clasts in such carpets were believed to be sheared as a dense dispersion just above the bed, maintained by dispersive pressure (Bagnold 1956), until a critical thickness was reached that prompted en masse deposition. Within each such deposit, intense grain interaction was believed to be responsible for both a basal inverse grading, and a strong alignment of grains with imbrication angles commonly >20° (Hiscott & Middleton 1979).

Hiscott (1994b) identified serious flaws in the physical model which had been used to explain shearing of a *traction carpet* beneath a sediment gravity flow. Specifically, shear stress should be constant throughout such a traction carpet (cf. Sumer *et al.* 1996; Pugh & Wilson 1999), so there is no reason to expect deposition to take place in a series of steps as each carpet individually 'freezes' from the top downward, as was proposed by Hiscott and Middleton (1979) and Lowe (1982). Legros (2002) subsequently discounted dispersive pressure as a viable mechanism to form the observed inverse grading. In addition, shear-cell experiments (Savage & Sayed 1984) suggest that even large shear stresses cannot shear a mobile bed to depths greater than about ten grain diameters. Hiscott (1994b) proposed a more descriptive term for the inversely graded deposits: *spaced stratification*. He interpreted this type of stratification to result from strongly fluctuating hydrodynamic conditions and vigorous burst–sweep cycles beneath large turbidity currents as they rain sediment onto the seabed. At the base of each stratum, inverse grading is attributed to a 'kinetic sieve' mechanism (Middleton 1970; Savage & Lun 1988) whereby small particles in a thin agitated dispersion are able to filter through the voids between larger particles, eventually dominating the lower part of the sheared layer. The conclusion that traction carpets are not the explanation for spaced stratification is supported by Sohn (1997), who demonstrated that deposition from traction carpets must occur by progressive aggradation rather than frictional 'freezing' of a sheared layer. This style of deposition will leave no layering in the deposit, and in sandy sediments is unlikely to produce inverse grading (Sohn 1997).

Sedimentary structure sequences for the deposits of concentrated density flows have been presented by Aalto (1976), Hiscott and Middleton (1979), Hein (1982), Lowe (1982) and Mulder and Alexander (2001). The analysis of Hiscott and Middleton (1979) is based on a transition matrix (9 states, Table 1.4) for 214 medium-to coarse-grained sandstone beds (mean thickness 380 cm) from inferred submarine-fan deposits (Hiscott 1980) of the Tourelle Formation of Québec, Canada. The preferred transitions, inferred from Markov Chain Analysis, are presented in Figure 1.51 with process interpretations. These transitions differ somewhat from those presented by Hiscott and Middleton (1979), due to a change in the method of calculation of the independent trials matrix (modified procedure includes iterative fitting of row and column totals; Powers & Easterling 1982). Except for some basal scour-and-fill structures, the first deposits accumulated by rapid en masse deposition, producing either a division of structureless coarse- to medium-grained sand or, in the case of highly unsteady flow, a division of spaced stratification. There is no evidence of grain-by-grain traction on the bed during the early stages of deposition, perhaps because the development of planar stratification is suppressed if the rate of bed aggradation
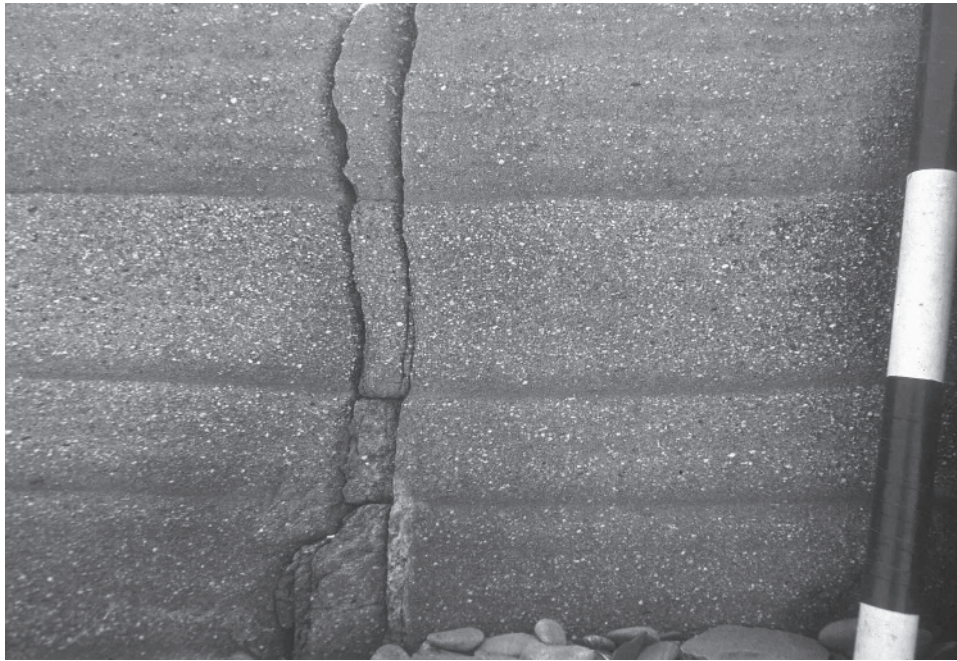
Fig. 1.50   *Spaced stratification* within a graded bed of coarse to medium sandstone. The base and top of the bed are not shown. Each 5–10 cm-thick stratification band is inversely graded at its base and then essentially structureless and ungraded above. The sandstone has a strong grain fabric with high grain imbrication angle. Scale divisions are 10 cm.

Table 1.4   Transition matrix for 214 thick sandstone beds, Tourelle Formation

'State'	Number of upward transitions								
	1	**2**	**3**	**4**	**5**	**6**	**7**	**8**	**9**
1 Basal scour	0	155	20	2	0	0	0	0	37
2 Structureless ('Massive') or graded	135	0	10	13	21	10	9	12	23
3 Internal scours	4	27	0	0	0	0	0	0	1
4 Planar lamination	7	1	0	0	5	1	2	0	0
5 Current-ripple lamination	25	0	0	0	0	0	0	3	0
6 Convolution	12	0	0	0	0	0	1	0	0
7 Cross-stratification	9	0	0	2	1	0	0	0	0
8 Muddy lamination	16	0	0	0	0	0	0	0	0
9 Spaced stratification	6	50	2	0	1	2	0	1	0

exceeds ∼ 4 cm min^{-1} (Arnott & Hand 1989). At the top of most beds, deceleration of the more dilute tail of the current produced a sequence of structures like the Bouma sequence. In other examples, the dilute tail of the current reworked the sandy top of the initial deposit into large ripples or dunes, and then presumably continued down the fan surface to deposit its fine load at more distal sites (cf. Lowe 1982).

Hein (1982) documented sequences of sedimentary structures in channelised conglomerates, pebbly sandstones and coarse sandstones that are similar to those recognised by Walker (1975a) for conglomerates and Hiscott and Middleton (1979) for sandstones. Important additional divisions recognised by Hein (1982) are those bearing the imprint of syn- and post-depositional fluid escape; dish structures are particularly abundant in these rocks. Also, the pebbly sandstones of Hein (1982) contain more cross-stratification than was observed in finer deposits by Hiscott and Middleton (1979). Hein (1982) interpreted some of this cross-stratification as the product of reworking of the tops of the deposits by dilute flows that spilled into the submarine

channel from other, nearby channels (see Section 7.4.5, flow stripping process of Piper & Normark 1983).

Soh (1987) studied the grain fabric of thickly bedded graded conglomerates from the Miocene–Pliocene of central Japan and concluded that the main transport process just before deposition changed from grain shearing, dominated by particle collisions near the base of flows, to viscous current drag near flow tops, where concentrations were lower.

A general theme that runs through these descriptions is an early phase of deposition dominated by grain-to-grain interactions and pore-fluid escape, followed by a transition to more turbulent conditions and slower, selective deposition. The implication is that these flows were density stratified with turbulence suppression limited to the lower parts of the flows. It is unclear whether there was a sharp interface between the different parts of these flows, whether the pronounced flow stratification was long-lived, or whether it was mainly an outcome of intense particle fallout as deposition started.
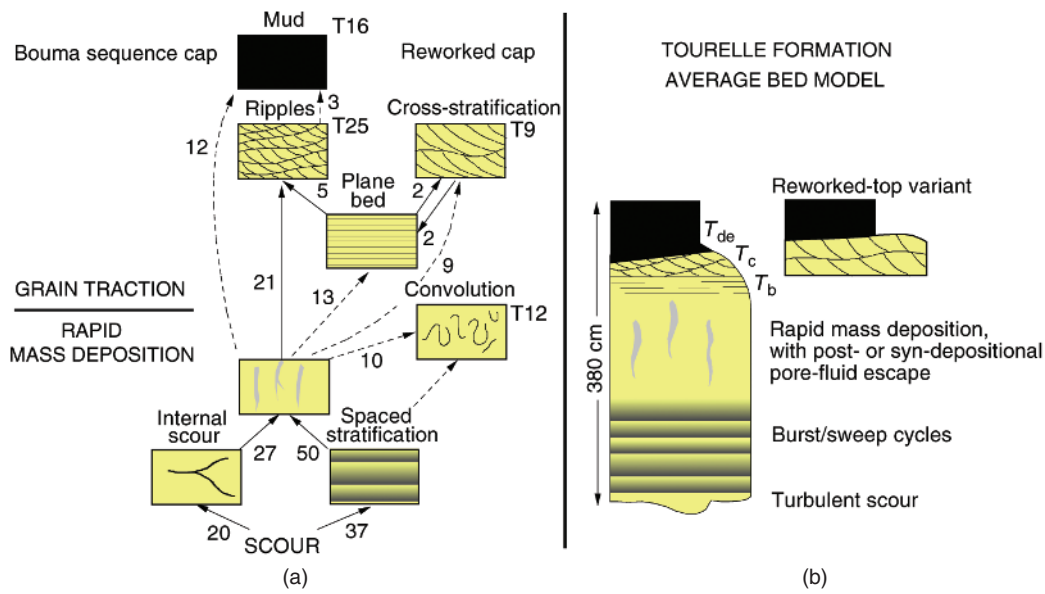
Fig. 1.51   (a) Preferred transitions between nine 'states' in 214 thick sandstone beds (average thickness 380 cm) deposited from concentrated density flows, Tourelle Formation, Québec, Canada. Numbers indicate the number of transitions between states; T25 signifies that a rippled division is the highest division in 25 beds. Complete beds (tops preserved) only occur 62 times – the other 152 beds had their tops bevelled during amalgamation. Structural divisions were produced either by rapid mass deposition ('freezing') or by selective grain-by-grain deposition with traction transport. In some cases, post-depositional reworking of the top of the bed is indicated by medium-scale cross-stratification. Arrow weight indicates the statistical significance of transitions (based on method of Powers & Easterling 1982: p. 922) with the levels of significance being >98% (solid arrow) and >93% (dashed arrow). No arrows are shown if there is only one transition between states, regardless of significance level. (b) Generalised bed model based on the transition diagram, with interpretation. Where appropriate, structural divisions have Bouma (1962) T_{a-e} labels.
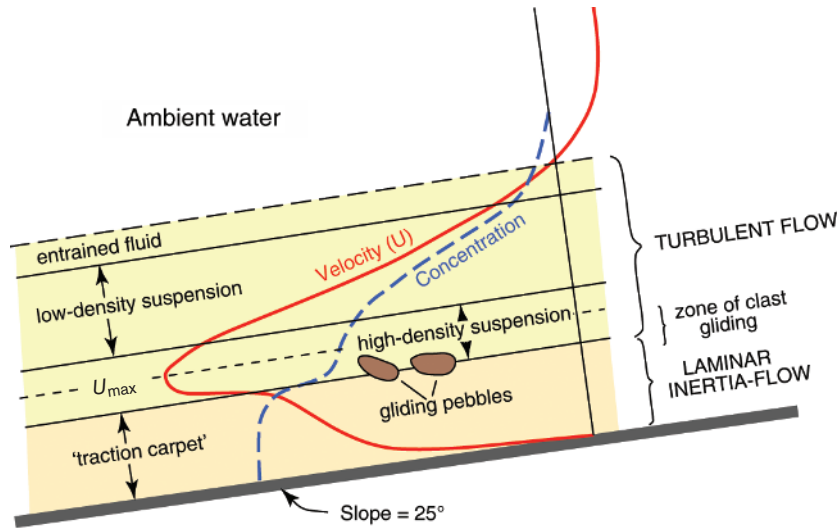

Fig. 1.52   Mechanism proposed by Postma *et al.* (1988) for the transport of large mud clasts within a strongly stratified SGF. At 25°, the slope for the experimental demonstration of this effect is unreasonably high for natural SGFs.

1.6.2   Large mud clasts in concentrated density-flow deposits

Many concentrated density-flow deposits contain large mud clasts, either dispersed well above the base of the bed, or concentrated into clusters or trains (Walker 1985; Postma *et al.* 1988; Shanmugam *et al.*

1995). Such clasts are commonly described to be 'floating' in the bed, and for this reason proposals have been made to explain how shale clasts can be suspended by sediment gravity flows, or by stratified two-layer flows. Postma *et al.* (1988) employed flume experiments on high slopes of 25° to show how large clasts can be carried along the interface between a highly concentrated, laminar, basal inertia-flow,

and a less concentrated, fully turbulent overriding flow (Fig. 1.52). They proposed that larger natural two-layer flows could operate in the same way on much lower slopes after undergoing a 'gravity transformation' (Fisher 1983). Shanmugam *et al.* (1995) instead interpreted 'floating' clasts in structureless sands as a strong indicator that the deposits were emplaced by inflated sandflows (his sandy debris flows), not turbidity currents or concentrated density flows. Hiscott *et al.* (1997a) disputed this generalisation, noting that concentrated density flows are deposited from the base upward through progressive aggradation (Kneller & Branney 1995), so that part way through the depositional phase the seafloor corresponds to some level well above the base of the eventual deposit. If a mud clast is rolling or sliding along the bed and then ceases to move, it will subsequently be buried by sand yet will appear to be suspended in sand. Outsized mud clasts rolling and sliding beneath a concentrated density flow might be expected to reach their final resting place well after deposition of some thickness of sand, because they would travel much more slowly than the mean velocity of the current (Hand & Ellison 1985).

Recent interpretations of 'hybrid event beds' (Haughton *et al.* 2009) explain large floating clasts in deposits having a graded sandy basal division as the product of flow transformation ('gravity transformation') from a turbulent density flow to a debris flow. The basal part of such deposits records accumulation from a turbulent flow, so is organised and graded (Fig. 1.28a). The clast-rich interval is more muddy and disorganised, because it was deposited from a cohesive late-stage phase of the flow capable of carrying large clasts. Alternatively, the large clasts might have been carried by a co-genetic debris flow that was triggered at the same time as a concentrated density flow (Fig. 1.29), leading to stacked deposits comprising a single event bed with large mud clasts in the upper part (Haughton *et al.* 2010).

1.7   Inflated sandflows and their deposits

Inflated sandflows are envisaged to range in density from ~40–70% by volume (Fig. 1.21), most of which is coarse silt or larger in size, and the bulk of which is sand. Variable amounts of gravel can also be present. Cohesion is minor (Figs 1.19 & 1.22), and voids between particles are well connected. Mulder and Alexander (2001) explain that this facilitates the ingesting of seawater and therefore the transition of many inflated sandflows to concentrated density flows. Inflated sandflows lack significant cohesive strength, but do possess frictional strength because of grain-to-grain interlocking when concentrations become very high, for example as velocity decreases and deposition starts. As a result, deposition from inflated sandflows takes place by frictional 'freezing'.

Even though cohesion is not a significant contributor to particle support, a small amount of interstitial mud, or very poor sorting, are required to permit these sandflows to operate on low slopes. Mud, or the very small pore throats that characterise poorly sorted sand, will dramatically reduce the permeability of the mobile sediment and therefore slow the dissipation of excess pore-fluid pressures that contribute to particle support (Fig. 1.19). Without the elevated pore-fluid pressures or cohesion provided by small amounts of clay, inflated sandflows would depend entirely on grain interaction for maintenance of the suspension, and would be pure grain flows. Grain flows, as noted earlier, cannot operate on slopes less than ~13°. As pointed out by Mulder and Alexander (2001), as little as 2% by volume clay will permit flow on low slopes if the remaining sediment is fine-grained sand. A maximum of ~20–25% by volume clay is required at water contents of 25–40% by volume if the rest of the

sediment is coarse-grained sand ± gravel (Hampton 1975; Marr *et al.* 2001). In natural poorly sorted mixtures of sand, the fine-grained sand between any larger sand grains will ensure that no more than ~2% by volume clay is required to significantly reduce the rate of pore-fluid escape.

When clay content is low and the sandy sediment is poorly sorted, inflated sandflows owe their mobility to the extended persistence of elevated pore-fluid pressures, and to grain-to-grain interactions. When mud forms ~10–25% of the detrital fraction, the flows may resemble the 'slurry flows' described by Lowe *et al.* (2003). As an explanation for the long runout distances seen in the more muddy sandflows, Mulder and Alexander (2001) point to the increased coherence of the flow mass that results from the presence of cohesive particles (i.e., clays). 'Coherence' is the ability of a mixture to hold together and support sediment (Marr *et al.* 2001). For flows with low coherence (i.e., low clay contents), the rheological strength of the material is unable to fully resist the dynamic stresses generated by the flow (Marr *et al.* 2001), leading to uninhibited internal deformation.

Inflated sandflows are more susceptible to 'shear mixing' with ambient seawater than clay-rich cohesive flows, because of their lower coherence and connected voids (Marr *et al.* 2001; Talling *et al.* 2002). Shear mixing is the erosion of the front and top of a SGF because of its movement beneath ambient fluid. This erosion produces a secondary dilute turbidity current (Hampton 1972).

1.7.1   Deposits of inflated sandflows

The high particle concentrations do not permit selective deposition and the formation of lamination by traction transport. Grain sorting cannot occur by the differential settling of coarser and finer grains (Mulder & Alexander 2001); hence, deposits lack normal grading or only show poor coarse-tail grading (Marr *et al.* 2001). They may be inversely graded, however, because of grain-to-grain interactions or because the base of the flow undergoes greatest and most prolonged shear, leading to reduced competence (Hampton 1975). The dissipation of elevated pore-fluid pressures often produces fluid-escape structures like dish structures and fluid-escape pillars. In more muddy deposits, a minor but significant amount of cohesion facilitates the development and preservation of a variety of shear laminae and banding, and deformation structures (Lowe *et al.* 2003). If a turbidity current is generated by shear mixing at the upper interface of the inflated sandflow, an organised turbidite might directly overlie the primary deposit, but more likely will accumulate more distally on lower slopes (Marr *et al.* 2001).

Although frictional 'freezing' is the cause of deposition, Mulder and Alexander (2001) conclude that the entire flow does not deposit en masse. They point to the experiments of Major (1997) on subaerial frictional flows, in which deposits formed by the successive accretion of thin layers which ultimately formed a thicker deposit. However, thick subaqueous flows might behave differently, and 'freeze' from the top downward as shear stress drops below the frictional strength of the material. Because the shear stress is lowest toward the flow top, the first grain interlocking and arrested internal motion might take place there, leading to the formation of a semi-rigid plug which would thicken downward as deceleration continues.

Branney and Kokelaar (2002) produced a set of synthetic bed models for deposition from mainly cohesionless gravity flows (Fig. 1.53). The main variables that distinguish the flows responsible for these deposits are flow concentration, shear rate and deposition rate (Fig. 1.54). For relatively low concentrations in turbidity currents, high shear rates produce tractional structures whereas low shear
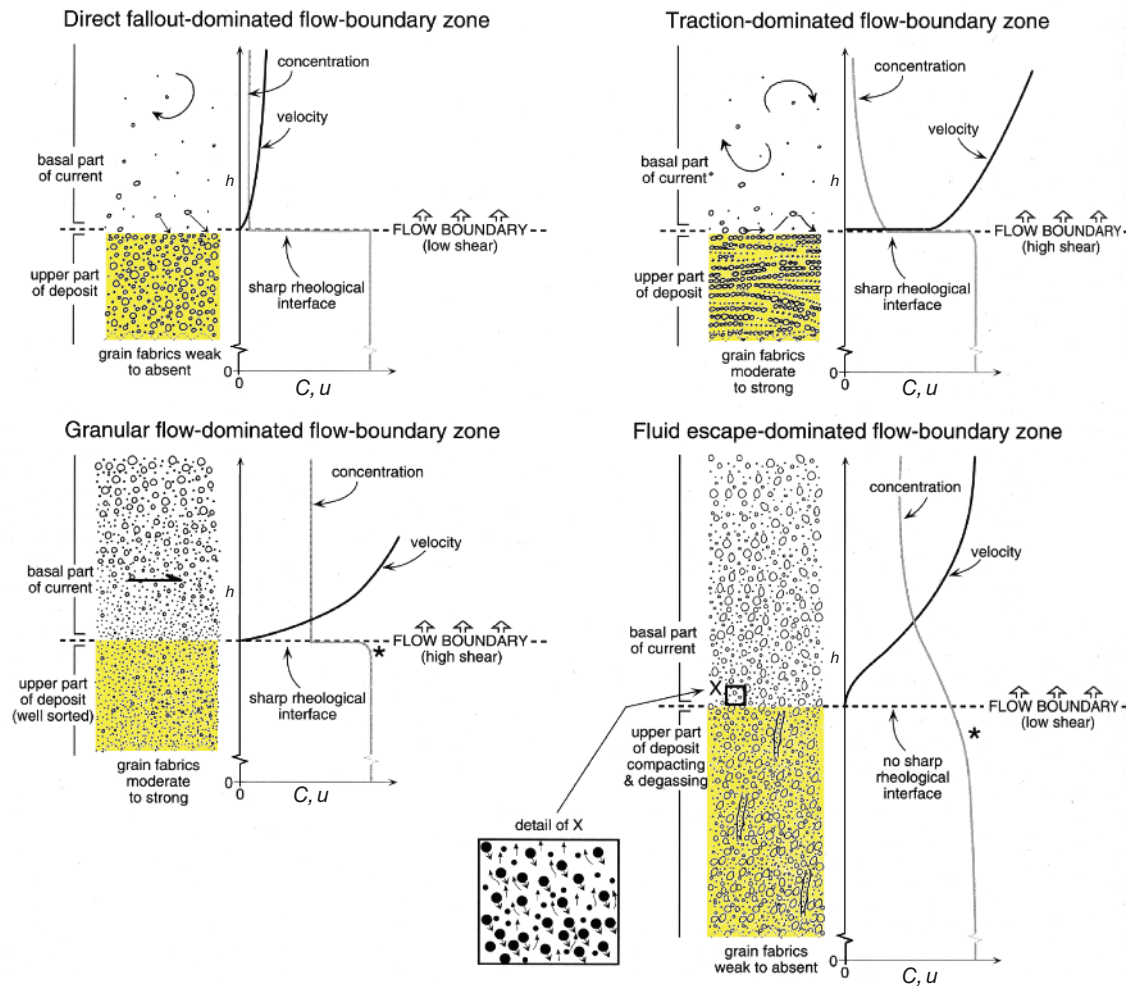
Fig. 1.53   Relationship between deposit characteristics, shear rate and flow concentration in sandy gravity-flow deposits. From Branney and Kokelaar (2002).

rates with fine-gained suspensions can lead to little traction and structureless deposits. For relatively high concentrations, high shear rates at the accumulating bed produce a sharp interface and strong grain fabrics, whereas low shear rates across a diffuse depositional boundary (perhaps because of strong pore-fluid escape and elutriation) lead to weak fabrics in deposits with signs of syndepositional liquefaction and fluid escape.

1.8   Cohesive flows and their deposits

1.8.1   Definitions and equations of flow

Cohesive flows are characterised by strong coherence, so that they hold together while flowing along the seabed (Marr *et al.* 2001). The coherence is created by cohesive forces between electrostatically charged clay minerals. Mulder and Alexander (2001) distinguish between *mudflows* and *debris flows*. Their mudflow deposits have less than 5% by volume gravel and more mud than sand. Their debris-flow deposits consist of more poorly sorted sediment (>5% by volume gravel with variable sand proportion) and may include boulder-sized

clasts of soft sediment or rock and very large sediment rafts. The name 'debris flow' commonly is used for both a flow process and a deposit. This usage generally does not create problems because the context makes the meaning clear. For clarity, however, we will henceforth use the term 'debris flow' for the process only, and *debrite* for the deposit.

Cohesive flows are only well described from modern subaerial settings (Johnson 1970, 1984; Pierson 1981; Takahashi 1981; Middleton & Wilcock 1994). According to Takahashi (1981: p. 58), cohesive flows are flows 'in which the grains are dispersed in a water or clay slurry with the concentration a little thinner than in a stable sediment accumulation … [and] in which all particles as well as the interstitial fluid are moved by gravity'. Subaerial cohesive flows are capable of transporting boulders up to 2.7 million kg (Takahashi 1981), have bulk densities in the range of 2.0–2.5 g cm^{-3}, and may move at speeds of 20 m s^{-1}. Catastrophic submarine cohesive flows may carry (or push) enormous slabs weighing up to about 2300 million kg (immersed weight, Marjanac 1985).

Experiments and theory (Hampton 1975, 1979; Rodine & Johnson 1976) suggest that only a small amount, about 5%, of interstitial matrix – mud + water slurry – is required to allow flow on surprisingly gentle slopes. The matrix serves several functions. It (i) lubricates the
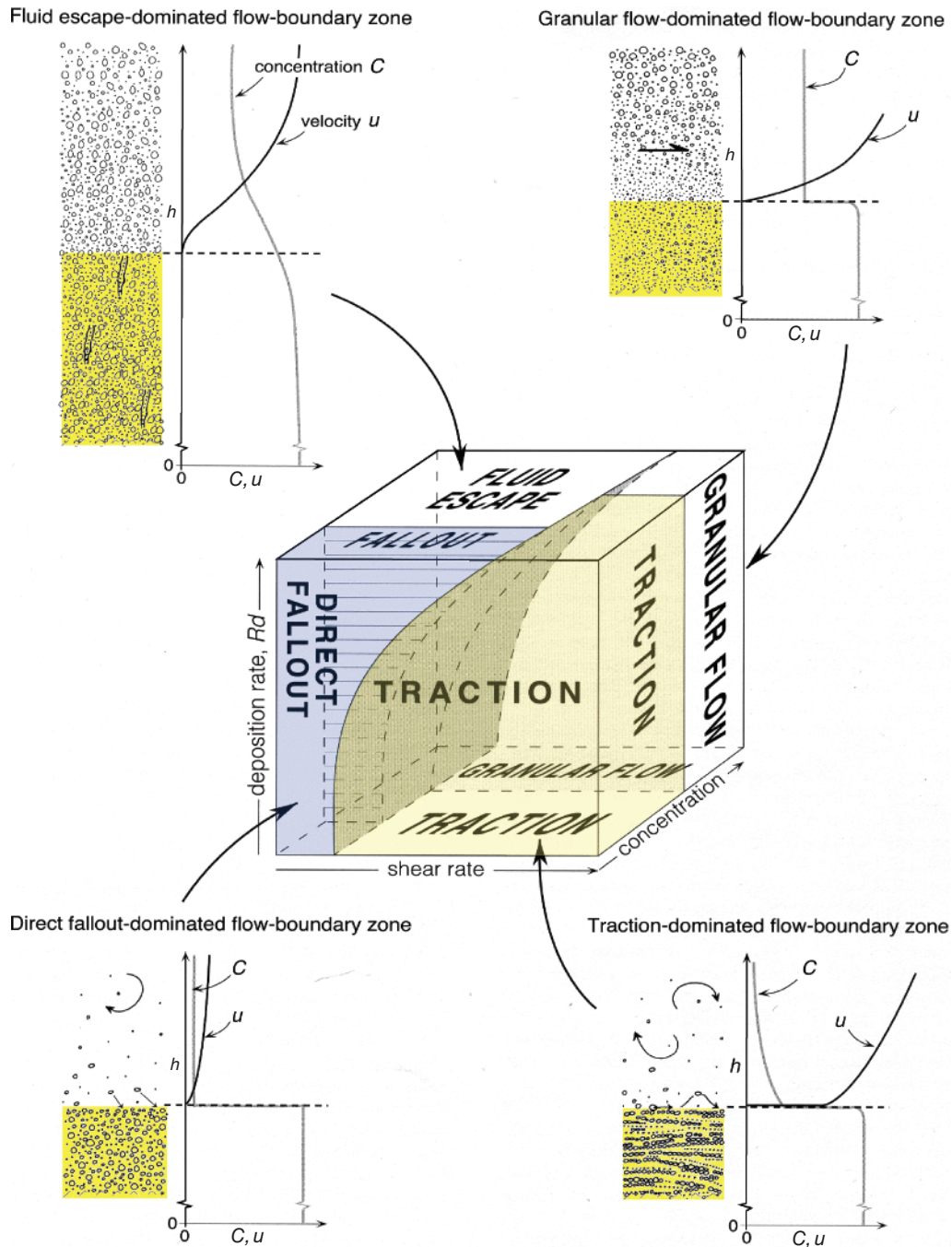
Fig. 1.54 Process cube to explain deposits from sandload SGFs. High concentrations (the two upper scenarios) form typical deposits of inflated sandflows and some concentrated density flows. From Branney and Kokelaar (2002).

larger clasts so that they are able to slide past one another, (ii) provides buoyant support for clasts of only slightly higher density and (iii) commonly exhibits elevated pore pressures that increase buoyancy and the lower frictional resistance to flow (Pierson 1981; Ilstad *et al.* 2004a).

In terms of rheology, cohesive flows resemble wet concrete and exhibit *strength*, which can be divided into two components: cohesive strength due to electrostatic attractions between clay-size particles, and frictional strength due to interlocking and surface contacts between clasts and between the flow and its bed. According to Pierson (1981), frictional strength far exceeds cohesive strength as a mechanism of clast support. Strength allows cohesive-flow deposits to stand up in relief above its surroundings, with steep meniscus-like margins called *snouts*. Strength, and buoyancy of clasts in the matrix, permits the flow to carry clasts above the bed that are more dense than the bulk density of the flow itself.

Materials with strength will not deform until a critical yield strength is exceeded. They therefore behave as *plastic* materials. Once

deformation (flow) begins, laminar flow generally prevails in those parts of the cohesive flow where the critical yield strength is less than the shear stress. Elsewhere, friction and/or cohesion resist deformation. Particle support during flow comes from a combination of (i) frictional resistance to settling through finer matrix, similar in explanation to the kinetic sieve process described by Middleton (1970); (ii) matrix cohesion or strength that is not exceeded by the downward-directed force exerted by dispersed clasts; (iii) buoyancy (partial support only); (iv) elevated pore pressures in the cohesive matrix and (v) dispersive pressure (Bagnold 1956, 1973; Pierson 1981). Lowe (1982) believes that, in many cases, the largest clasts are not actually suspended, but remain in contact through rolling, sliding and intermittent bouncing downslope.

Cohesive flows move as a result of deformation in a basal zone of high shear stress. Lower shear stresses high in the flow, or at the flow margins, do not always exceed the yield strength of the material, so that the upper part of the flow may be rafted along as a semi-rigid plug (Johnson 1970). As total shear stress decreases (i.e., as bottom slope decreases), or as intergranular friction increases, the semi-rigid plug thickens by downward growth until the entire mass ceases to move ('freezes') when bed shear stress declines to a value lower than the yield strength. Likewise, low shear stresses at flow margins result in marginal 'freezing' and construction of levées. Johnson (1970) favoured either a Bingham plastic or Coulomb viscous rheological model for debris flow (see Iverson 1997 for other models). A mathematical expression for Bingham plastics is:

$$\tau = k + \mu \left[\frac{du}{dy} \right]; \quad \tau_{\text{crit}} = k \tag{1.11}$$

where k = strength of the cohesive flow = critical shear stress for movement (τ_{crit}), μ = dynamic viscosity of the sediment-water mixture after movement begins, and du/dy = the rate of change of velocity at any level, y, in the flow. Note that for $k = 0$, this equation reduces to Newton's law of viscosity. A similar expression for Coulomb viscous materials is:

$$\tau = C + \sigma_n \tan \phi + \mu \left[\frac{du}{dy} \right]; \quad \tau_{\text{crit}} = C + \sigma_n \tan \phi \tag{1.12}$$

where C = the cohesive strength component, due to electrostatic attractions between clay particles; $\sigma_n \tan \phi$ = the frictional strength component, due to intergranular friction; σ_n = normal stress; and ϕ = angle of internal friction. In contrast, Takahashi (1981) favours a 'dilatant-fluid' rheological model based on dispersive pressure (Bagnold 1956). Locat (1997) has developed a bilinear rheological model with two viscosity terms. At high strain rates, the debris behaves as a Bingham material {Eq. 1.11) with low viscosity, and at low strain rates it behaves as a Newtonian fluid with a high viscosity. The bilinear model provides a good fit to experimental data (Imran *et al.* 2001).

Although cohesion is a primary support mechanism in both mudflows and debris flows, natural flows exhibit a wide variation in the relative importance of grain-support mechanisms. In particular, elevated pore-fluid pressures are important in explaining the mobility of many cohesive flows (Pierson 1981; Pierson & Costa 1987; Ilstad *et al.* 2004a). Once mud-rich sediments fail and the electrostatic bonds responsible for cohesion are broken, the material tends to remain mobile throughout its downslope flow, even on low slopes. This is a reflection of the *thixotropic behaviour* of clays and fine silts, in which strength is dependent on the recent deformation history of the material.

1.8.2   Turbulence of cohesive flows

Most cohesive flows are laminar, with no fluid mixing across streamlines. Large flows may be turbulent (Enos 1977; Middleton & Southard 1984), but should not be classified as turbidity currents or concentrated density flows because they lack the strong vertical concentration gradients of more dilute currents (e.g., Fig. 1.30), and because they re-acquire laminar behaviour and develop a semi-rigid plug with deceleration. Even in laminar flows devoid of eddies, secondary circulation due to clast rotations and encounters, or due to flow meandering, may cause churning and internal mixing.

For Bingham plastics, the criterion for turbulence is based on both the *Reynolds Number, R.* and the *Bingham Number, B,* where

$$R = \frac{Ud\rho}{\mu} \tag{1.13}$$

and

$$B = \frac{\tau_{\text{crit}} d}{\mu U} \tag{1.14}$$

In these equations, U = mean flow velocity, d = flow thickness, ρ = flow density, and μ = dynamic viscosity after flow begins. Experimental data (Fig. 1.55), originally plotted by Hampton (1972), indicate that for large values of either R or B, a conservative criterion for turbulence is:

$$R \geq 1000B \tag{1.15}$$

which is equivalent to

$$\frac{\rho U^2}{\tau_{\text{crit}}} \geq 1000 \tag{1.16}$$

This last dimensionless product was named the *Hampton Number* by Hiscott and Middleton (1979), who used reasonable values for
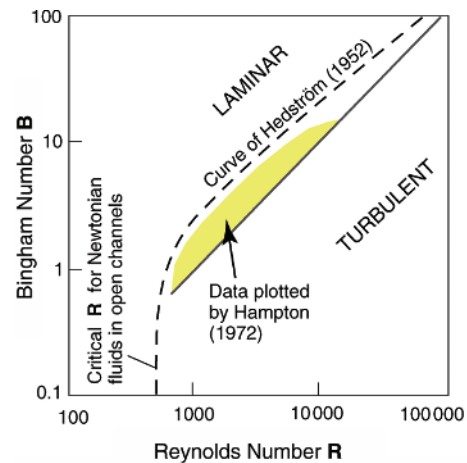

Fig. 1.55 Relation of Bingham Number to critical Reynolds Number for turbulence in a Bingham plastic. Experimental data are for pipe flow but scales have been adjusted to the correct values for 2D SGFs using the thickness of the flow as the length scale. From Hiscott and Middleton (1979), based on Hampton (1972).

flow strengths and densities to show that even large, fast debris flows probably would not be turbulent.

Basal scour beneath fully freighted laminar cohesive flows generally is insignificant (Takahashi 1981), possibly because in cases where hydroplaning results this allows the flow to ride along on top of a thin sheet of overpressured water or wet, low-viscosity, mud (Mohrig *et al.* 1998; Ilstad *et al.* 2004b). Also, the lack of turbulence decreases the chance of erosion because fluid scour is inoperative. Nevertheless, underlying sediments may be plucked up and incorporated into the flow because of high shear stresses along the basal interface (Hiscott & James 1985; Dakin *et al.* 2012). Where large cohesive flows impinge upon the base of submarine slopes, they can gouge and disrupt the underlying strata (e.g., Hiscott & Aksu 1994) and produce 10–30 m-deep erosional channels, grooves and scour pits, perhaps facilitated by partial liquefaction of the rapidly loaded substratum of unconsolidated or weakly lithified sediments (Dakin *et al.* 2012). Cohesive-flow deposits also may occur in channels cut by other processes, as these flows seek out bathymetric lows.

1.8.3 Competence of cohesive flows

The competence – largest clast that can be carried (D_{max}) – of cohesive flows was determined by Hampton (1975) to be:

$$D_{max} = \frac{8.8k}{g(\rho_{clast} - \rho_{matrix})} \qquad (1.17)$$

where k = strength, g = gravitational acceleration and ρ = density. Using kaolinite-water slurries as matrix, Hampton (1975) determined that (i) competence decreases approximately exponentially with increasing weight percent water, from about 20 cm at 40% water to about 2 cm at 60% water (approximate lower limit of cohesive flows, Fig. 1.21), (ii) competence of slurries is less after shear than before shear – by about 0.5 mm at 60% water, (iii) competence decreases with flow duration for durations less than about one hour and (iv) competence is independent of flow velocity.

For debris flows with more than 20 volume% coarse sand and gravel, the competence increases dramatically with increasing concentration of coarse clasts (Hampton 1979). This is because the large clasts load the matrix and produce elevated pore-fluid pressures that counteract the tendency of the clasts to settle. These excess pressures (above hydrostatic) also reduce the strength of the flow by reducing normal stress (Eq. 1.12). At volume concentrations above 50%, clast collisions and near collisions provide additional support (Rodine & Johnson 1976), and competence continues to increase dramatically above that predicted by Equation 1.17 (Hampton 1979). At these concentrations, grain-to-grain interactions may be the dominant support mechanism (Pierson 1981; Takahashi 1981), and the more sand-laden flows are transitional into inflated sandflows.

Natural subaerial analogues to submarine cohesive flows commonly flow in an unsteady manner as a series of advancing 'waves' that may overtake one another or be separated in time by more fluid flows (Fig. 1.56). This process affects the streamwise texture of the flow and the eventual vertical profile of the deposit.

1.8.4 Deposits of cohesive flows, including debrites

Because of the mode of deposition, cohesive-flow deposits are poorly sorted, lack distinct internal layering but may have crude stratification due to non-uniform migration through the flow of the base of the semi-rigid plug during deceleration (Hampton 1975; Thornton 1984; Aksu 1984), have a poorly developed clast fabric (Lindsay 1968; Aksu 1984; Hiscott & James 1985), irregular mounded tops and tapered flow margins or snouts. Grading is generally poor, but both normal and inverse grading may occur (Naylor 1980; Aksu 1984; Shultz 1984). Inverse grading may develop because the base of the flow undergoes the greatest and most prolonged shear, leading to reduced competence (Hampton 1975). Individual cohesive-flow events may deposit separate tongues or lobes of material that have quite different textural characteristics (for a subaerial example, see Johnson 1984: pp. 266–74), making it difficult to distinguish separate flows in the geological record (Fig. 1.57).
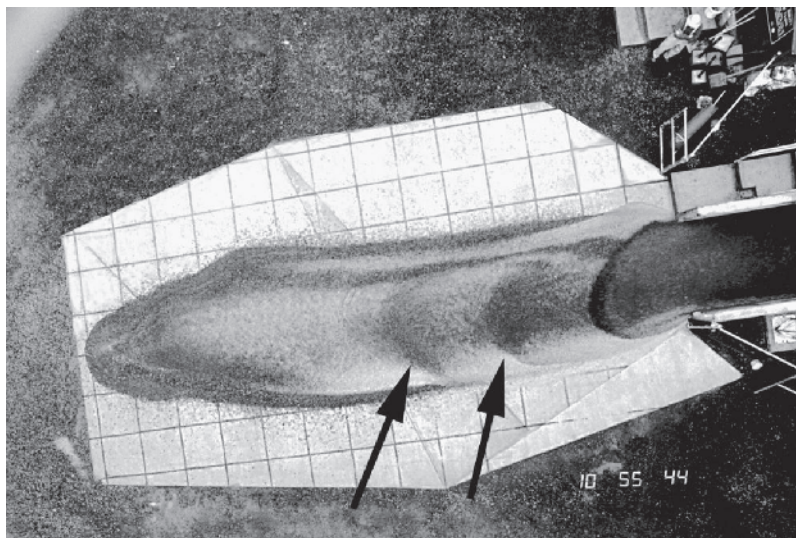

Fig. 1.56 Experimental subaerial debris flow with a series of advancing surface waves (arrows). The grid squares have sides of 1 m, and a human figure in the top right also provides scale. From Major (1997: his fig. 7E).
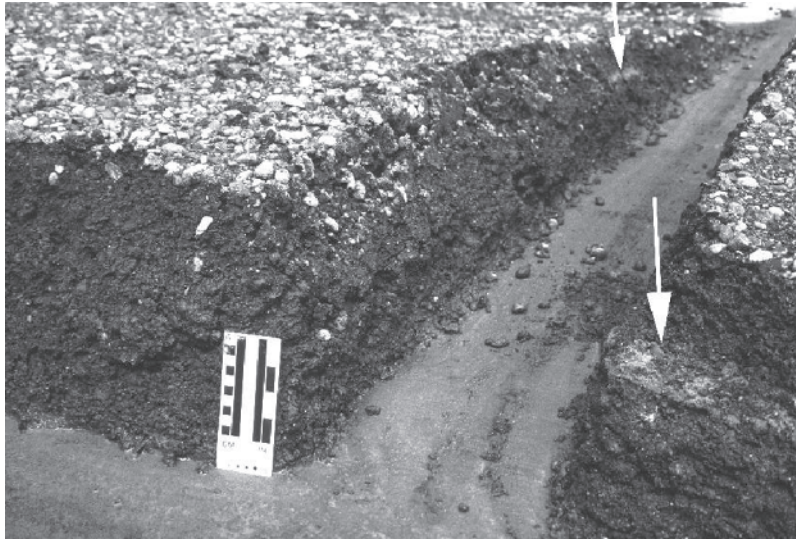
Fig. 1.57 Amalgamated experimental debris flow deposits separated by a cryptic surface (arrow) that could easily be missed in a natural exposure. Leftmost scale divisions are in centimetres. Photograph courtesy of J. J. Major. A different view of the arrowed amalgamation surface is shown in Major (1997: his fig. 10A).
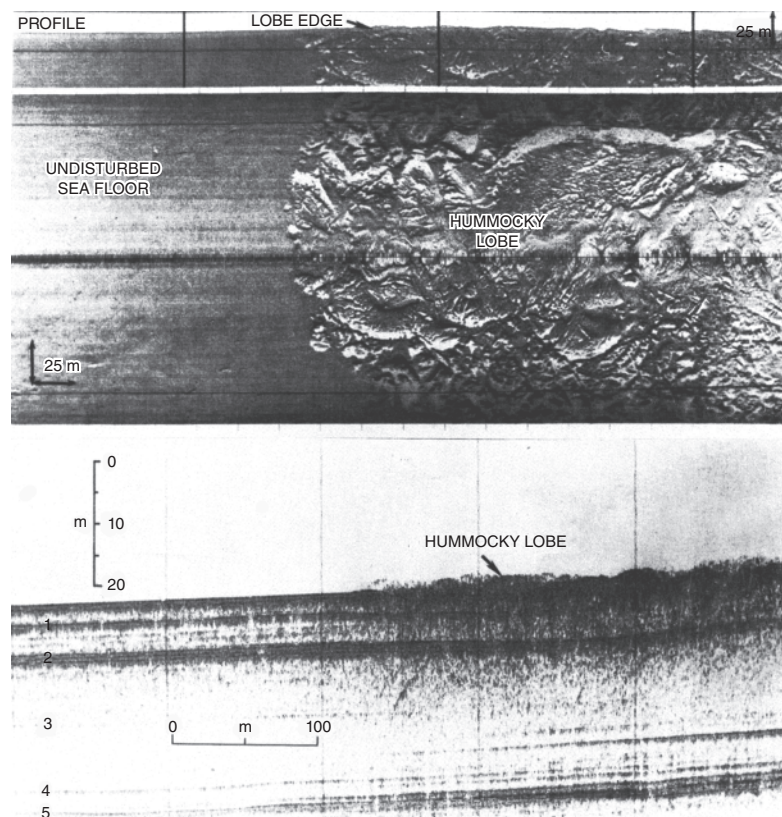

Fig. 1.58 100 kHz side-scan sonar image (and relief profile), and matching sub-bottom profile of hummocky debrite lobe in Bute Inlet, Canada. From Prior *et al*. (1984).
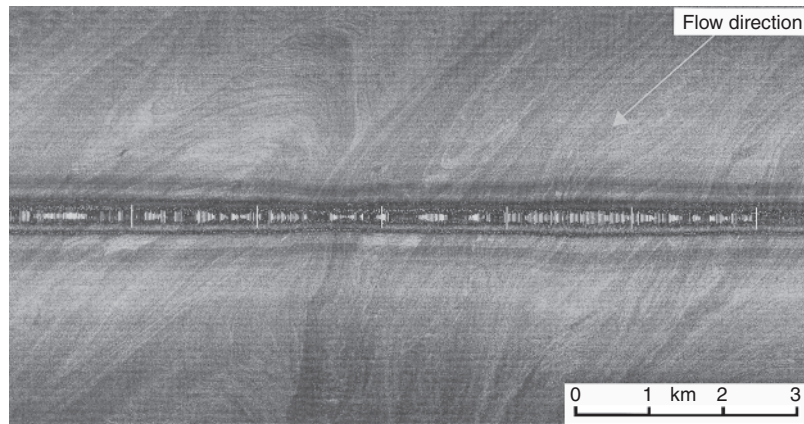
Fig. 1.59 TOBI 30 kHz sonograph of 'woodgrain' texture, consisting of flow-parallel banding, pressure ridges and longitudinal shears, on the surface of the Saharan Debris Flow deposits at ~4350 m water depth. Light tones are high backscatter and the vehicle track is along the centre-line of the image. From Weaver *et al*. (1995).
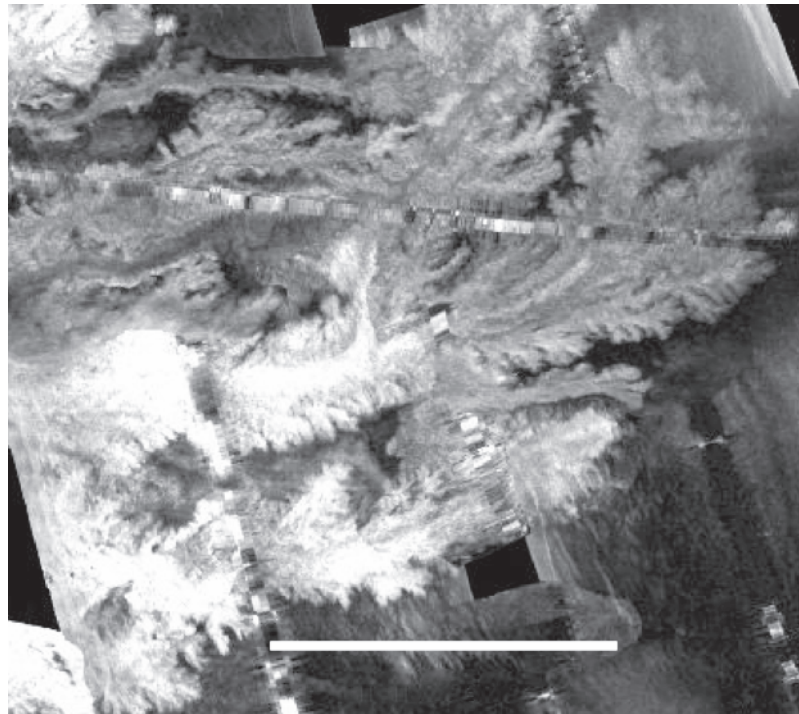

Fig. 1.60 SeaMarc1A mosaic showing shrub-shaped SGF deposits at the terminations of dendritic channel network on the Mississippi Fan, and interpreted by Schwab *et al*. (1996) and Talling *et al*. (2010) as the deposits of mudflows. From Paskevich *et al*. (2001) and http://pubs.usgs.gov/of/2000/of00-352/htmldocs/images.htm.

Increasingly, submarine cohesive flows are being imaged by high-resolution side-scan sonar systems. Some flows have irregular blocky surfaces (Fig. 1.58) (Prior *et al.* 1984), whereas others show prominent woodgrain-like flow lines like the surfaces of some glaciers, indicating ductile flow (Fig. 1.59) (Masson *et al.* 1993; Weaver *et al.* 1995). These flow lines resemble the compression ridges produced in small-scale experiments by Marr *et al.* (2001). Low-viscosity flows that transited the Mississippi Fan channel system form shrub-like digitate deposits (Fig. 1.60) just beyond the channel mouths and over the tops of low distal levées (Twichell *et al.* 1992; Schwab *et al.* 1996; Talling *et al.* 2010). These digitate deposits have been interpreted by Talling *et al.* (2010) as ~1 m-thick mudflow deposits carrying large clay and fine-sandstone slabs, passing downward into clean graded sand deposited during a turbulent phase of the same flow event. According to Talling *et al.* (2010), a body transformation occurred along the flow path as clay concentration increased in the upper part of the flow, leading to damping of turbulence and development of cohesion. Similar finger-like sandy deposits (inferred to be hyperconcentrated-flow deposits – the inflated sand-flow deposits of this chapter) are present in channel-mouth lobes of the Monterey Fan channel (Klaucke *et al.* 2004). Extensively cored 'mass-transport complexes' on the Amazon Fan, with the acoustic characteristics of mudflows, predominantly consist of contorted and disoriented blocks of silt and mud (Piper *et al.* 1997). The blocky flows and the woodgrain-banded flows presumably possess different rheology and viscosities.

Shultz (1984) attributed grading style and volume concentration of matrix in debrites to the relative importance of cohesion, clast interaction (dispersive pressure) and fluid behaviour. The result is a continuum of deposit characteristics (Fig. 1.61) intermediate in character between four distinct end-member facies: *Dmm* = 'massive' (structureless) matrix-supported debrite, *Dmg* = graded matrix-supported debrite, *Dci* = inversely graded clast-supported debrite, and *Dcm* = 'massive' (structureless) clast-supported debrite (Shultz 1984).

The larger clasts – cobbles and boulders – of some cohesive-flow deposits are concentrated near the base or in the middle of the deposit. Some large boulders may be grounded on the underlying substrate (Masson *et al.* 1993), whilst others project from the tops of the beds (Fig. 1.22), allowing a quantitative assessment of rheological strength using a Bingham plastic model (Johnson 1970: p. 487).
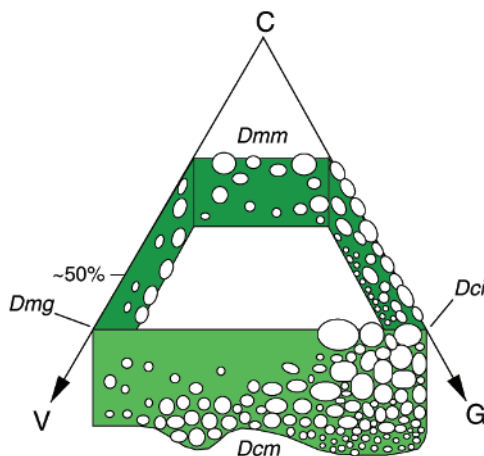
Bingham plastic strength can also be calculated from the shape of debris snouts and from the thickness, T_{crit}, at which flow ceased (Johnson 1970: p. 488), according to the following equation:

$$T_{crit} = \frac{k}{\gamma_d \sin \alpha} \tag{1.18}$$

where γ_d = specific weight of the cohesive flow and α = slope angle. Note that $\gamma_d = g' \rho_{flow}$ where $g' = g(\rho_{flow} - \rho_{water})/\rho_{flow}$.

Calculations of cohesive-flow strength based on either the extent of clast projection or snout shape are given by Hiscott and James (1985) and Kessler and Moorhouse (1984), who calculated strengths in the range 10^2 to 1.0 Pa (1 Pa $= 10^5$ dynes cm^{-2} = 1 N m^{-2}) for Cambro-Ordovician and Jurassic deposits, respectively. These estimates are in the same range as values calculated for subaerial flows by Johnson (1970).

1.8.5   Submarine versus subaerial cohesive flows

All evidence suggests that submarine cohesive flows and their deposits differ only in minor ways from subaerial equivalents, although associated facies and processes of post-depositional modification are clearly different. Shear stress is dependent on the density difference between the flow and the ambient fluid, so one might predict that somewhat higher slopes would be needed to permit subaqueous versus subaerial cohesive flow, given similar yield strengths. Recall, however, that submarine cohesive flows have been documented from very low slopes. Hydroplaning might help explain this high degree of mobility (Mohrig *et al.* 1998). In general, submarine flows probably have lower yield strengths than subaerial flows as a result of entrainment of seawater and wet mud, lack of downward percolation of water from the flow itself into the substrate, and elevated pore-fluid pressures (Pierson 1981) due to greater amounts of interstitial fluid. This suggestion is supported by the observation that, for deposits of equal thickness, subaqueous cohesive-flow deposits contain smaller boulders than subaerial deposits (Nemec *et al.* 1980; Gloppen & Steel 1981; Nemec & Steel 1984), that is, subaqueous cohesive flows are weaker than subaerial flows.

1.9   Accumulation of biogenic skeletons and organic matter

Far from continental sources of detritus, four main types of pelagic input dominate the world oceans: *biogenic silica* in high-productivity zones along the equator (radiolarians) or at about 60° latitude (diatoms); *biogenic carbonate* (foraminifera, nannofossils, pteropods) in other areas shallower than the carbonate compensation depth (CCD); ice-rafted particles along the trackways of drifting icebergs; and red clays where no biogenic or glaciogenic particles are supplied (Figs 1.62 and 1.63). Under special circumstances, pelagic sediments may accumulate near continents, but only where terrigenous input is relatively very low (e.g., Gulf of California; Calvert 1966). Unconsolidated biogenic pelagic sediments are called *ooze*. If sufficiently buried and lithified, siliceous ooze becomes diatomite or radiolarite, and eventually *chert*, whereas calcareous ooze becomes *chalk* and eventually aphanitic limestone.

It is appropriate here to differentiate between the terms *pelagic* and *hemipelagic* as they apply to sedimentary deposits. In this book, pelagic grains are defined as those grains that initially enter the marine hydrosphere beyond the shelf-slope break, or are created by
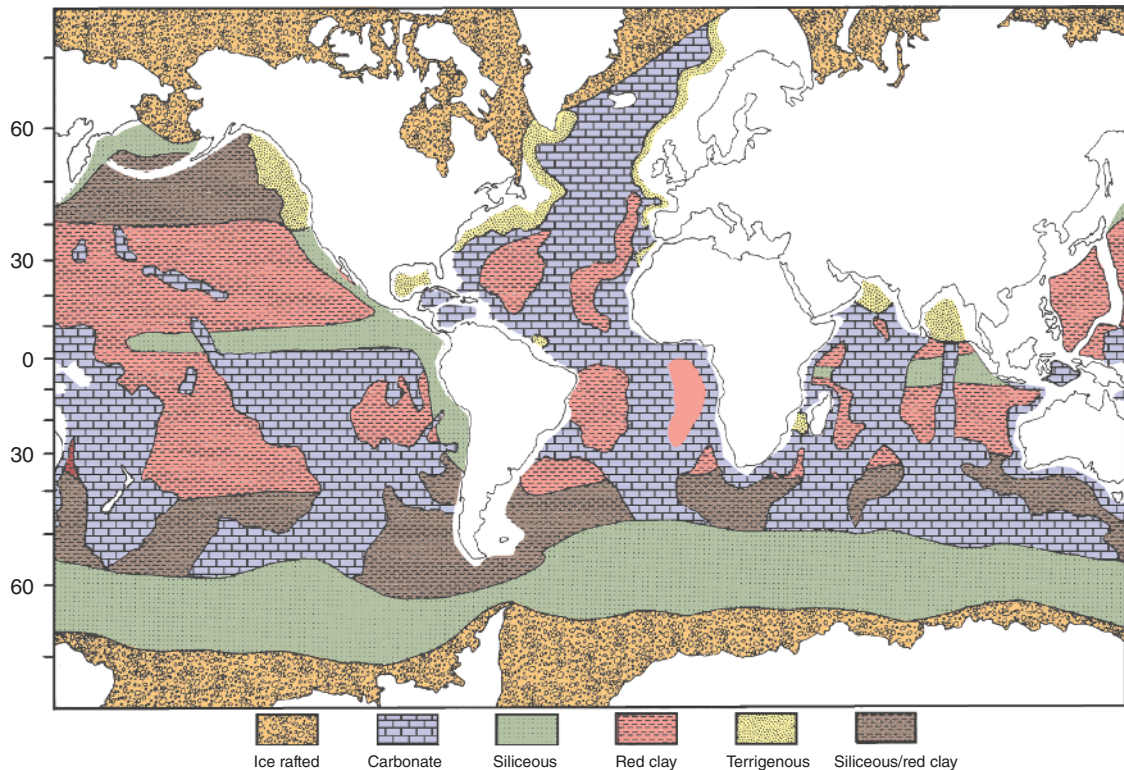

Fig. 1.61   Schematic diagram of relationships among debrite types. See text for abbreviations. Redrawn from Shultz (1984).

Fig. 1.62 World distribution of dominant sediment types in the oceans. Redrawn from Jenkyns (1986).
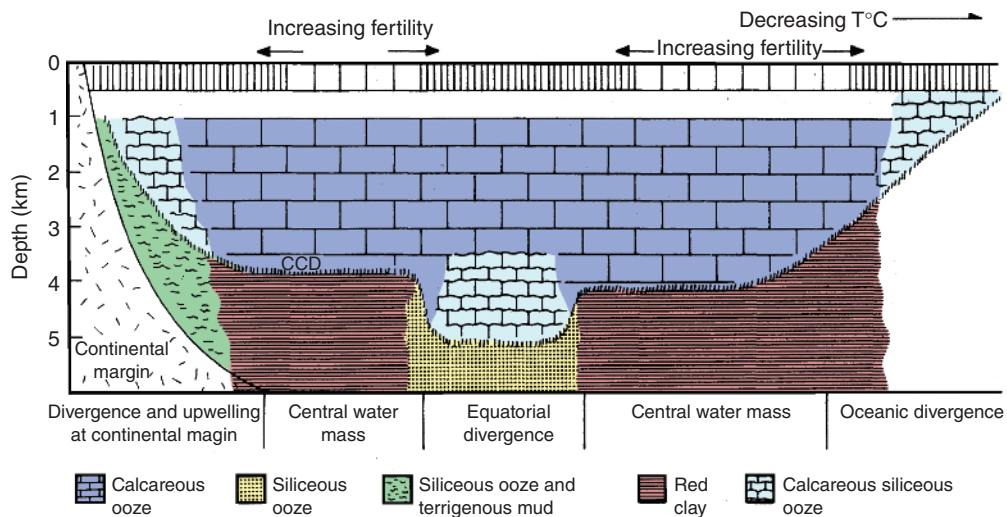

Fig. 1.63 Schematic diagram, based on the Pacific Ocean, to show the main location of sediment types relative to the CCD and near-surface organic productivity. Redrawn from Ramsay (1977).

organisms in this open-ocean region, and that subsequently settle to the seafloor. Pelagic particles, therefore, include biogenic siliceous skeletons (diatoms, radiolaria), calcareous skeletons (foraminifera, nannofossils), wind-blown dust (e.g., Staukel *et al.* 2011; Wan *et al.* 2012; Xu *et al.* 2012) or volcanic ejecta that lands on the sea surface of the open ocean, and debris liberated by melting icebergs. Hemipelagic sediments contain a pelagic component, generally 5–50% but locally

as much as 75%, with the remainder consisting of terrigenous mud that initially enters the ocean at the coast, either by coastal erosion or through river systems (deltas, estuaries etc.). This terrigenous component is advected off the shelf by storms and ocean currents.

The tests of dead planktonic organisms, with their empty chambers, settle more slowly than would be anticipated based on diameter alone. For example, planktonic foraminifera settle at the same rate as quartz

particles with a diameter approximately 2.4 times less (Berger & Piper 1972). Because of advection by ocean currents, such slow settling might be expected to result in geographic mismatches between areas of plankton productivity and areas of their seafloor accumulation. Serious mismatches are, in fact, not observed in the modern oceans for a number of reasons (Berger & Piper 1972): (i) surface currents mostly transport settling tests parallel with the pelagic facies belts; (ii) deep currents commonly return settling tests closer to the place where they originated in surface waters and (ii) many tests travel to the seafloor in faecal pellets, and therefore settle (as a group) far more rapidly than they would as single tests.

Organic matter can be derived from land masses as *terrestrial organics*, or from the preservation of algal and other *marine organic compounds*. The two main processes which may lead to burial of organic matter are high rates of accumulation (leaving inadequate time or oxidising agents to decompose the material at the seafloor), and accumulation under anoxic to dysaerobic seabed conditions. High rates of accumulation, particularly of marine organic matter, are favoured by oceanographic upwelling of nutrient-rich waters along continental margins or at open-ocean divergence zones. Fully or partly enclosed bodies of water may have their own particular chemistry (e.g., stratification and poorly oxygenated bottom water) which can lead to accumulation of organic-rich sediments. Examples are *sapropels* in the Mediterranean Sea (Kidd *et al.* 1978; Rossignol-Strick 1985; Emeis & Weissert 2009; Möbius *et al.* 2010) and Japan Sea (Ishiwatari *et al.* 1994; Stax & Stein 1994) which formed periodically in the Neogene and Quaternary, and Albian *black shales* which have widespread distribution in the world's oceans (Jenkyns 1980). Sapropel is defined as mud with >2% total organic matter (Kidd *et al.* 1978). Decomposition of this organic matter in the sediment uses up the available oxygen and makes the pore-water anoxic. If the bottom water is also anoxic, then neither deposit feeders nor filter feeders can live in the sediment, and it is entirely undisturbed by burrowers, leading in many cases to the finely laminated deposits typical of ancient black shales.

The maximum depth for accumulation of deep-marine biogenic carbonate particles is dependent upon the position of the *carbonate compensation depth* (CCD), and the shallower *aragonite compensation depth* (ACD) for pteropods. These critical depths, below which calcareous remains do not occur, are functions of ocean circulation, latitude, seawater chemistry and geologic time (Fig. 1.64). The net result of the spatial and temporal variation of these controls is the generation of vertically and laterally changing facies, facies associations and sequences. Such changes result in geographically and stratigraphically distinct units or 'packets' of sediments, each with their own environmental interpretation.

Highstands of sea level are associated with an amelioration in climate, increased biological diversification, reduced mid-water oxygen concentration, an open-ocean shoaling of the CCD (Fig. 1.64), a proliferation of deep-marine 'condensed successions' of pelagic sediment and the accumulation of muddy abandonment facies over many deep-marine clastic systems. At the present time, during the Holocene sea-level highstand, most of the world's deep-marine clastic systems are essentially dormant and being mantled by pelagic or hemipelagic sediments. The surfaces of many submarine fans are veneered by about 1 m of light-brown, pelagic, foraminiferal ooze or marl, representing approximately the last 11 kyr; for example on the Amazon Fan (Damuth & Kumar 1975a; Damuth & Flood 1985), and the Mississippi Fan (Bouma *et al.* 1986).

Pelagic depositional rates are typically 1–60 mm kyr^{-1} (Fig. 1.65). However, these rates may reach about 100 mm kyr^{-1} on outer shelves and upper slopes in areas of upwelling. Ocean currents control the mixing of cold and warm water masses, biological productivity, sites of upwelling and the distribution of various chemogenic sediments such as phosphorites. Oceanic circulation, interacting with water depth and basin physiography, oxygen minima or anoxia, and biological productivity, govern the potential distribution of open-ocean (e.g., biogenic) sediments.

Although modern ocean circulation patterns are well known, and despite their profound impact on the distribution of fine-grained
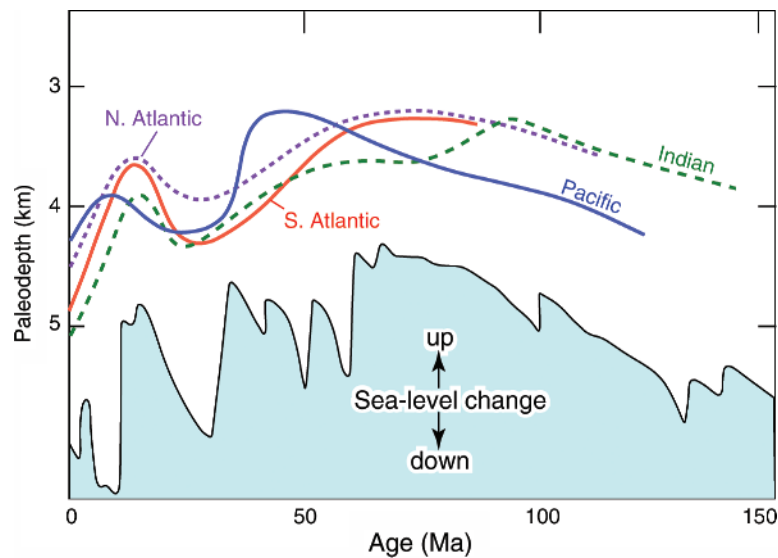

Fig. 1.64 Fluctuations in the depth of the CCD since 150 Ma in the Atlantic, Pacific and Indian oceans and the variation in global sea level. Redrawn from Kennett (1982).
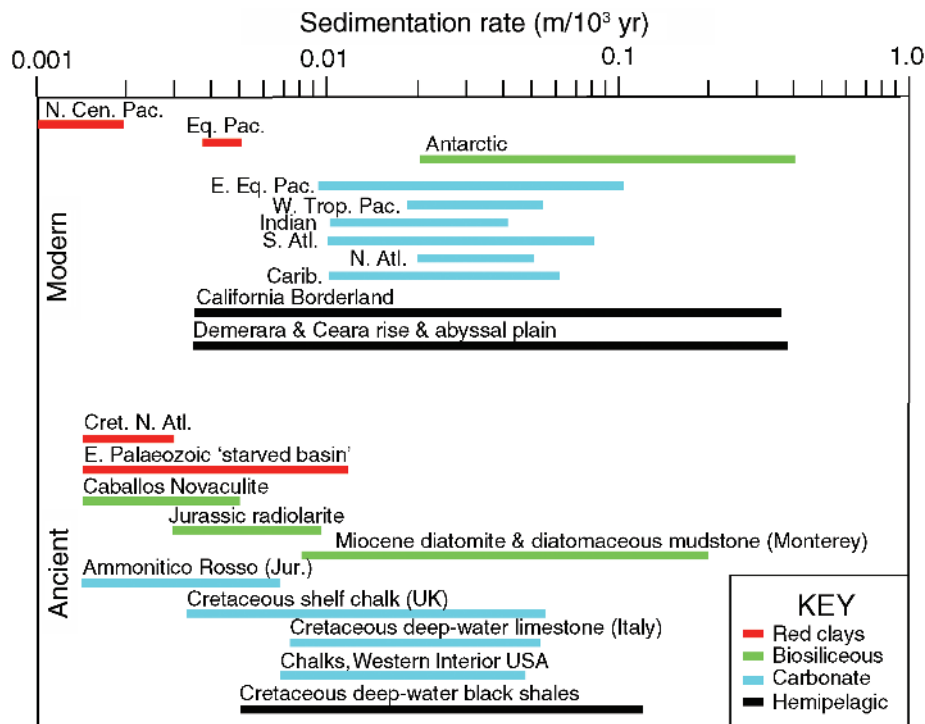
Fig. 1.65 Rates of sediment accumulation of some modern and ancient pelagic and hemipelagic sediments. Note that estimated rates for ancient sediments are ~60–70% of modern rates. Redrawn from Scholle and Ekdale (1983).

and biogenic facies, there are few data on ancient ocean current patterns, except constraints provided by DSDP and ODP drilling. For example, a comparison of Palaeocene and Oligocene world oceans, based partly on DSDP data (Fig. 1.66) shows the important role that the distribution of continents plays in controlling ocean circulation. In the Palaeocene, prior to the collision of India with the Asian Plate, there was an equatorial circum-global Pacific-Tethys current, and clockwise subpolar gyres inferred for the Southern Pacific and Atlantic. By the Oligocene, the remnant of Tethys was a relatively small fragmented ocean basin, and much of the present-day ocean circulation was established, including the Circum-Antarctic Current.

Results from various DSDP sites around the Central Atlantic show that even in the Early Cretaceous, a proto-Gulf Stream was established (Fig. 1.67), with pelagites and hemipelagites comprising varve-type laminations, graded claystones and limestone–shale couplets (Robertson 1984; Sheridan, Gradstein *et al.* 1983). The fine-grained varve-type lamination, formed by fluctuating proportions of terrigenous plant material, marine plankton and clastics, may reflect short-periodicity (tens to hundreds of years) climatic changes. The graded claystones and black shales represent fine-grained turbidite redeposition from within or near the oxygen minimum zone on the upper continental slope. The limestone–shale couplets suggest climatic variation on time scales of 20 000–60 000 years, with the organic-rich shales formed during wetter periods when abundant plant material entered the sea (Robertson 1984). The abundance of radiolaria in the pelagic chalks suggests upwelling to produce fertile surface waters, possibly due to the inflow of nutrient-rich waters from western Tethys (Fig. 1.67). This is just one example

of the importance of palaeoceanography in interpreting ancient deep-marine mixed siliciclastic and carbonate sediments, including organic-rich shales.

1.9.1 Environmental information from biogenic skeletons

A number of fossil groups can provide information on past values of seawater salinity (e.g., dinoflagellate cysts, benthic foraminifera, ostracods) and temperature (e.g., planktonic foraminifera). These constraints are largely based on species proportions (through statistically based transfer functions) and morphological variations including test abnormalities. Here, we emphasise two criteria from benthic foraminiferal studies that provide constraints on palaeo water depth and water-column oxygenation.

Pioneering work in the California Borderland and Neogene successions of the western United States established the technique of determining palaeo water depth from the assemblage of the benthic foraminifera, in particular (Natland 1933; Bandy 1953; Ingle 1975). Ingle (1975, 1980) explains procedures and limitations, and provides some statistical data for offshore California. For example, planktonic foraminifera constitute 0–10%, 10–50%, 20–80% and <30% of total fauna for inner shelf, outer shelf, upper slope (<1000 m) and basin, respectively, whereas radiolarians increase dramatically at the shelf edge from <5 to ~500–1000 specimens per gram. Only the known upper depth limits of benthic foraminiferal species can be used to establish the palaeo water depth, because post-mortem downslope
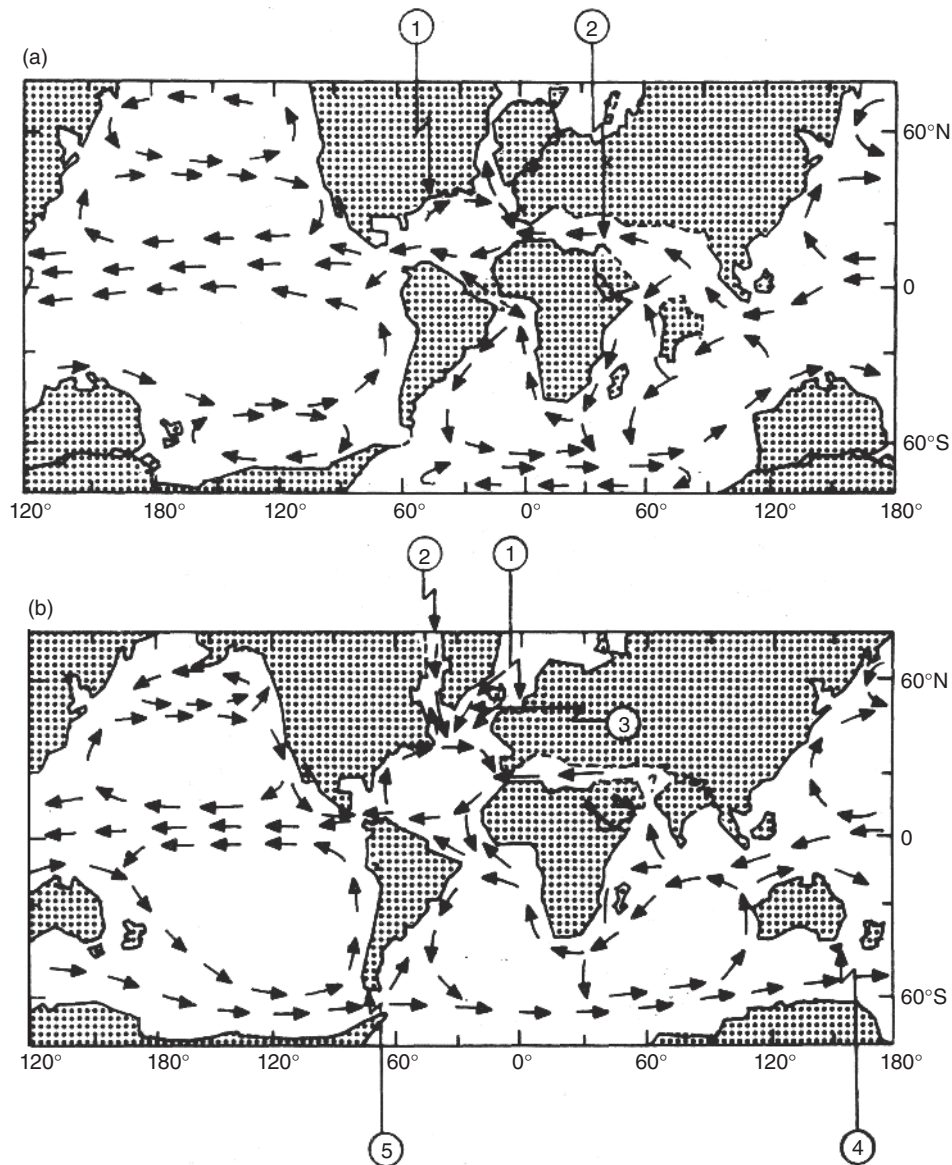
Fig. 1.66 Schematic reconstruction of the Palaeocene and Oligocene distribution of continents and ocean surface-circulation patterns. Numbers refer to following: (a) Palaeocene; 1, Proto Gulf Stream; 2, Tethys Current; (b) Oligocene; 1, Norwegian-Greenland Sea; 2, North Labrador Passage; 3, Greenland-Iceland-Faroe Ridge; 4, South Tasman Rise; 5, Drake Passage. From Leggett (1985) after Haq (1981).

transport contaminates samples with the skeletons of upslope fauna. For example, 50–100% of benthic foraminiferal tests found beyond the shelf edge offshore California have been displaced from upslope. When applied to ancient successions, great care must be taken because the modern upper depth limits depend on the stratification of temperature, nutrients, oxygen concentration, etc. in the modern ocean. As a result, Ingle (1980) advises that modern upper depth limits from offshore California can be used for cool periods in the Palaeogene and Neogene, but that for warmer climatic periods (e.g., late Palaeocene – early middle Eocene, latest Oligocene, middle Miocene) the upper depth limits from more tropical areas in the eastern Pacific and Gulf of Mexico are more reliable. The water-depth ranges which can be discriminated using benthic foraminifera become wider with increasing depth (e.g., upper bathyal = 150–500 m, whereas upper middle bathyal = 500–1500 m).

The use of benthic foraminifera to estimate palaeo water depth is most reliable in the Neogene and Palaeogene, where species are likely to have had similar behaviour to modern relatives. However, this approach has also been used successfully in Upper Cretaceous rocks (Sliter 1973; England & Hiscott 1992).

Benthic foraminifera can also be used to quantify past concentrations of dissolved oxygen in bottom waters, unless conditions were too anoxic for life. Kaiho (1991) defined a *benthic foraminiferal oxygen index* (BFOI), which displays a linear correlation to the oxygen content of bottom waters at least in the range of values below $3 \, \text{ml} \, \text{l}^{-1}$ (Kaiho 1994). The BFOI uses the relative proportions of three benthic foraminiferal morphogroups to estimate past bottom water oxygen content. Kaiho adapted the morphogroup concepts of Bernhard (1986), and Corliss and Chen (1988), to define these groups. 'Dysoxic' species have flattened, tapered, or elongate tests
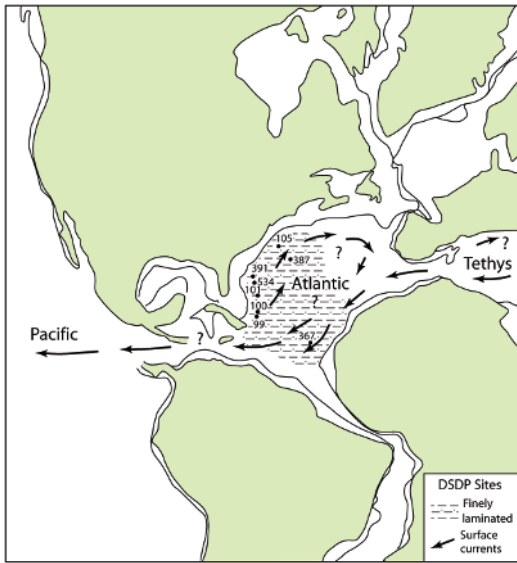
Fig. 1.67 Reconstruction of the central Atlantic Ocean in the Early Creta-ceous, showing location of some DSDP sites, the inferred surface circulation and probable distribution of varve-type laminated sediments. Redrawn from Robertson (1984).
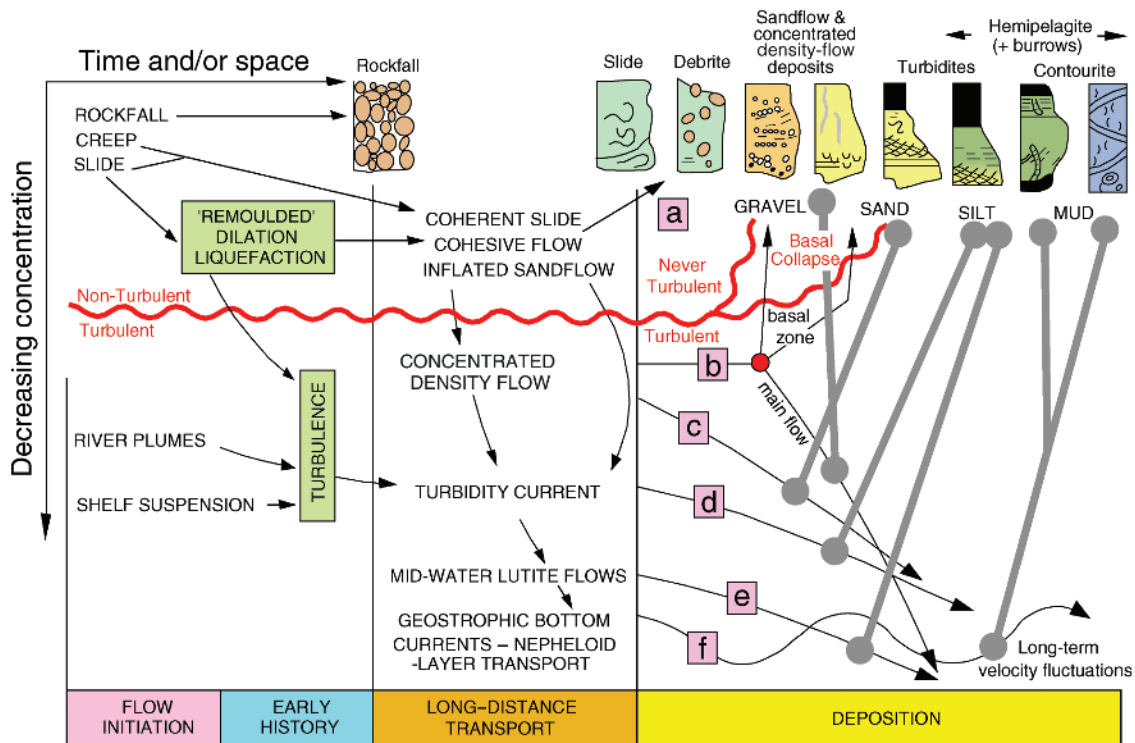

Fig. 1.68 Summary of the evolution of sediment gravity flows and other deep-marine transport processes as a function of particle concentration. Compare with Figure 1.1. Deposits are arranged across the top of the diagram at the end of each evolutionary pathway. The box labelled with the letter a relates to dense, cohesive SGFs that never became turbulent. Box b corresponds to concentrated density flows which, during their depositional phase, become strongly stratified into a non-turbulent lower part and a thicker turbulent upper part. The lower part of this flow eventually deposits en masse rather than by suspension settling. Boxes with letters c–e correspond to turbulent SGFs of variable concentration – these lose their sediment load by selective (grain-by-grain) deposition, forming graded beds with tractional structures. Eventually, all sediment is dropped and concentration approaches zero. Grey 'dumbells' link each evolving flow with its deposit. The box and flow labelled *f* is a thermohaline contour current with low concentration and very long-period velocity fluctuations (e.g., thousands of years). Clearly, the time scale for these currents and their fluctuations is much longer than the time scales for other flows in the diagram, which might be no longer than hours to days. Modified from Middleton and Hampton (1973) and Walker (1978).

which typically display a thin, porous wall and lack ornamentation. 'Oxic' species display a variety of test forms, including spherical, plano-convex, biconvex, and rounded trochospiral. This group includes species that have large, ornamented tests and thick walls. Finally, the 'intermediate' or 'suboxic' group contains taxa that are typically larger than the 'dysoxic' forms, and display some ornamentation. This group includes tapered and cylindrical forms, planispiral forms, and those trochospiral forms that have small, thin test walls. The BFOI has been used successfully by Kaminski *et al.* (2002) to assess past environmental conditions in the salinity-stratified water column of the Marmara Sea, Turkey, where dysoxic conditions have existed for the last 10,000 years.

Summary

The main mechanisms for long-distance lateral transport of sediment in the deep sea are: (i) turbidity currents; (ii) concentrated density flows; (iii) cohesive flows; (iv) deep, thermohaline, clear-water currents that commonly flow parallel to bathymetric contours; (v) movement of dilute mud suspensions in water masses that drift or cascade off the shelf and (vi) mass movement in the form of sediment slides. The summary Figure 1.68 is a more developed version of Figure 1.1, and relates the various transport processes to their deposits. The deposits of cohesive flows are poorly sorted, generally lack stratification, have a poorly developed clast fabric, and stand up above their surroundings as irregular mounds with a tapered marginal snout. Deposits of concentrated density flows (and less common inflated sandflows) show evidence for grain-to-grain interaction (as inverse grading) and pore-fluid escape (as dish structures or pillars); however, these processes are restricted to the time of deposition and reveal little about the long-distance transport mechanism.

Fine-grained sediment can be deposited by turbidity currents, by bottom currents (contour currents), or by settling from dilute suspensions at the top of, or within, the water column (pelagites and hemipelagites). The deposits have some diagnostic characteristics, but are in many cases difficult to interpret because of a superposition of more than one process, or because of post-depositional bioturbation.

Sediment slides can involve all size grades of sediment, but are most common in poorly consolidated, water-rich muds found in areas with high depositional rates. The susceptibility of sediment masses to sliding, even on very low slopes, is sharply increased by cyclic vibrations generated by earthquakes.

Biogenic sediments and organic-rich muds are not shown in Figure 1.68 because they do not form beneath discrete flow events. Biogenic sediments accumulate where biological productivity is high in surface waters, and where post-mortem dissolution of hard parts is prevented or reduced by favourable shallow depositional depths (carbonate) or high accumulation rates (silica). Organic-rich sediments accumulate in areas of high productivity (e.g., upwelling zones) where accumulation rates are too high to allow significant seabed oxidation of organic matter, or where bottom waters are anoxic because oxidising organic matter consumes dissolved oxygen faster than it can be supplied by sluggish marine currents.